

SEISMIC RESPONSE OF PILE FOUNDATION IN
SATURATED SAND USING BEAM ON NONLINEAR
WINKLER FOUNDATION APPROACH

MOHAMMAD KAMRUZZAMAN TALUKDER



**SEISMIC RESPONSE OF PILE FOUNDATION IN SATURATED
SAND USING BEAM ON NONLINEAR WINKLER FOUNDATION
APPROACH**

by

© Mohammad Kamruzzaman Talukder

(B.Sc. in Civil Eng., Bangladesh University of Engineering and Technology)

Faculty of Engineering and Applied Science

Memorial University of Newfoundland

St. John's, NL, Canada.

A thesis submitted to the School of Graduate Studies
Memorial University of Newfoundland, Canada
in partial fulfillment of
the requirements for the degree of
Master of Engineering (Civil Engineering)

May, 2009

Memorial University of Newfoundland

St. John's, NL, Canada.

Abstract

Evaluating the interaction of soil-pile systems to earthquake ground motions is an important step in the seismic design of piles. Three Dimensional Finite Element Models have been developed by a number of researchers. But these models are computationally expensive, complicated and not readily used in design offices. In this study, a Beam on Nonlinear Winkler Foundation (BNWF) approach consisting of simple nonlinear springs, dashpots and pile elements is used to account for nonlinearity of soil-pile relative movement, energy dissipation through radiation damping of soil and material damping of pile. The p-y curves within the framework of two dimensional Winkler foundation approach are widely used in design offices to calibrate soil springs where p is the unit soil reaction and y is the pile lateral deflection. The p-y curves proposed by American Petroleum Institute (2000) are used to estimate the lateral response of single flexible pile that is embedded in saturated sand. An effective stress based ground response analysis is performed to predict input motions to soil springs at various depths of soil. Performance of the BNWF model when compared with centrifuge test results is shown to be an inexpensive procedure and compatible with readily available structural analysis software, ABAQUS, for prediction of dynamic response of pile foundations in design offices. Pile peak response curves are given by comparing maximum computed and experimental pile peak responses (pile peak head accelerations, pile peak superstructure acceleration and pile peak bending moments) for a range of peak ground input accelerations, and pile material damping parameter, so the designer can choose peak pile response quantities within the resulting range based on conservativeness of the design.

Acknowledgement

I would like to express my deep appreciation to my research advisors professor Dr. Stephen Butt and Dr. Radu Popescu for their supervision and research support. I also thank School of Graduate Studies, Memorial University of Newfoundland for providing me with graduate fellowship that made my thesis possible. I express my gratitude to Dr. Dan Wilson of University of California, Davis for providing me with necessary centrifuge tests data that made validation of Finite Element modeling possible. I am filled with gratitude to my parents whose prayers have always been a constant source of strength and encouragement in the pursuit of my graduate research.

Table of Content

Abstract	ii
Acknowledgement	iii
Table of Contents	iv
List of Tables	vii
List of Figures	viii
List of Symbols	xvi

Chapter 1 Introduction

1.1 General	1
1.2 Objective.....	1
1.3 Outline of Study.....	2
1.4 Contribution to Seismic Response Analysis of Piles.....	2

Chapter 2 Literature Review

2.1 Introduction.....	3
2.2 Numerical Methods of Soil Structure Interactions.....	8
2.2.1 Three Dimensional Finite Element Approach.....	8
2.2.2 BNWF approach.....	10
2.3 Free Field Analysis.....	15
2.4 Determination of Shear Wave Velocity.....	16

Chapter 3	Discussion on Centrifuge Tests	
3.1	Introduction.....	17
3.2	Layout of Csp2 Model	17
3.3	Layout of Csp3 Model.....	19
3.4	Results of Csp2 and Csp3 Tests.....	21
Chapter 4	Nonlinear Seismic Free Field Response Analysis of Saturated Sand	
4.1	Introduction.....	23
4.2	Cyclic1D Model description.....	25
4.3	Modeling Soil Profile in Cyclic1D.....	25
4.4	Cyclic1D Model Input Parameters.....	25
4.5	Artificial Damping in Cyclic1D Analyses.....	28
4.6	Comparison of Numerical and Experimental Results.....	29
4.7	Conclusion.....	50
4.8	Acknowledgement.....	50
Chapter 5	Evaluation of Seismic Lateral Response of a Pile in Saturated Sand	
5.1	Introduction.....	51
5.2	Pile-Soil Interaction Analysis with BNWF Models.....	52
5.2.1	Pile Modeling.....	55
5.2.2	Soil Stiffness Modeling.....	55
5.2.3	Calibration of Soil Stiffness Model.....	56
5.2.4	Pile Material Damping.....	57
5.2.5	Modeling Radiation Damping of Soil.....	58

	5.3	ABAQUS Methodology in BNWF Model.....	58
	5.4	Free Field Excitation.....	60
	5.5	Comparison of Numerical and Experimental Results.....	61
	5.6	Discussion on the Numerical Results.....	74
	5.7	Acknowledgement.....	75
Chapter 6		Pile Peak Response Curves for Seismic Analysis of Piles in Saturated Sand	
	6.1	Introduction.....	76
	6.2	Analysis of Predicted Pile Head Accelerations.....	76
	6.3	Analysis of Predicted Superstructure Accelerations.....	77
	6.4	Analysis of Predicted Superstructure Displacements.....	77
	6.5	Analysis of Predicted Bending Moments.....	83
	6.6	Discussion on the pattern of PPBM vs. PGA curves.....	88
Chapter 7		Conclusion and Recommendation for future Research	
	7.1	Conclusions.....	94
	7.2	Recommendation for Future Research	97
References		98
Appendix	A	Excess Pore Water Pressure Time Histories.....	101
Appendix	B	Pile Response Time Histories.....	102
Appendix	C	Peak Pile Bending Moment Profiles.....	127

List of Tables

Table	Description	Page
3.1	Ground Input Motion for Csp2 Tests (Wilson et al., 1997a).....	18
3.2	Ground Input Motion for Csp3 Tests (Wilson et al., 1997b).....	21
3.3	Soil Properties (Wilson, 1998).....	22
3.4	Pile Properties (Wilson, 1998).....	22
4.1	Ground Input Motions for Cyclic1D Analysis.....	26
4.2	Input parameters for Cyclic1D Analysis.....	27
5.1	Verification of effect of time step used in ABAQUS analysis.....	60
6.1	Design Pile Material Damping Ratios, ξ input to the current BNWF model.....	85
6.2	Analyses of Spectral Acceleration of Ground Input Motions.....	89

List of Figures

Figure	Description	Page
2.1	Nonlinear p-y Springs at Various Depths (Reese and Van Ampe, 2001).....	4
2.2	Typical p-y and Soil Modulus Reduction Curves (Reese and Van Ampe, 2001).....	6
2.3	Comparison of Shapes of Reese's and Murchison's p-y Curves (After, Murchison et al. 1984).....	7
2.4	Schematic BNWF Model (Boulanger et al., 1999).....	11
2.5	Structured p-y Elements (Boulanger et al., 1999).....	12
2.6	Normalized API Recommended p-y Curves for Soil (Boulanger et al., 1999).....	12
2.7	One Dimensional Radiation damping (Berger et al., 1977).....	14
3.1	Single Pile, SP1 Instrumentation, (from Wilson, 1998).....	18
3.2	Centrifuge Test Layout of Csp2 Model (from Wilson, 1998).....	19
3.3	Centrifuge Test Layout of Csp3 Model (from Wilson, 1998).....	20
4.1	Finite Element Model of Soil Profile Developed in Cyclic1D for Free Field Analysis.....	26
4.2	Horizontal acceleration time histories and corresponding Fast Fourier Transform for Event D of Csp2 Test(soil depths, 1 m to 3 m).....	31
4.3	Horizontal acceleration time histories and corresponding Fast Fourier Transform for Event D of Csp2 Test (soil depths, 5 m to 8 m).....	32
4.4	Horizontal acceleration time histories and corresponding Fast Fourier Transform for Event D of Csp2 Test (soil depths, 11 m to 14 m).....	33
4.5	Horizontal Acceleration Time Histories and corresponding Fast Fourier Transform for Event J, Csp2 (soil depths, 1 m to 3 m).....	34
4.6	Horizontal Acceleration Time Histories and corresponding Fast Fourier Transform for Event J, Csp2 (soil depths, 5 m to 8 m).....	35
4.7	Horizontal Acceleration Time Histories and corresponding Fast Fourier Transform for Event J, Csp2 (soil depths, 11 m to 14 m).....	36
4.8	Horizontal Acceleration Time Histories and corresponding Fast Fourier Transform for Event J, Csp2 (soil depth, 17 m).....	37
4.9	Excess Pore Water Pressure Time Histories for Event J, Csp2 (soil depths, 1 m to 12 m).....	38

4.10	Horizontal Acceleration Time Histories and corresponding Fast Fourier Transform for Event J, Csp3 (soil depths, 2 m to 4 m).....	39
4.11	Horizontal Acceleration Time Histories and corresponding Fast Fourier Transform for Event J, Csp3 (soil depths, 7 m to 13 m).....	40
4.12	Horizontal Acceleration Time Histories and corresponding Fast Fourier Transform for Event J, Csp3 (soil depth, 17 m).....	41
4.13	Excess Pore Water Pressure Time Histories of Event J, Csp3 (soil depths, 1 m to 13 m).....	42
4.14	Horizontal Acceleration Time Histories and corresponding Fast Fourier Transform of Event M, Csp3 (soil depths, 2 m to 4 m).....	43
4.15	Horizontal Acceleration Time Histories and corresponding Fast Fourier Transform of Event M, Csp3 (soil depths, 7 m to 13 m).....	44
4.16	Horizontal Acceleration Time Histories and corresponding Fast Fourier Transform of Event M, Csp3 (soil depths 17 m).....	45
4.17	Excess Pore Water Pressure Time Histories of Event M, Csp3 (soil depths, 1 m to 8 m).....	46
5.1	Schematic diagram of BNWF model for simulation of Csp2 using ABAQUS.....	53
5.2	Schematic diagram of BNWF model for simulation of Csp3 using ABAQUS.....	54
5.3	Schematic p-y curve for calibration of soil springs of BNWF model.....	56
5.4	Comparison of Superstructure Displacement Time History for Event D, Csp2.....	62
5.5	Comparison of Super Structure Acceleration Time History for Event D, Csp2.....	62
5.6	Comparison of Pile Head Acceleration Time History for Event D, Csp2.....	62
5.7	Comparison of Bending Moment Time History for Event D, Csp2 at soil depth 0.5 m.....	63
5.8	Comparison of Bending Moment Time History for Event D, Csp2 at soil depth 1.5 m.....	63
5.9	Comparison of Bending Moment Time History for Event D, Csp2 at soil depth 2.5 m.....	63
5.10	Comparison of Bending Moment Time History for Event D, Csp2 at soil depth 4.0 m.....	64
5.11	Comparison of Bending Moment Time History for Event D, Csp2 at soil depth 5.5 m.....	64
5.12	Comparison of Bending Moment Time History for Event D, Csp2 at soil depth 8.5 m.....	64

5.13	Comparison of Super Structure Displacement Time History for Event J, Csp2.....	65
5.14	Comparison of Super Structure Acceleration Time History for Event J, Csp2.....	65
5.15	Comparison of Pile Head Acceleration Time History for Event J, Csp2.....	65
5.16	Comparison of Bending Moment Time History for Event J, Csp2 at soil depth 0.5 m.....	66
5.17	Comparison of Bending Moment Time History for Event J, Csp2 at soil depth 1.5 m.....	66
5.18	Comparison of Bending Moment Time History for Event J, Csp2 at soil depth 2.5 m.....	66
5.19	Comparison of Bending Moment Time History for Event J, Csp2 at soil depth 4.0 m.....	67
5.20	Comparison of Bending Moment Time History for Event J, Csp2 at soil depth 5.5 m.....	67
5.21	Comparison of Bending Moment Time History for Event J, Csp2 at soil depth 8.5 m.....	67
5.22	Comparison of Super Structure Displacement Time History for Event J, Csp3.....	68
5.23	Comparison of Super Structure Acceleration Time History for Event J, Csp3.....	68
5.24	Comparison of Pile Head Acceleration Time History for Event J, Csp3.....	68
5.25	Comparison of Bending Moment Time History for Event J, Csp3 at soil depth 0.5 m.....	69
5.26	Comparison of Bending Moment Time History for Event J, Csp3 at soil depth 1.5 m.....	69
5.27	Comparison of Bending Moment Time History for Event J, Csp3 at soil depth 2.5 m.....	69
5.28	Comparison of Bending Moment Time History for Event J, Csp3 at soil depth 4.0 m.....	70
5.29	Comparison of Bending Moment Time History for Event J, Csp3 at soil depth 5.5 m.....	70
5.30	Comparison of Bending Moment Time History for Event J, Csp3 at soil depth 8.5 m.....	70
5.31	Comparison of Super Structure Displacement Time History for Event M, Csp3.....	71
5.32	Comparison of Super Structure Acceleration Time History for Event M, Csp3.....	71
5.33	Comparison of Pile Head Acceleration Time History for Event M, Csp3.....	71
5.34	Comparison of Bending Moment Time History for Event M, Csp3 at soil depth 0.5 m.....	72
5.35	Comparison of Bending Moment Time History for Event M, Csp3 at soil depth 1.5 m.....	72

5.36	Comparison of Bending Moment Time History for Event M, Csp3 at soil depth 2.5 m.....	72
5.37	Comparison of Bending Moment Time History for Event M, Csp3 at soil depth 4.0 m.....	73
5.38	Comparison of Bending Moment Time History for Event M, Csp3 at soil depth 5.5 m.....	73
5.39	Comparison of Bending Moment Time History for Event M, Csp3 at soil depth 8.5 m.....	73
6.1	Calculated and Recorded Peak Pile Head Accelerations for Csp2 tests.....	78
6.2	Calculated and Recorded Peak Pile Head Accelerations for Csp3 tests.....	79
6.3	Calculated and Recorded Peak Superstructure Accelerations for Csp2 tests.....	80
6.4	Calculated and Recorded Peak Superstructure Accelerations for Csp3 tests.....	81
6.5	Calculated and Recorded Peak Superstructure Displacements for Csp2 tests.....	82
6.6	Calculated and Recorded Peak Superstructure Displacements for Csp3 tests.....	83
6.7	Maximum Pile Peak Bending Moment vs. Peak Ground Input Acceleration Curves for Csp2 tests.....	87
6.8	Maximum Pile Peak Bending Moment vs. Peak Ground Input Acceleration Curves for Csp3 tests.....	88
6.9	Spectral acceleration vs. Period curves for the Ground Input Motions of Csp2 tests (after, Wilson et al. 1997a).....	90
6.10	Spectral acceleration vs. Period curves for the Ground Input Motions of Csp3 tests (after, Wilson et al. 1997b).....	91
A-1	Excess Pore Water Pressure Time Histories of Event J, Csp2 (soil depths, 20 m).....	101
A-2	Excess Pore Pressure Time Histories of Event J, Csp3 (soil depths, 20 m).....	101
A-3	Excess Pore Pressure Time Histories of Event M, Csp3 (soil depth 20 m).....	101
B-1	Parameters C_1 , C_2 and C_3 (API, 2000).....	102
B-2	Initial modulus of subgrade reaction for sands (API, 2000).....	102
B-3	Typical p-y curves for loose sand layer ($D_r = 35\%$) in Csp2 centrifuge model using API, 2000.....	103
B-4	Typical p-y curves for loose sand layer ($D_r = 55\%$) in Csp3 centrifuge model using API, 2000.....	103
B-5	Shear Wave Velocity Profile for the soil in Csp2 centrifuge model.....	104
B-6	Shear Wave Velocity Profile for the soil in Csp3 centrifuge model.....	104
B-7	Verification of effect of time step 0.005 s on predicted response the pile.....	105

B-8	Verification of effect of time step 0.01 s on predicted response the pile.....	105
B-9	Verification of effect of time step 0.02 s on predicted response the pile.....	105
B-10	Comparison of Super Structure Displacement Time History for Event F, Csp2.....	106
B-11	Comparison of Super Structure Acceleration Time History for Event F, Csp2.....	106
B-12	Comparison of Pile Head Acceleration Time History for Event F, Csp2.....	106
B-13	Comparison of Bending Moment Time History for Event F, Csp2 at soil depth 0.5 m.....	107
B-14	Comparison of Bending Moment Time History for Event F, Csp2 at soil depth 1.5 m.....	107
B-15	Comparison of Bending Moment Time History for Event F, Csp2 at soil depth 2.5 m.....	107
B-16	Comparison of Bending Moment Time History for Event F, Csp2 at soil depth 4.0 m.....	108
B-17	Comparison of Bending Moment Time History for Event F, Csp2 at soil depth 5.5 m.....	108
B-18	Comparison of Bending Moment Time History for Event F, Csp2 at soil depth 8.5 m.....	108
B-19	Comparison of Super Structure Displacement Time History for Event E, Csp2.....	109
B-20	Comparison of Super Structure Acceleration Time History for Event E, Csp2.....	109
B-21	Comparison of Pile Head Acceleration Time History for Event E, Csp2.....	109
B-22	Comparison of Bending Moment Time History for Event E, Csp2 at soil depth 0.5 m.....	110
B-23	Comparison of Bending Moment Time History for Event E, Csp2 at soil depth 1.5 m.....	110
B-24	Comparison of Bending Moment Time History for Event E, Csp2 at soil depth 2.5 m.....	110
B-25	Comparison of Bending Moment Time History for Event E, Csp2 at soil depth 4.0 m.....	111
B-26	Comparison of Bending Moment Time History for Event E, Csp2 at soil depth 5.5 m.....	111
B-27	Comparison of Bending Moment Time History for Event E, Csp2 at soil depth 8.5 m.....	111
B-28	Comparison of Super Structure Displacement Time History for Event L, Csp2.....	112
B-29	Comparison of Super Structure Acceleration Time History for Event L, Csp2.....	112
B-30	Comparison of Pile Head Acceleration Time History for Event L, Csp2.....	112

B-31	Comparison of Bending Moment Time History for Event L, Csp2 at soil depth 0.5 m.....	113
B-32	Comparison of Bending Moment Time History for Event D, Csp2 at soil depth 1.5 m.....	113
B-33	Comparison of Bending Moment Time History for Event D, Csp2 at soil depth 2.5 m.....	113
B-34	Comparison of Bending Moment Time History for Event D, Csp2 at soil depth 4.0 m.....	114
B-35	Comparison of Bending Moment Time History for Event D, Csp2 at soil depth 5.5 m.....	114
B-36	Comparison of Bending Moment Time History for Event D, Csp2 at soil depth 8.5 m.....	114
B-37	Comparison of Super Structure Displacement Time History for Event G, Csp3.....	115
B-38	Comparison of Super Structure Acceleration Time History for Event G, Csp3.....	115
B-39	Comparison of Pile Head Acceleration Time History for Event G, Csp3.....	115
B-40	Comparison of Bending Moment Time History for Event G, Csp3 at soil depth 0.5 m.....	116
B-41	Comparison of Bending Moment Time History for Event G, Csp3 at soil depth 1.5 m.....	116
B-42	Comparison of Bending Moment Time History for Event G, Csp3 at soil depth 2.5 m.....	116
B-43	Comparison of Bending Moment Time History for Event G, Csp3 at soil depth 4.0 m.....	117
B-44	Comparison of Bending Moment Time History for Event G, Csp3 at soil depth 5.5 m.	117
B-45	Comparison of Bending Moment Time History for Event G, Csp3 at soil depth 8.5 m.....	117
B-46	Comparison of Super Structure Displacement Time History for Event D, Csp3.....	118
B-47	Comparison of Super Structure Acceleration Time History for Event D, Csp2.....	118
B-48	Comparison of Pile Head Acceleration Time History for Event D, Csp2.....	118
B-49	Comparison of Bending Moment Time History for Event D, Csp3 at soil depth 0.5 m.....	119
B-50	Comparison of Bending Moment Time History for Event D, Csp3 at soil depth 1.5 m.....	119
B-51	Comparison of Bending Moment Time History for Event D, Csp3 at soil depth 2.5 m.....	119
B-52	Comparison of Bending Moment Time History for Event D, Csp3 at soil depth 4.0 m.....	120
B-53	Comparison of Bending Moment Time History for Event D, Csp3 at soil depth 5.5 m.....	120

B-54	Comparison of Bending Moment Time History for Event D, Csp3 at soil depth 8.5 m.....	120
B-55	Comparison of Super Structure Displacement Time History for Event I, Csp3.....	121
B-56	Comparison of Super Structure Acceleration Time History for Event I, Csp3.....	121
B-57	Comparison of Pile Head Acceleration Time History for Event I, Csp3.....	121
B-58	Comparison of Bending Moment Time History for Event I, Csp3 at soil depth 0.5 m.....	122
B-59	Comparison of Bending Moment Time History for Event I, Csp3 at soil depth 1.5 m.....	122
B-60	Comparison of Bending Moment Time History for Event I, Csp3 at soil depth 2.5 m.....	122
B-61	Comparison of Bending Moment Time History for Event I, Csp3 at soil depth 4.0 m.....	123
B-62	Comparison of Bending Moment Time History for Event I, Csp3 at soil depth 5.5 m.....	123
B-63	Comparison of Bending Moment Time History for Event I, Csp3 at soil depth 8.5 m.....	123
B-64	Comparison of Super Structure Displacement Time History for Event O, Csp3.....	124
B-65	Comparison of Super Structure Acceleration Time History for Event O, Csp3.....	124
B-66	Comparison of Pile Head Acceleration Time History for Event O, Csp3.....	124
B-67	Comparison of Bending Moment Time History for Event O, Csp3 at soil depth 0.5 m.....	125
B-68	Comparison of Bending Moment Time History for Event O, Csp3 at soil depth 1.5 m.....	125
B-69	Comparison of Bending Moment Time History for Event O, Csp3 at soil depth 2.5 m.....	125
B-70	Comparison of Bending Moment Time History for Event O, Csp3 at soil depth 4.0 m.....	126
B-71	Comparison of Bending Moment Time History for Event O, Csp3 at soil depth 5.5 m.....	126
B-72	Comparison of Bending Moment Time History for Event O, Csp3 at soil depth 8.5 m.....	126
C-1	Pile Peak Bending Moment (PPBM) in Event D of Csp2 test.....	127
C-2	Pile Peak Bending Moment (PPBM) in Event F of Csp2 test.....	127
C-3	Pile Peak Bending Moment (PPBM) in Event J of Csp2 test.....	128
C-4	Pile Peak Bending Moment (PPBM) in Event E of Csp2 test.....	128
C-5	Pile Peak Bending Moment (PPBM) in Event L of Csp2 test.....	129
C-6	Pile Peak Bending Moment (PPBM) in Event G of Csp3 test.....	129
C-7	Pile Peak Bending Moment (PPBM) in Event D of Csp3 test.....	130
C-8	Pile Peak Bending Moment (PPBM) in Event J of Csp3 test.....	130

C-9	Pile Peak Bending Moment (PPBM) in Event M of Csp3 test.....	131
C-10	Pile Peak Bending Moment (PPBM) in Event I of Csp3 test.....	131
C-11	Pile Peak Bending Moment (PPBM) in Event O of Csp3 test.....	132

List of Symbols

Symbol	Description
<i>A</i>	Empirical Adjustment Factor
<i>A_{area}</i>	Cross Sectional Area of the Elastic Medium
<i>B</i>	Pile Diameter
<i>BNWF</i>	Beam on Nonlinear Winkler Foundation
<i>c</i>	Radiation Damping Coefficient
<i>C</i>	Material Damping Matrix of the Pile Foundation System
<i>CF</i>	Coincidence Factor
<i>C_u</i>	Soil Uniformity Coefficient
<i>C₁, C₂ and C₃</i>	Empirical Coefficients Determined from Figure B-1
<i>D₅₀</i>	Diameter of soil Particles corresponding to 50 % finer
<i>D_r</i>	Relative Density
<i>e₀</i>	Initial Void Ratio of Soil
<i>EPWP</i>	Excess Pore Water Pressure
<i>FEM</i>	Finite Element Methods
<i>G_{max}</i>	Dynamic Soil Shear Modulus
<i>K</i>	Stiffness Matrix of the Pile Foundation System
<i>k</i>	Initial Modulus of Subgrade Reaction
<i>M</i>	Mass Matrix of the Pile Foundation System
<i>OCR</i>	Over Consolidation Ratio
<i>p</i>	Soil Reaction
<i>P_u</i>	Ultimate Soil Resistance
<i>PGA</i>	Peak Ground Input Acceleration
<i>PPBM</i>	Pile Peak Bending Moment
<i>SPSI</i>	Soil Pile Structure Interaction
<i>SSI</i>	Soil Structure Interaction
<i>V</i>	Velocity of Wave propagation in Elastic Medium
<i>V_p</i>	P-wave Velocity
<i>V_s</i>	Shear Wave Velocity in Soil
<i>y</i>	Pile Lateral Displacement
<i>z</i>	Depth below Ground Surface
<i>α</i>	Rayleigh Mass proportional Damping Coefficient
<i>β</i>	Rayleigh Stiffness proportional Damping coefficient
<i>f</i>	Natural frequency of vibration in Hz
<i>η</i>	Pile Shape Adjustment Factor
<i>λ_{elem}</i>	Hysteretic Damping Ratio
<i>ω</i>	Natural Frequency of Each Mode of Pile Vibration in rad/s
<i>σ_m'</i>	Mean Effective Confining Stress in Soil
<i>ρ_s</i>	Mass Density of Elastic Medium
<i>ρ</i>	Bulk Density of soil
<i>ξ</i>	Pile Material Damping Ratio
<i>Δu / σ_{v0}'</i>	Excess Pore Water Pressure Ratio

Chapter 1

Introduction

1.1 General

The design of a particular type of pile foundation is often a tedious process, because a geotechnical engineer must consider tolerable settlement of the pile foundation under various types of loading from superstructure, subsoil conditions, economy and the requirements of the local building code. The pile foundations are also subjected to seismic ground motion in addition to superstructure loading and the pile experiences lateral displacement. The judgment of the geotechnical engineer is necessary in assessing the lateral response of the pile under seismic loading conditions. This includes the variation of soil properties with depth, nonlinear soil behavior, nonlinear behavior of pile-soil interfaces, and energy dissipation through radiation and material damping. The analysis of response for soil-pile-structure systems is called soil-structure interaction (SSI) analysis. SSI analysis is crucial when heavy and important structures are supported by the foundation system. Seismic motions make the SSI analyses complicated. Although the history of pile foundations is as old as shallow foundations, the interaction of the soil-pile-structure during earthquakes has sparked great research interest in the last decade (Boulangier et al., 1999, Kimiaei et al., 2004, Liyanapathirana and Poulos, 2005, El Naggar et al., 2005).

1.2 Objective

The main objective of this study is to present a simplified practical Beam on Nonlinear Winkler Foundation (BNWF) model using the general finite element code ABAQUS (version 6.7) that can be readily used for capturing the soil-pile-interaction effects observed in saturated sand during dynamic centrifuge experiments. The model will take into account nonlinear behaviour of soil-pile interface, energy dissipation through radiation and pile material damping. The current study gives special attention to the evaluation of free field excitation where saturated sand is concerned.

1.3 Outline of Study

Chapter 2 presents a brief review of previous studies focusing on soil structure interaction and discusses advancements made in the field. Very recently used approaches to the analysis of dynamic pile response were studied. Attention was given to various approaches for modeling soil stiffness, soil damping, and predicting free field accelerations. Chapter 3 describes a brief presentation of centrifuge tests performed by Wilson et al. (1997 a, b). This chapter summarizes centrifuge testing since the following chapters use results of the centrifuge tests for comparing dynamic response of the BNWF model. Chapter 4 discusses prediction of free field motions that are used as boundary conditions at the free ends of spring dashpot pair. Free field motions are predicted by using a well known Finite Element multi-yield surface plasticity model called Cyclic1D computer program (Elgamal et al., 2006). Chapter 5 describes the calibration of API based p-y curves and investigates the validity of the Finite Element BNWF model against the centrifuge tests. A commercial Finite Element code ABAQUS, 6.7 was used to directly model pile and soil behaviour under seismic loading. Chapter 6 uses results from the BNWF model to prepare pile peak response quantities (peak pile head accelerations, peak superstructure accelerations, peak superstructure displacements and peak pile bending moments) versus peak ground input acceleration curves so design engineers can estimate those quantities within the range of peak ground input acceleration and soil profile discussed in this study. Chapter 7 summarizes the findings of the thesis and make recommendations for future research.

1.4 Contribution to Seismic Response Analysis of Piles

- Implementing a dynamic BNWF model for piles in sand in the Finite Element Program ABAQUS.
- Accounting for soil liquefaction effects on free field ground motion.
- Providing practical design recommendations in the form of peak response (maximum moments in piles and peak displacements and accelerations of superstructure) for piles in saturated sand.

Chapter 2

Literature Review

2.1 Introduction

Soil Structure Interaction analyses are performed mainly by Finite Element Method (FEM) and BNWF method. FEM can treat the soil as a medium along a continuum of an assemblage of discrete elements. The boundaries of the elements are defined by nodal points with an assumption that the response of the continuum can be described by the response of the nodal points. The stress applied at any nodal point on the mesh is directly related to surrounding nodal stresses developed through the behavior of adjoining elements. The main advantage of such an approach is its capability to perform a fully coupled SSI analysis of piles without resorting to independent calculations of the site or superstructure response. However, continuum FEM is not commonly used in design offices mainly because of their excessive computational time and their complexity for common pile dynamic response analysis.

The BNWF method is a simplified approach that can account for nonlinear SSI and is commonly used in professional engineering practices. The basic assumption for this method is that the displacement at any point of the soil medium is directly proportional to the stress represented by p , applied at that depth and independent of any other stresses applied at other points along the soil pile interface. In this method, the nonlinear force-displacement relationship for soil-pile interaction is expressed as $p = E_{py}y$ where E_{py} is the reaction modulus of pile under lateral load and y is lateral pile displacement. The stresses developed between the pile and the soil act normal to the face of the pile. The stiffness can be determined using p - y curves. In the BNWF method, the pile is modeled as a series of beam-column elements resting on a series of springs and dashpots representing the nonlinear dynamic characteristic of the soil. Ground motion time histories are usually computed in a separate site response analysis. The computed ground motion at different levels within the soil is then applied to the spring supports as boundary conditions in BNWF models. A singular disadvantage of the BNWF model is

the two-dimensional simplification of the soil–pile contact, because it ignores the radial and three-dimensional components of interaction. The shear stress acting along the sides of pile is ignored. The theory assumes that response of each soil layer to the pile loading is independent of the response of adjacent soil layer, and therefore, the shear transfer between soil layers is ignored. Thus springs elements can be used to represent the soil-pile stiffness in each layer. The dynamic Winkler model can be employed into two types of analyses, one is the frequency domain method and the other is the time domain approach. Although the frequency domain method is computationally efficient, nonlinear soil pile behavior during seismic excitation can only be accounted for by using step by step time domain method.

The nonlinear force displacement concept of p-y curves is illustrated in Figure 2.1 showing a longitudinal section through a deep foundation.

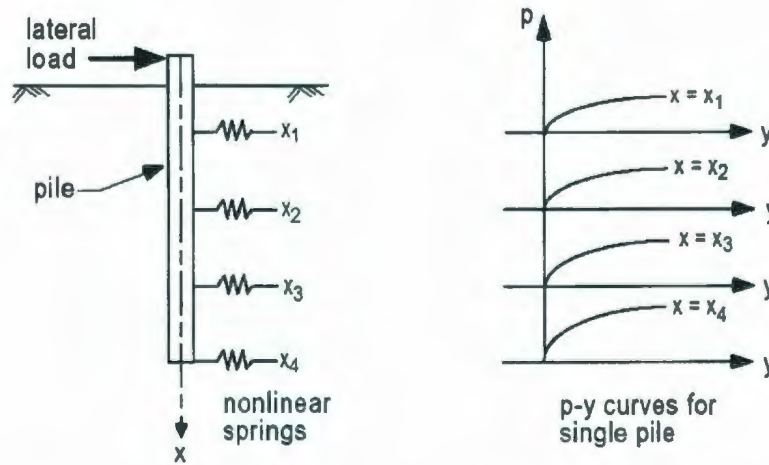


Figure 2.1: Nonlinear p-y springs at various depths (Reese and Van Ampe, 2001).

For the solution of a laterally loaded pile subjected to any static load, it is necessary to predict a set of p-y curves such as those shown in Figure 2.1 for obtaining deflection, pile rotation, bending moment, and shear force.

The discrete p-y springs have lateral soil stiffness E_{py} with the unit of force per length squared $\left(\frac{F}{L^2}\right)$ where the first L refers to the unit length of the pile and the second L refers to the lateral displacement (Reese and Van Ampe, 2001). E_{py} is calculated as follows:

$$E_{py} = \frac{P}{y}$$

in which p is the unit soil reaction and y is the lateral deflection of the pile. The coefficient of horizontal subgrade reaction k (F/L^3) is related to E_{py} as shown below:

$$k = \frac{E_{py}}{B} \text{ where } B \text{ is the pile diameter.}$$

Nonlinear p-y curves are obtained from field experiments with full sized piles (Reese and Van Ampe, 2001). The procedure for obtaining experimental p-y curves involves field testing of a pile foundation instrumented with strain gauges so that the bending moment can be measured along the length of the pile foundation. From sets of experimental bending moment curves, values of p and y at any point, z along the pile can be obtained by solving Equation 2.1.

$$p = \frac{d^2 M}{dz^2} \tag{2.1}$$

Double integration over the entire curvature M/EI with respect to depth, z is performed to obtain lateral displacement y.

$$y = \int \left(\int \frac{M}{EI} dz \right) dz \tag{2.2}$$

An example of typical p-y curve using the Winkler approach is shown in Figure 2.2.

The main assumptions in this approach include:

- the pile material is isotropic homogeneous
- Elastic modulus of the pile, E_p is the same in both tension and compression
- the pile is vertical and the cross section is uniform.
- under bending moment, plane sections remain plane.

The portion of the curve from points a to b in Figure 2.2a show that the value of p is increasing at a decreasing rate with increasing deflection y . Figure 2.2b shows the variation of E_{py} with a steady increase in y . This behavior undoubtedly is reflecting the nonlinear behavior of the in situ stress-strain curve. The part of the curve starting from point a to b is empirical and based on the results of full scale tests of pile in a variety of soils with both monotonic and cyclic loading (Reese and Van Ampe, 2001).

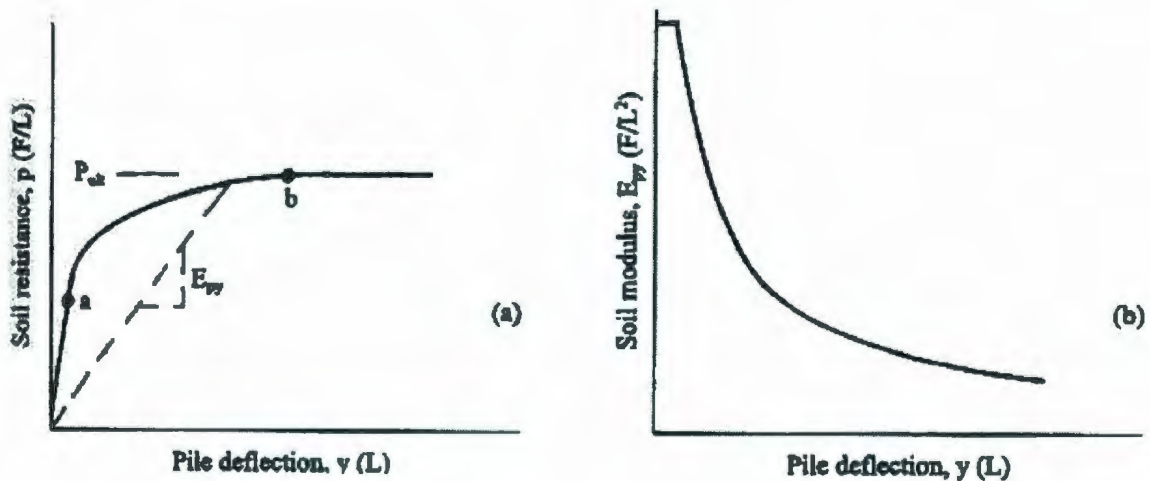


Figure 2.2: Typical p-y and soil modulus reduction curves (Reese and Van Ampe, 2001).

A number of p-y curves were developed for sands (Murchinson et al., 1984 and Reese et al., 1974). Reese et al. (1974) developed p-y curves from the results of full scale lateral load tests on two 21m long, 0.610 m diameter piles. The piles were driven into saturated sand at Mustang Island. The soil at the site was uniformly graded, fine sand with a friction angle of 39° . The effective unit weight of the soil was 10.4 kN/m^3 and average relative density of the sand at the site was 90%. The Reese p-y curve (Reese et al., 1974) consists of three segments having two straight lines connecting by a parabola as shown in Figure 2.3. The initial straight portion of the curve connects the origin of axes and the point m. The parabolic part is joined by the points m and n. The parabolic part is followed by another straight portion starting from the point n to t. The initial portion of the curve represents elastic behavior of sand under small (about 1% of pile diameter) lateral displacement of pile. The later section of the curve starting from the point m to point t is

constructed to account for large lateral displacement of pile when the pile is under cyclic loading situation. For the results at Mustang Island, Reese et al. (1974) found that the values of y at n and t are $B/60$ and $3B/80$ respectively. Here B is pile diameter. Therefore, the Reese p - y curves (Reese et al., 1974) are not continuous and the diameter dependence of the p - y curve at large scale deformation is empirical. Based on full scale static and cyclic loading of piles in similar soil, Murchison et al. (1984) described a continuous hyperbolic tangent function to describe the p - y curves as shown in Figure 2.3.

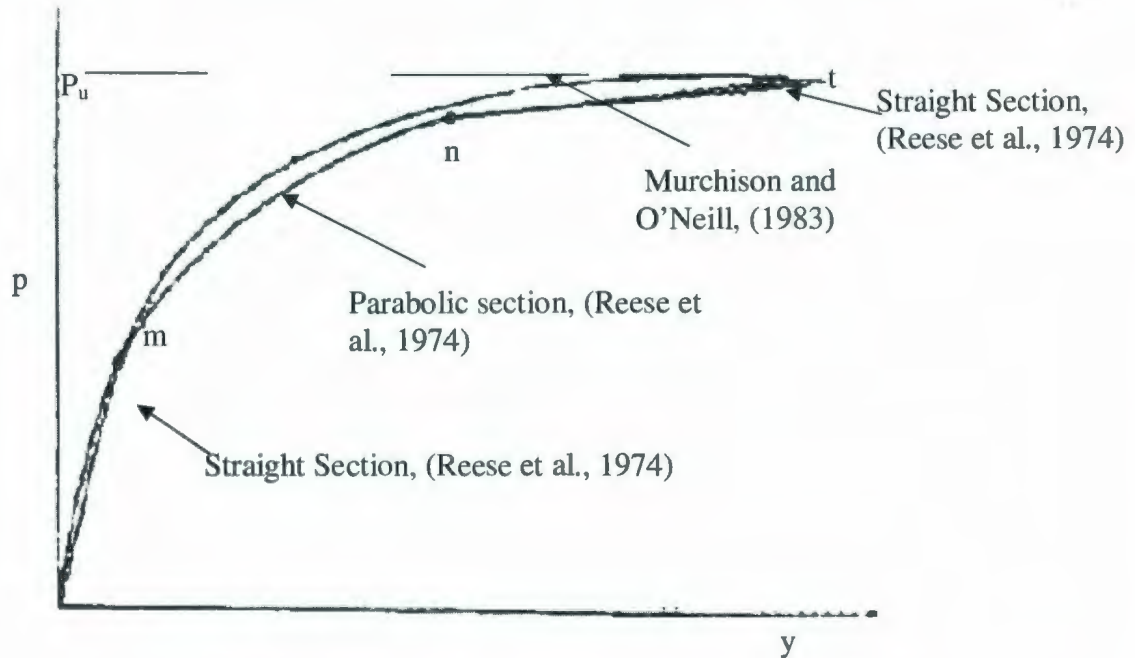


Figure 2.3: Comparison of shapes of Reese's and Murchison's p - y curves (After, Murchison et al. (1984)).

The hyperbolic tangent function is shown below:

$$p = \eta A P_u \tanh \left[\left(\frac{kz}{\eta A P_u} \right) y \right] \quad (2.3)$$

where A is the empirical adjustment factor for loading type namely cyclic and static while η is a factor used to describe the pile shape.

Equation 2.3 incorporates depth (z) of soil in the formulation of p - y curves as lateral soil reaction is the function of soil depth and pile deflection. The single analytical p - y curves

derived by Equation 2.3 are smooth and differentiable at any point along the curve as compared to the 3 segmented p-y curves proposed by Reese et al. (1974). The nonlinear p-y curves for flexible pile recommended by API (2000) are based on Murchison et al.'s (1984) method. The horizontal, straight-line portion of the p-y curve in Figure 2.2a means that the in situ soil is behaving plastically with no loss of strength with increasing displacement. Therefore, according to API (2000) ultimate soil resistance, P_u is calculated using an analytical formula relating soil and pile properties. Chapter 5 discusses the details of the API recommendations on generating p-y curves.

2.2 Numerical Methods of Soil Structure Interactions

It is known that p – y curves can be employed in comprehensive numerical soil–structure interaction analysis methods such as Finite Element Method (FEM) to model the soil–pile response of a structural problem involving the superstructure along with the substructure. The methods used to analyze the response of single piles are mainly categorized into two approaches, (1) three dimensional (3D) Finite Element Methods and (2) two dimensional (2D) Beam on Nonlinear Winkler Foundation approach. In 3D Finite Element methods, soil-pile-superstructure interaction is modeled in a coupled manner in which seismic response of pile and soil are computed in one step. But in BNWF approach, response of soil and pile due to seismic loading are computed in a decoupled way. In this method seismic response of soil layers are performed by free field analysis methods and then computed soil response is applied to the finite element BNWF model for predicting dynamic behavior of the pile. The following section provides brief description of advancements made in dynamic soil pile analyses.

2.2.1 Three Dimensional Finite Element Approach

El Naggar and Bentley (2000) developed a 3D Finite Element program in ANSYS to model dynamic behavior of piles surrounded by homogeneous clay. The dynamic loading was applied to the rigid base of the 3D model as a one dimensional horizontal acceleration and only the horizontal response was measured. It is important to note that the acceleration data were for bedrock motions and not free field motions. Bed rock motion can either increase or decrease in terms of peak horizontal acceleration due to

local site effects. Vertical accelerations were ignored because the margins of safety against static vertical forces usually provide adequate resistance to dynamic forces induced by vertical accelerations. Clay soil was assumed to have 16.5° angle of internal friction. They compared acceleration time histories and Fourier spectra of the pile head with that of the free field. Acceleration time histories of floating and socketed pile head were almost identical. The Fourier amplitude of socketed pile showed both a decrease and increase depending on the level of frequency.

Wu and Fin (1997) developed a 3D Finite Element model in the time domain to predict seismic response of pile foundations. They considered nonlinearity of soil (sand) by focusing on modeling shear strain dependence of soil moduli and damping ratios. Eight noded brick elements were used to represent soil and two noded beam elements were used to simulate the pile. An equivalent linear model was employed to model the nonlinear hysteretic behavior of soil. The damping matrix for a soil element in this analysis was given by:

$$[C]_{elem} = \lambda \left(\omega_1 [M]_{elem} + \frac{[K]_{elem}}{\omega_1} \right) \quad (2.4)$$

in which ω_1 is the fundamental frequency of the soil pile system and is applied to each element. The fundamental frequency was obtained from eigen value analysis. The hysteretic damping ratio, λ_{elem} was prescribed as a function of element shear strain. The 3D Finite Element analysis was carried out in the time domain to account for the changes in shear modulus and damping ratios due to dynamic shear strains. The low strain shear modulus G_{max} is determined using the equation given by Hardin et al. (1972) which gives G_{max} as a function of void ratio and effective mean normal stress. The soil model in this model incorporates soil yielding and potential gapping. They explained soil yielding as the continuing phenomena of deformation at a constant stress representative of the shear strength of soil. This phenomena was accomplished by ensuring normal stress in a soil element in the direction of shaking without exceeding the assigned tensile strength which is normally zero for sand. The Finite Element mesh of the soil had 456 elements. The soil deposit was 12 m thick and divided into 11 layers of Finite Element mesh. The pile was

modeled using 15 beam elements including 5 elements above the soil surface. During comparison, predicted bending moment time history of the pile agreed with the centrifuge test results. The average CPU time using a PC-486 (33 MHz) needed 3 hr to carry out the time domain analysis of the pile foundation for an input seismic record of 1550 steps.

2.2.2 BNWF approach

El Naggar et al. (2005) developed an inexpensive and practical numerical model for estimating the lateral response of flexible piles embedded in clay soil overlying sand deposits subjected to seismic loading. In the proposed model, the BNWF approach is consisted of simple nonlinear springs, dashpots and contact elements. The steel pile structure was modeled by using 12 pipe elements (11 elements below the soil surface and 1 element above the soil surface) of ANSYS elements library. The soil stiffness was modeled by nonlinear spring elements. The spring stiffness was established by using p-y curves based on API (2000). The damping component of soil resistance was modeled by dashpot elements from ANSYS library. The paper considered two kinds of damping mechanisms for soil, soil hysteretic and radiation damping. Soil hysteretic damping was taken care of by performing free field analysis. Radiation damping was addresses by using viscous dashpot elements. Dashpot coefficients were established by Berger at al. (1977).

Free field analysis was performed by using a nonlinear earthquake site response analysis program NERA (Nonlinear Earthquake Response Analysis). NERA does not consider pore pressure generation in clay or sand layers (Bardet and Tobita, 2001). The results of such free-field analysis (acceleration-time histories at different soil layers) were then assigned as input excitation at the support nodes of the BNWF model. The authors did not take into consideration cyclic degradation of soil stiffness due to seismic loading to keep the soil modeling as simple as possible. Despite these limitations, the authors were able to achieve good agreement between numerical and centrifuge test results by having variation in pile material damping ratio, ξ . In the proposed BNWF model, linear dashpots were used in parallel with nonlinear p-y based springs. Pile nodes below ground surface were connected to nonlinear p-y based spring elements in parallel with linear

dashpot elements on each side of the pile. The contact and discontinuity conditions and the development of gapping at the pile-clay interface were established by using interface elements from ANSYS. The authors reported that if a pile is embedded in sand, no gapping will form in the vicinity of the soil and pile, so this interface element is not necessary for modeling pile movement in sand.

Boulangier et al. (1999) evaluated a dynamic BNWF method (Figure 2.4) for analyzing seismic soil-pile-superstructure interaction (SPSI) against the results of a series of dynamic centrifuge model tests.

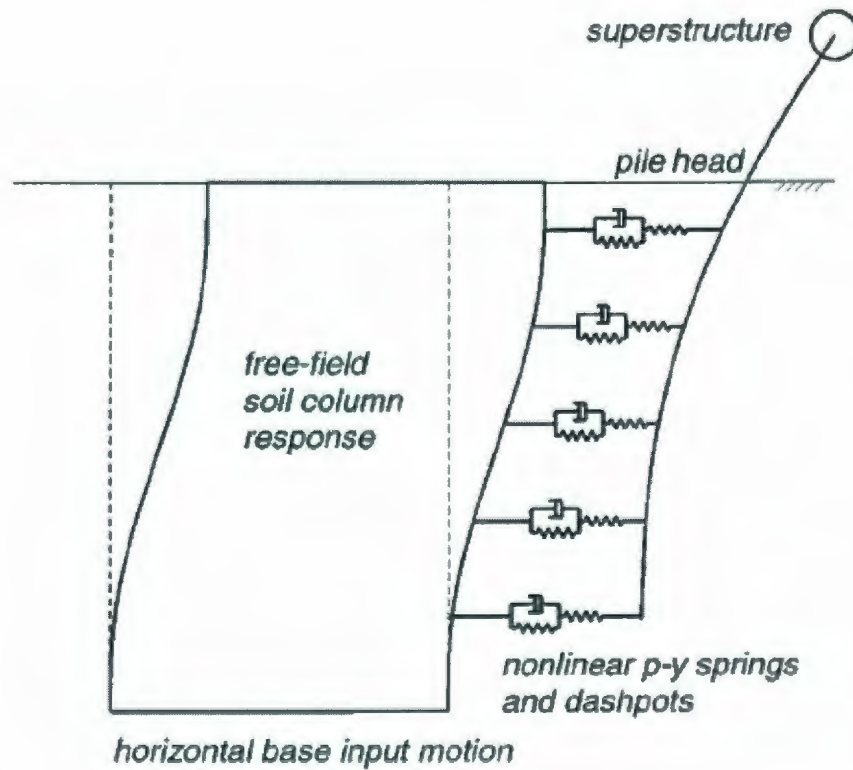


Figure 2.4: Schematic BNWF model (Boulangier et al., 1999).

The analyses were performed in the time domain. The pile was modeled using linear elastic beam elements and supported superstructure mass. The soil profile consisted of soft clay overlying dense sand. The free field site response was calculated by SHAKE 91

(Idriss and Sun, 1991). The displacement profile obtained from the free field analysis was inputted to the support nodes of p-y elements. The equations used to describe dynamic p-y behavior were structured consisting of elastic, plastic and gap component in series. The gap component consisted of a nonlinear closure spring in parallel with a nonlinear drag spring as shown in Figure 2.5.

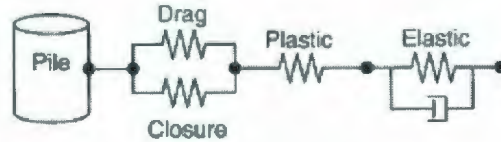


Figure 2.5: Structured p-y elements (Boulanger et al., 1999).

The inclusion of the gap component permits simulation of inverted s-shaped p-y curves (Boulanger et al., 1999) that may represent the influence of a physical gap and the undrained hysteretic behavior of the clay soil. This closure spring allows for a smooth transition in the load-displacement behavior as the gap opens or closes. The backbone of the p-y curves for the sand layer was based on API recommendations (Figure 2.6).

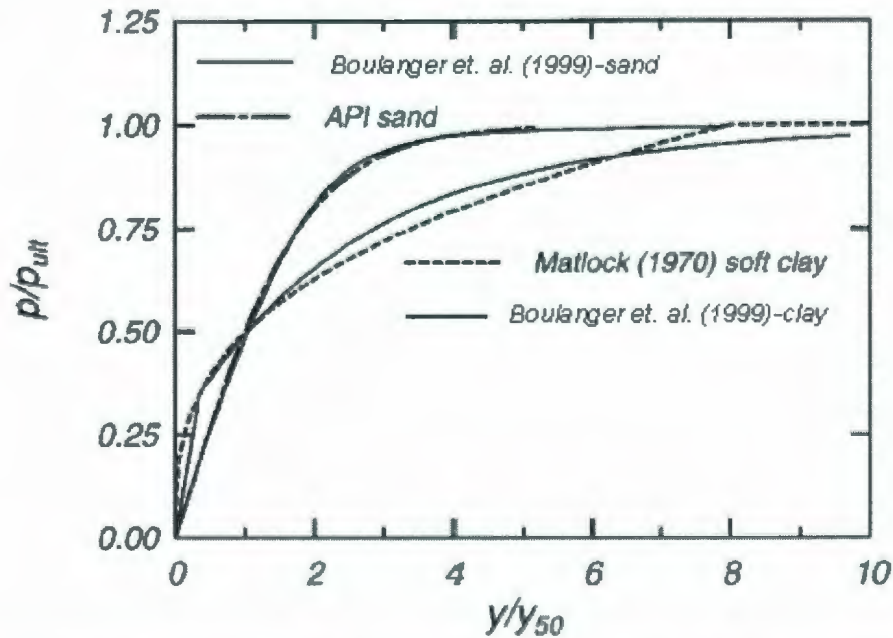


Figure 2.6: Normalized API recommended p-y curves for soil (Boulanger et al., 1999).

The calibration of these gap closure and drag elements require a number of parameters and these parameters were derived from curve fitting experimental p-y behaviors observed in centrifuge tests. Radiation damping component was modeled by a dashpot in parallel with the elastic component of p-y springs. The authors made comparison between calculated and recorded peak bending moment profile of the model pile. Calculated peak superstructure motions were underestimated. It was found that the depth to maximum bending moment increases with increasing magnitude of base input acceleration to the system. They compared recorded and calculated peak superstructure accelerations and displacements versus maximum base input accelerations. Calculated peak superstructure accelerations and displacements were underestimated by about 15-20 %. In order to find the root cause of this anomaly, they recalculated peak super structure displacements vs. maximum base input acceleration by applying recorded motion to the support nodes of p-y element instead of using input acceleration deduced from free field site analysis. The use of recorded input motions to the support nodes reduced the differences between calculated and recorded superstructure response. Therefore, the authors acknowledge the short comings in the site response analysis method of SHAKE 91.

Liyanapathirana and Poulos (2005) developed a Finite Element Winkler model for the analysis of piles founded in saturated dense sand underlying medium dense sand. An effective stress based free field ground response analysis was carried out to determine the external soil movement and degradation of soil stiffness and strength due to pore pressure generation. A seismic analysis of the pile was performed by applying computed ground displacements dynamically to the pile. The effect of radiation damping was taken into account by adding linear viscous dashpots in parallel with springs. Time integration of the equation of motion of pile-soil system was integrated by the average acceleration method. The paper mentioned that in the design of pile foundations subjected to earthquake loading, the maximum bending moment developed in the pile is the most important design parameter. The paper made the comparison between calculated and experimental bending moment and superstructure acceleration time histories. The time histories were in good agreement with experimental ones.

Berger et al. (1977) presented a simplified analytical procedure for evaluating SPSI effects for pile supported offshore structures. The soil profile used in this study was a clay deposit. The foundation was modeled as beam on elastic foundation to which a series of springs and dashpots were attached. Springs were in parallel with linear viscous dashpots. Free field motions were directly assigned to the free ends of spring and dashpot elements at each layer in the soil. These springs and dashpots were used to represent the stiffness and three dimensional wave propagation effects respectively during seismic excitation. The authors mentioned that a horizontally moving square pile cross section generates solely one dimensional compression (P-waves) waves traveling in the direction of shaking and one dimensional shear waves traveling in the direction perpendicular to the direction of shaking (Figure 2.7).

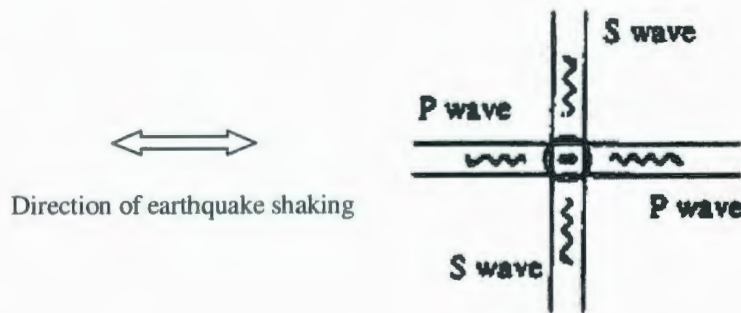


Figure 2.7: One Dimensional Radiation damping (Berger et al. 1977)

When the pile is subjected to seismic induced incremental displacement, it deforms soil around the pile and generates waves which will radiate away from the pile into the soil. This radiation of energy was modeled by using the concept of an elastic half space loaded with uniformly distributed normal force. The authors mentioned that a frequency independent viscous dashpot with a coefficient $c = \rho VA$ fully absorbs the energy of wave traveling with a velocity V in one dimension along an elastic medium with cross section A and mass density ρ_s of the elastic medium. The radiation damping coefficient for dashpot elements is calculated as shown below:

$$c = 2B\rho_s V_p + 2B\rho_s V_s \quad (2.5)$$

in which B is the pile diameter; ρ_s is the density of the elastic medium, V_p is p-wave velocity and V_s is shear wave velocity of wave propagation through the medium. Representation of three dimensional propagation of energy was handled in a two dimensional form as stated in Equation 2.5. The paper compared displacement histories of soil in the free field with that of the pile. The study found that the displacement history of the pile is smaller than those in the free field indicating the pile with its much larger stiffness tends to resist the displacements imposed by the soil during seismic excitation.

2.3 Free Field Analysis

Any seismic analysis of pile requires the calculation of free field response which is the response of the soil mass in the absence of the pile. As the incident seismic waves are often assumed to be vertically incident SH waves, the principles of wave propagation in a horizontally layered and laterally infinite soil layer is used to obtain free field response (Kramer, 1996). The program SHAKE which uses this principle is widely used for prediction of free field motions. Boulanger et al. (1999) used SHAKE for free field motion analysis. It obtains the nonlinear response of the soil mass under strong seismic motion by an equivalent linear methodology. Although the equivalent linear approach is computationally convenient and provides reasonable results for many practical problems, it remains an approximation to actual nonlinear process of a seismic ground response (Kramer, 1996). An alternative approach is to analyze the actual nonlinear response of a soil deposit using direct numerical integration in the time domain (Kramer, 1996). Most currently available nonlinear one dimensional ground response analysis computer programs characterize the stress strain behavior of soil by cyclic stress strain models such as the hyperbolic model, the Mroz type model, the Iwan type model etc (El Naggar et al. 2005). A computer program NERA (Nonlinear Earthquake Response Analysis) is a Iwan type model (Bardet and Tobita, 2001) and is widely used for one dimensional ground response analysis. El Naggar et al. (2005) used this software for predicting free field input motions at different depths of clay and sand layer. But both NERA and SHAKE are formulated in terms of total stress concepts. These programs do not allow modeling of the

generation, redistribution and eventual dissipation of excess pore pressure in cohesionless soil during and after earthquake shaking. Advanced constitutive model such as Cyclic 1D has this capability (Elgamal et al. 2006). Nonlinearity is simulated by the incremental plasticity formulation to allow for modeling permanent deformation and for generation of hysteretic damping.

2.4 Determination of Shear Wave Velocity

Soil damping provides a major source of energy dissipation in pile–soil systems subjected to dynamic loading. In seismic pile–soil interaction problems, two types of damping should be considered: radiation and material damping (El Naggar et al. 2005). Determination of radiation damping requires magnitude of shear wave velocity.

Hardin and Drnevich (1972) discussed about computing low strain shear modulus G_{\max} . It is reported in their work that for many undisturbed cohesive soil, as well as sands, G_{\max} (psi) can be calculated from

$$G_{\max} = 1230 \frac{(2.973 - e)^2}{(1 + e)} (OCR)^K (\sigma'_m)^{0.5} \quad (2.6)$$

in which e is the initial void ratio of soil; OCR is the overconsolidation ratio; K is the plasticity index of clay soil; σ'_m mean effective confining stress (psi). The author mentioned that values of G_{\max} computed from Equation 2.6 may be too low for void ratios in excess of 2.

Shear wave velocity V_s is measured by relating G_{\max} as shown below:

$$G_{\max} = \rho V_s^2 \quad (2.7)$$

where ρ is the bulk density of soil.

Chapter 3

Discussion on Centrifuge Tests

3.1 Introduction

Wilson et al. (1997 a, b) conducted several centrifuge tests on single pile and pile groups using Kobe (1995) and Santa Cruz (1989) earthquake data as the input motions. Data from two of these, Csp2 and Csp3 are used in this study. Three pile supported structures were tested in the Csp2 test and four pile supported structures were tested in the Csp3 test. A total of 17 shaking events were performed at a centrifugal acceleration of 30g. All data reported in Wilson et al. (1997a, b) is in prototype units. The thesis used centrifuge tests Csp2 and Csp3 for analyzing performance of the BNWF model of single pile. The following section describes the key configuration of Csp2 and Csp3.

3.2 Layout of Csp2 Model

Csp2 tests were performed using a 9-m radius centrifuge at the University of California at Davis in a flexible shear beam container. The inside dimensions of the container were 1.7 m long, 0.7 m deep and 0.7 m wide. Details of the modeling procedure are described in Wilson et al., (1997a). The location of the instruments along the pile SP1 is shown in Figure 3.1. The soil profile, structural models and instrumentation for the tests are shown in Figure 3.2. Location of instrument in the container is mentioned in Wilson et al. 1997a. The soil profile of Csp2 consisted of two horizontal soil layers. The lower layer was fine, uniformly graded Nevada sand ($C_u=1.5$ and $D_{50}=0.15$ mm) at a dry density of 16.2 kN/m^3 which corresponds to a relative density D_r of about 80%. The sand was air pluviated, flushed with carbon dioxide and saturated under vacuum. The water table was approximately at the surface of the soil. The upper layer was loose fine, uniformly graded Nevada sand at a dry density of 14.9 kN/m^3 which corresponds to D_r of about 35 %. The single-pile-supported systems SP1 analyzed in this study consisted of a superstructure mass attached to an extension of the pile. The mass was 49,100 kg. The steel pipe pile had an outer diameter of 0.67 m and a thickness of 19 mm. The piles were installed at 1g (prior to spinning the centrifuge) and remained elastic during all earthquake events.

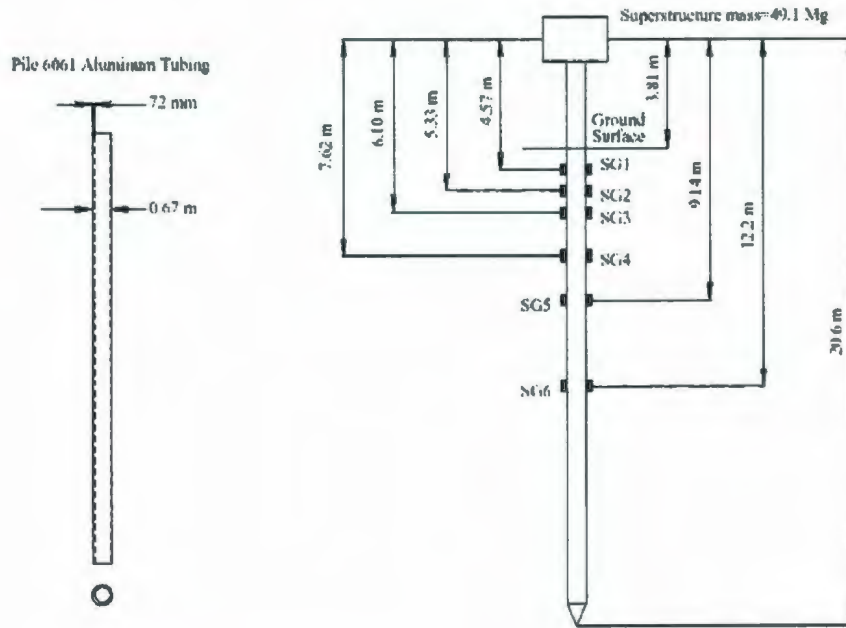


Figure 3.1: Single Pile, SP1 Instrumentation, (from Wilson, 1998).

Shaking events of Csp2 that were analyzed in the thesis are mentioned in Table 3.1. Each event was a scaled version of a record prepared by filtering and integrating strong motion records from the Kobe earthquake in 1995 or the Santa Cruz earthquake in 1989. Each earthquake event was separated by sufficient time to allow dissipation of any shaking induced excess pore pressures.

Table 3.1 Ground Input Motion for Csp2 Tests (Wilson et al., 1997a)

Event	Input	PBA (g)
D	Kobe	0.04
F	Kobe	0.22
J	Santa Cruz	0.45
E	Santa Cruz	0.49
L	Kobe	0.62

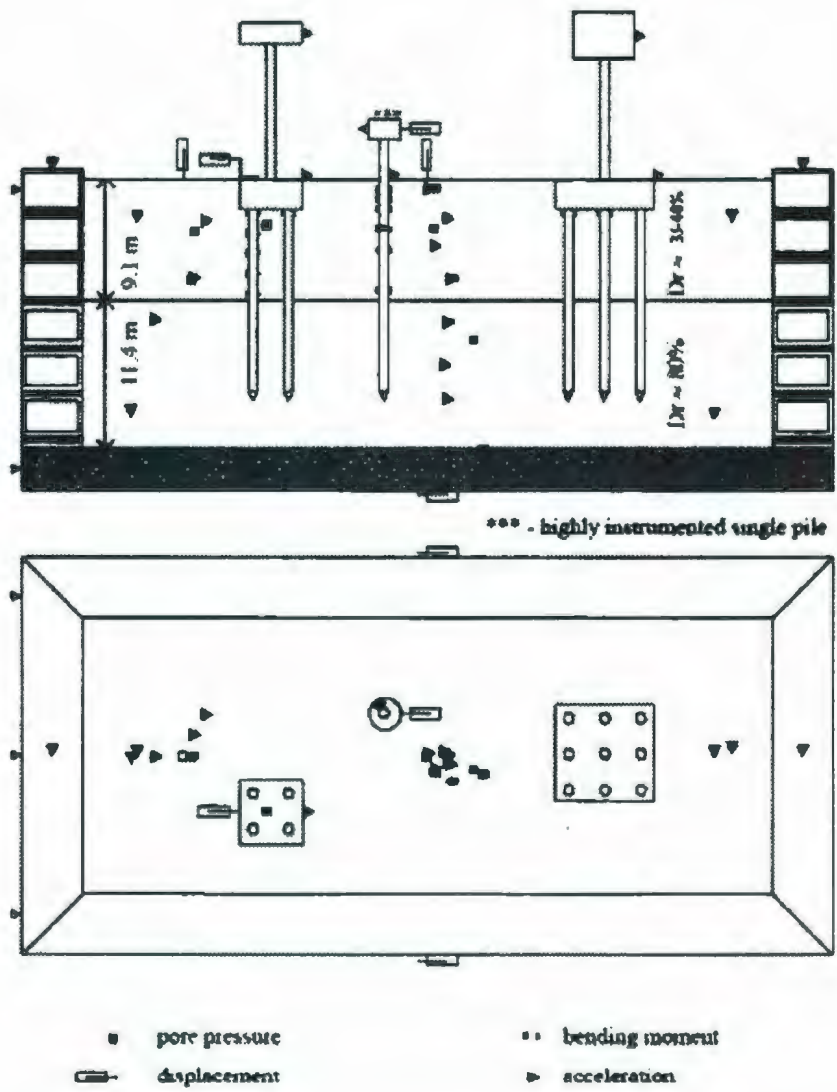


Figure 3.2: Centrifuge Test Layout of Csp2 Model (from Wilson, 1998).

3.3 Layout of Csp3 Model

The same soil profile was used in Csp3 tests but the model structures and instrumentation were rearranged. The soil profile, structural models and instrumentation for the tests are shown in Figure 3.3.

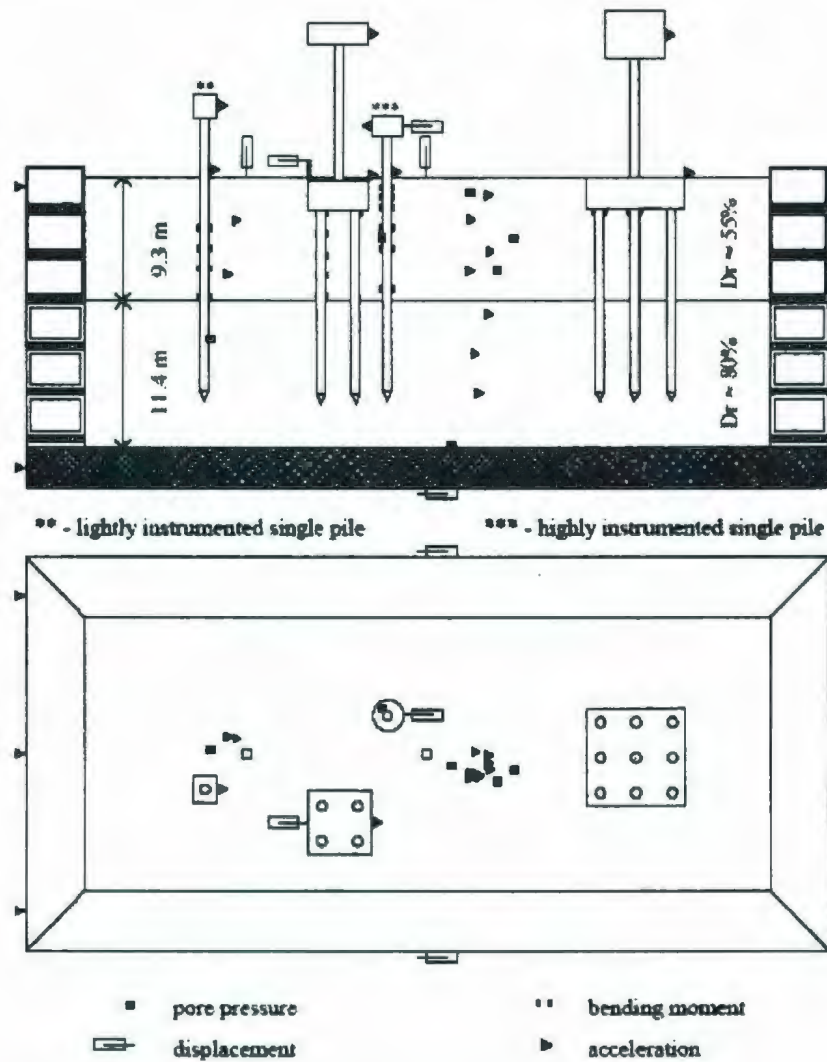


Figure 3.3: Centrifuge Test Layout of Csp3 Model (from Wilson, 1998)

The location of instrument in the container is mentioned in Wilson et al., (1997b). The lower layer was fine, uniformly graded Nevada sand at a dry density of 16.2 kN/m^3 , which corresponds to relative density D_r of about 80%. The water table was approximately at the surface of the soil. The upper layer was loose fine, uniformly graded Nevada sand at a dry density of 15.5 kN/m^3 , which corresponds to D_r of about 55%. The highly instrumented single pile SP1 was analyzed in this study and it supported a superstructure mass of 49,100 kg. The piles were installed at 1g (prior to spinning the

centrifuge) and remained elastic during all earthquake events. Shaking events of Csp3 that were analyzed in this thesis are shown in Table 3.2.

Table 3.2 Ground Input Motion for Csp3 Tests (Wilson et al., 1997b)

Event	Input	PBA (g)
G	Santa Cruz	0.025
D	Santa Cruz	0.04
J	Kobe	0.22
M	Santa Cruz	0.41
I	Santa Cruz	0.49
O	Kobe	0.60

Each event was a scaled version of a record prepared by filtering and integrating strong motion records from the Kobe earthquake in 1995 or the Santa Cruz earthquake in 1989. Each earthquake event was separated by sufficient time to allow dissipation of any shaking induced excess pore pressures.

The steel pipe pile had an outer diameter of 0.67m and a thickness of 19 mm. Soil and pile properties used in Csp2 and Csp3 tests are shown at a glance in Table 3.3 and Table 3.4 respectively.

3.4 Results of Csp2 and Csp3 Tests

Details of recorded time histories of ground accelerations, pore pressures, pile head accelerations, pile superstructure accelerations, superstructure displacements and bending moments of Csp2 and Csp 3 tests can be obtained from Wilson et al (1997a,b). The test results of Csp2 and Csp3 along with simulation results have been plotted in Chapter 5.

Table 3.3 Soil Properties (Wilson, 1998)

Soil Sample Properties (from Wilson, 1998)			
		Csp2 Soil Model	Csp 3 Soil Model
Upper Layer (Nevada Sand)	Depth, (m)	9.10	9.30
	Relative Density (%)	35-40	55
	Effective Unit Weight (kN/m ³)	9.30	9.70
	Specific Gravity	2.65	2.65
	Void ratio	0.743	0.677
	Friction angle	30 ⁰	35 ⁰
Lower Layer (Nevada Sand)	Depth, (m)	11.4	11.4
	Relative Density (%)	80	80
	Effective Unit Weight (kN/m ³)	10.10	10.10
	Specific Gravity	2.65	2.65
	Void ratio	0.606	0.606
	Friction angle	42 ⁰	42 ⁰

Table 3.4 Pile Properties (Wilson, 1998)

Pile Material	Steel
Superstructure Mass	49,100 kg
Young's Modulus	200 GPa
Outside Diameter	0.667 m
Wall Thickness	19 mm

Chapter 4

Nonlinear Seismic Free Field Response Analysis of Saturated Sand

Co Authorship: Chapter 4 has been prepared in accordance with the regulations for a Manuscript format thesis stipulated by Faculty of Applied Science and Engineering at The Memorial University of Newfoundland, Canada and has been co-authored as:

Nonlinear Seismic Free Field Response Analysis of Saturated Sand, co-authored by Mohammad K. Talukder and Dr. Stephen D. Butt. A version of this paper is published in the refereed conference proceedings of the 1st International/1st Engineering Mechanics and Materials Specialty Conference, St John's, Newfoundland, May 28, 2009. Mohammad K. Talukder conducted the research and wrote the manuscript. Based on the thesis examination report, this manuscript is modified from the previously published version. Specifically Table 4.2 has some modified values and Figures 4.2 to 4.17 have modified computed results. Dr. Stephen D. Butt supervised the research and reviewed the manuscript.

4.1 Introduction

Free field ground acceleration time histories are used as input excitation at support boundaries of the BNWF (Beam on Nonlinear Winkler Foundation) approach. The importance of predicting the free field motions has long been recognized by the researchers who are interested in analyzing soil-structure interaction utilizing the well known BNWF method. This interest has triggered the development of computer programs for performing one dimensional (1D) seismic response analyses of soil deposits since the early 1970s. One Dimensional ground response analyses are based on two assumptions: all boundaries between different geologic materials are horizontal and the response of soil deposit is predominantly caused by SH-waves propagating vertically from the underlying bedrock (Kramer, 1996). For 1D ground response analyses, the soil and rigid bedrock are assumed to extend infinitely in the horizontal direction (Kramer, 1996). SHAKE is perhaps the most popular program on the list of 1D response analyses programs that implements a 1D equivalent-linear analysis of a soil deposit idealized as a

stratified, viscoelastic medium (Idriss and Sun, 1991). In the code SHAKE, nonlinear response of soils to a seismic excitation is modeled through a frequency domain equivalent-linear analysis where stiffness and damping parameters of the soil layers are adjusted in each iteration. This is continued until they are made compatible with the strain level induced by the earthquake loading (Kramer, 1996). Even though the process of iteration toward strain compatible soil properties allows nonlinear soil behaviour to be approximated, it is important to remember that the complex response method is still a linear method of analysis (Kramer, 1996). The strain compatible properties are constant throughout the duration of an earthquake, regardless of whether the strains at particular time are small or large (Kramer, 1996). The method is incapable of representing the changes in soil stiffness that actually occurs during the earthquake. On the other hand, nonlinear time-domain analysis methods allow soil properties within a given layer to change with time as the strains change in that layer (Kramer, 1996). The most currently available nonlinear 1D ground response analysis computer programs for predicting free field input motions are ONDA (Lo Presti et al. 2006) and NERA (Bardet and Tobita, 2001). Results from these two well known softwares often do not agree with the recorded motions since they are capable of performing total stress based analysis. One must use effective stress based free field analysis methods that can generate both pore pressure and acceleration time histories for cohesionless saturated soil. With this requirement in mind, this study used a solid-fluid coupled finite element code called Cyclic1D (Elgamal et al. 2006) for predicting free field acceleration time histories at any depth in saturated sand deposits. Nonlinear method Cyclic1D being formulated in terms of effective stresses can allow modeling of the generation, redistribution and eventual dissipation of excess pore pressure during and after earthquake shaking (Elgamal et al., 2006). Equivalent linear SHAKE or nonlinear methods NERA and ONDA do not have this capability.

The objective of this study is to predict free field acceleration time histories for saturated sand deposit by using Cyclic1D to compare them with recorded results of centrifuge tests performed by Wilson et al. (1997a, b). This chapter also tabulates values of the model parameters to be used in Cyclic1D simulation for better agreement with the recorded motions at various depths of saturated sand deposits.

4.2 Cyclic1D Model description

Cyclic1D is a nonlinear Finite Element program for one dimensional (1D) Horizontal dynamic site response simulations. The soil model employed in Cyclic1D is developed within the framework of multi-yield-surface plasticity model (Elgamal et al., 2002). For analysis of dry as well as saturated strata, the Finite Elements in Cyclic1D are defined within a coupled solid-fluid (u-p) formulation. In this model, emphasis is placed on controlling the magnitude of cycle-by-cycle permanent shear strain accumulation in clean loose and dense sands (Elgamal et al., 2002). The program operates in the time domain, allowing for linear and nonlinear studies. Nonlinearity is simulated by the incremental plasticity formulation to allow for modeling permanent deformation and for generation of hysteretic damping of sand (Elgamal et al., 2006).

4.3 Modeling Soil Profile in Cyclic1D

This paper predicts free field motions for saturated sand profiles of centrifuge models Csp2 and Csp3 (Wilson et al 1997a, b). The two dimensional finite element model of soil profile developed in this study for Cyclic1D analysis is shown in Figure 4.1. The soil profile was divided into 200 finite elements each of which is 0.1 m high. Horizontal motion was applied at the base of the model. The soil profile developed in Cyclic1D model is excited by weak and strong ground motions mentioned in Table 4.1.

4.4 Cyclic1D Model Input Parameters

Cyclic1D requires several traditional soil input parameters, such as effective friction angles saturated unit weight and permeability constant. Saturated unit weights of the soils in Csp2 and Csp3 model were determined by Wilson, (1998) and have been used in Cyclic1D simulation. Wilson, (1998) reported the values of effective friction angles based on API, 1993. This study used those values of effective friction angles in Cyclic1D analyses. Coefficient of Hydraulic conductivity was ascertained by Hazen's, (1930) method and was used in Cyclic1D response analyses. It may be noted that coefficient of

permeability of Nevada sand was not reported in Wilson, (1998) and its magnitude at 30g level was not found in the literature.

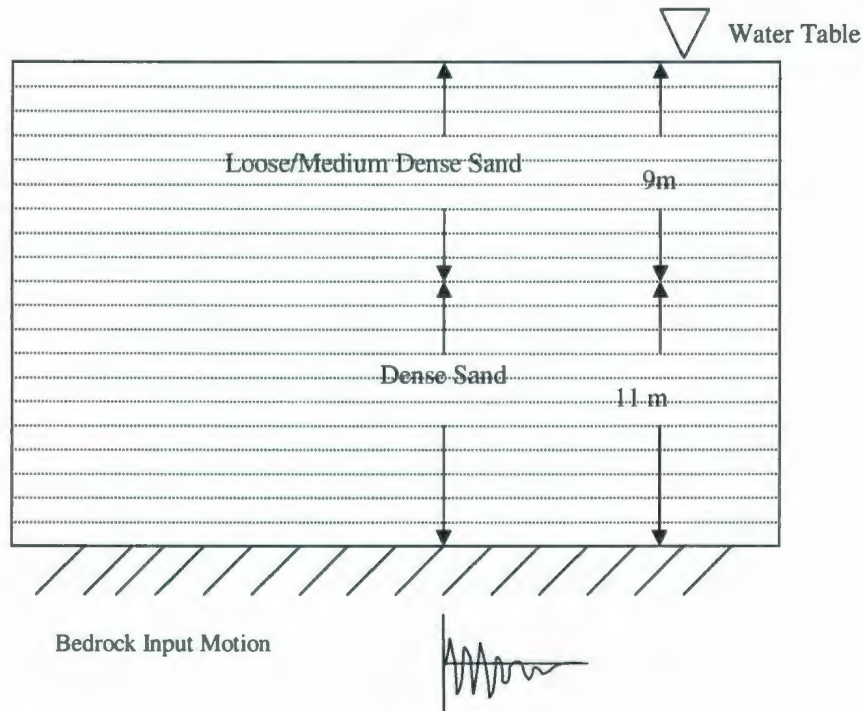


Figure 4.1: Finite Element Model of Soil Profile Developed in Cyclic1D for Free Field Analysis.

Table 4.1 Ground Input Motions for Cyclic1D Analysis

Experiments	Event	Motion	Peak Ground acceleration, PGA (g)
Csp2	D	Kobe	0.04
Csp2	J	Santa Cruz	0.45
Csp3	J	Kobe	0.22
Csp3	M	Santa Cruz	0.41

Apart from the basic soil properties, there are a number of model parameters relating to the multi-yield surface soil plasticity model employed in Cyclic1D, namely, dilation angles, dilation parameters and contraction parameters (Elgamal et al., 2003).

Table 4.2 Input parameters for Cyclic1D Analysis

	Soil properties used in Cyclic1D analyses of Csp2 (Wilson, 1998)		Soil properties used in Cyclic1D analyses of Csp3 (Wilson, 1998)	
	Parameters for upper loose soil layer	Parameters for lower dense soil layer	Parameters for upper loose soil layer	Parameters for lower dense soil layer
Relative Density (%)	35	80	55	80
Soil effective Unit weight (kN/m ³)	9.1	10	9.3	10
Reference Shear wave velocity (m/s)	100	350	200	350
Peak Shear Strain (%)	3	3	3	3
Effective friction angle (degree)	30 ⁰	42 ⁰	35 ⁰	42 ⁰
Dilation angle (degree)	30 ⁰	30 ⁰	30 ⁰	30 ⁰
Hydraulic Conductivity(m/s)	0.0002*	0.0001*	0.00015*	0.0001*
Contraction Parameter 1	0.01	0.01	0.001	0.05
Contraction Parameter 2	0.6	0.6	0.6	0.3
Dilation Parameter 1	0.6	0.6	0.6	0.6
Dilation parameter 2	10	10	10	10
Soil Poisson's Ratio	0.4	0.4	0.4	0.4
Number of Yield Surface	20		20	
Rayleigh Damping Parameter (α)	0.039		0.047	
Rayleigh Damping Parameter (β)	0.0024		0.0016	

* In this study, coefficients of hydraulic conductivity for Nevada sand (C_u , 1.5 and d_{50} , 0.15 mm) were estimated by using Hazen's (1930) empirical method and adjusted for relative density.

Dilation angle in Cyclic1D model is also termed as Phase Transformation angle (Elgamal et al., 2003) and expressed in degrees. Dilation angle divide the domain of shear induced volume contraction of sand from that of volume dilation (Elgamal et al., 2003). Elgamal et al. (2006) suggest that one should set dilation angle to zero to remove contraction behavior completely. To remove dilation behavior completely, one should set this angle larger than the friction angle employed in the Cyclic1D ground response analysis (Elgamal et al., 2006).

Dilation parameters are of two kinds. These are Dilation parameter 1 and 2. Dilation parameter 1 dictates the rate of volume expansion or reduction of pore water pressure (Elgamal et al., 2006). Recommended range of values (Elgamal et al., 2006) of Dilation parameter 1 is 0.00~0.60 (very loose to very dense sand). Dilation parameter 2 reflects the effect of shear strain on dilation behavior (Elgamal et al., 2003). Recommended range of Dilation parameter 2 is 10 (Elgamal et al., 2006).

Contraction parameters are also of two kinds. These are Contraction parameter 1 and 2. Contraction parameter 1 dictates the rate of pore water pressure buildup under undrained conditions (Elgamal et al., 2003). Recommended range of values (Elgamal et al., 2006) of Contraction parameter 1 is 0.30~0.00 (very loose to very dense sand). Contraction parameter 2 reflects the effect of overburden pressure on contraction behavior. Elgamal et al. (2006) suggest that Contraction parameter 2 should be chosen between 0.2 to 0.6 (very loose to very dense)

Input parameters used in this study for generating free field input motions are shown in Table 4.2.

4.5 Artificial Damping in Cyclic1D Analyses

Rayleigh damping is a kind of artificial damping applied to finite element models for dynamic response analyses (Elgamal et al., 2006). Soil profiles developed in the finite

element framework within Cyclic1D model require manipulation of mass and stiffness proportional Rayleigh damping coefficients as given by Equation 4.1

$$[C] = \alpha[M] + \beta[K] \quad (4.1)$$

where M is the mass matrix, C is viscous damping matrix, K is initial stiffness matrix, α mass proportional Rayleigh damping coefficient and β initial stiffness proportional Rayleigh damping coefficient. These two damping Rayleigh coefficients α and β are obtained by solving Equations 4.2 and 4.3 as shown below:

$$\xi_1 = \frac{\alpha}{4\pi f_1} + \beta\pi f_1 \quad (4.2)$$

$$\xi_2 = \frac{\alpha}{4\pi f_2} + \beta\pi f_2 \quad (4.3)$$

By specifying two frequencies, $f_1 = 0.5$ Hz and $f_2 = 20$ Hz and two damping ratios $\xi_1 = 1\%$ and $\xi_2 = 15\%$, we can solve Eqs. 4.2 and 4.3 for α and β . We then find $\alpha = 0.039$ and $\beta = 0.0024$. These values of α and β have been used in this study for simulating free field motions observed in centrifuge test Csp2 (Wilson et al., 1997a). Similarly, $\alpha = 0.047$ and $\beta = 0.0016$ are achieved for predicting free field response recorded in centrifuge test Csp3 (Wilson et al., 1997b) by specifying two frequencies, $f_1 = 0.5$ Hz and $f_2 = 20$ Hz and damping ratios $\xi_1 = 1\%$ and $\xi_2 = 10\%$; respectively.

4.6 Comparison of Numerical and Experimental Results

Cyclic1D model employs the Newmark time integration procedure with two user defined coefficients γ and β . In this study, default values for γ and β are used. The default values for γ and β are 0.55 and 0.27 respectively.

The calculated free field motions for event D of Csp2 are shown in Figures 4.2-4.4. In event D, with a low level of peak ground acceleration (PGA, 0.04 g), a good agreement on peak accelerations between recorded and computed results, particularly for lower soil layers with depths of 8 m to 14 m is seen in Figures 4.3-4.4. Cyclic1D tends to underestimate recorded motions for upper soil layers with depths of 1 m to 5 m (Figures 4.2-4.3). The calculated and recorded horizontal acceleration time histories at different depths of soil for Event J of Csp2 are shown in Figures 4.5-4.8. In event J with strong

peak ground acceleration (PGA, 0.45 g), an excellent agreement between predicted and experimental acceleration time histories is achieved for shallow to deep soil layers with depths of 5 m to 17 m (Figures 4.6-4.8). However, agreement is not good for layers with depths of 1 m to 3 m that are close to the soil surface as Cyclic1D tends to overestimate recorded motions. Time histories of excess pore water pressure ratios ($\Delta u / \sigma'_{v0}$; where Δu is excess pore water pressure and σ'_{v0} is initial effective vertical stress at any depth) at different layers of the soil profile of Csp2 for shaking event J are shown in Figure 4.9. Agreement between predicted and experimental time histories of excess pore water pressure (EPWP) ratios is achieved reasonably well for shallow to deep soil layers with depths of 1 m to 12 m (Figure 4.9).

The calculated and recorded horizontal acceleration time histories at different layers of the soil profile of Csp3 for shaking events J are shown in Figures 4.10-4.12. EPWP time histories at different layers of the soil profile of Csp3 for shaking event J are shown in Figure 4.13 and compared with experimental data. The calculated and recorded horizontal acceleration time histories at different layers of the soil profile of Csp3 for shaking event M are shown in Figures 4.14-4.16. EPWP time histories at different layers of the soil profile of Csp3 for shaking event M are shown in Figure 4.17 and compared with experimental data. For events J and M of Csp3 with moderate (0.22 g) to strong peak ground acceleration (0.41 g), excellent agreement on peak accelerations was obtained between measured and computed results for all soil layers with depths of 1 m to 17 m.

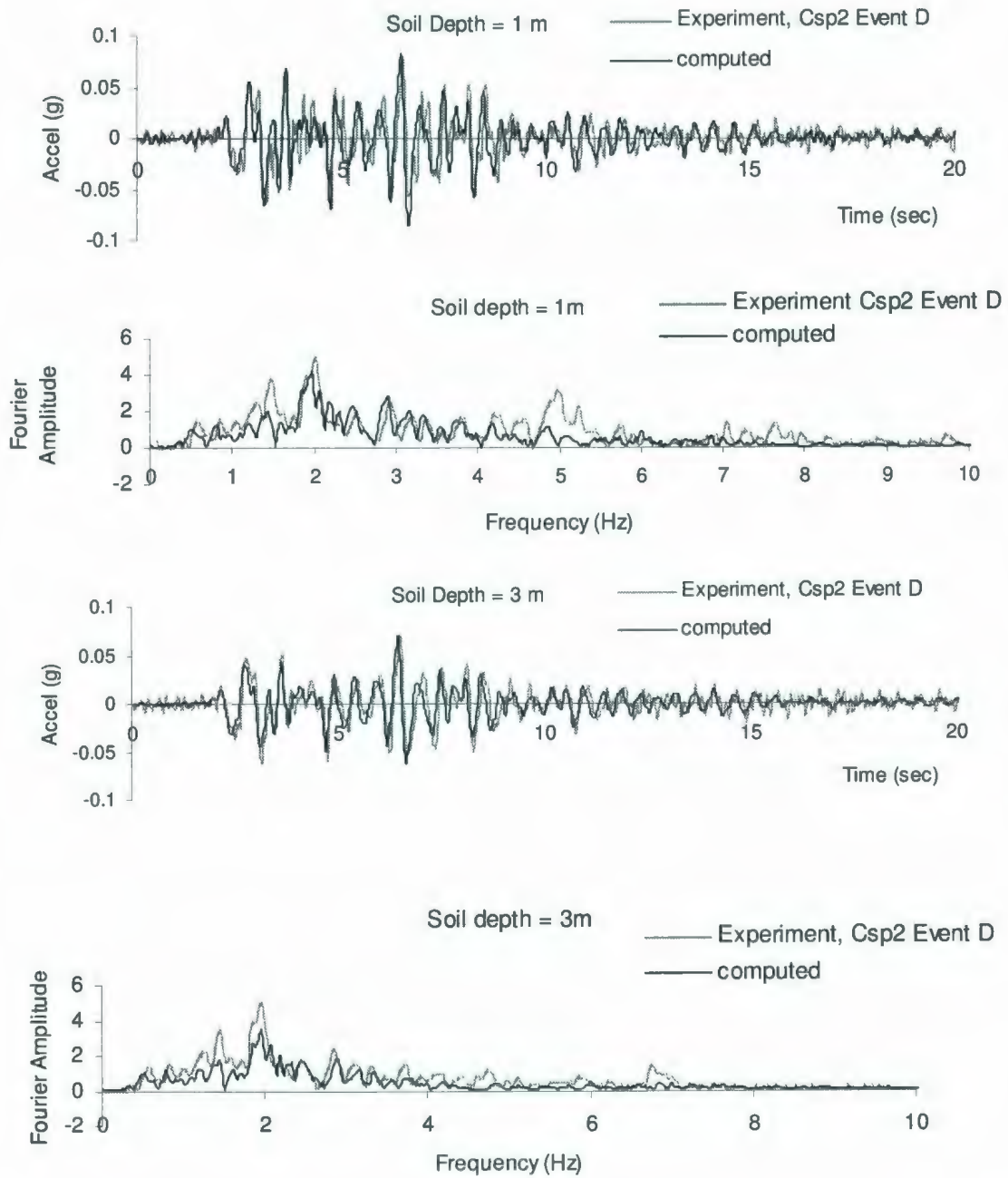


Figure 4.2: Horizontal acceleration time histories and corresponding Fast Fourier Transform for Event D of Csp2 Test (soil depths, 1 m to 3 m).

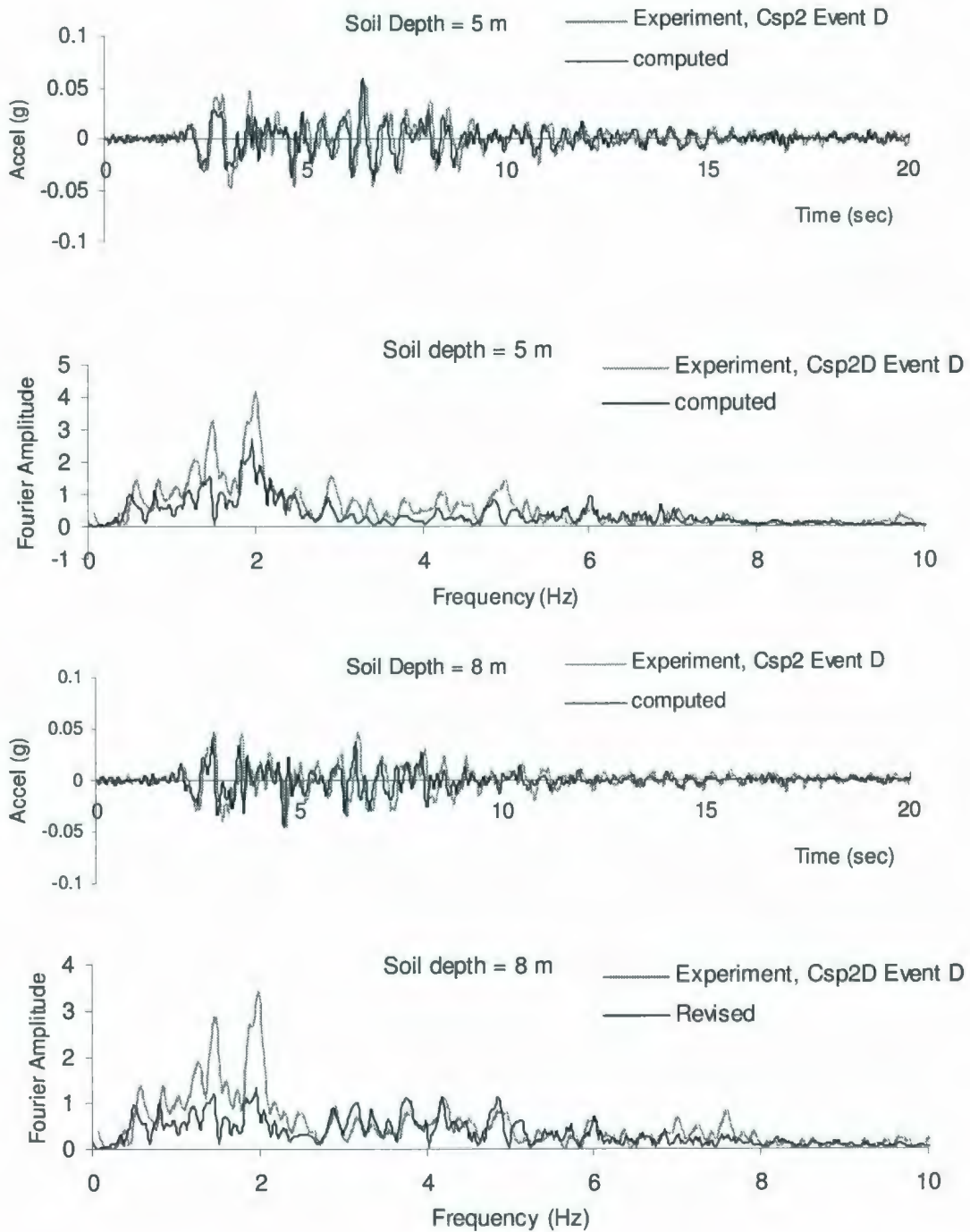


Figure 4.3: Horizontal acceleration time histories and corresponding Fast Fourier Transform for Event D of Csp2 Test (soil depths, 5 m to 8 m).

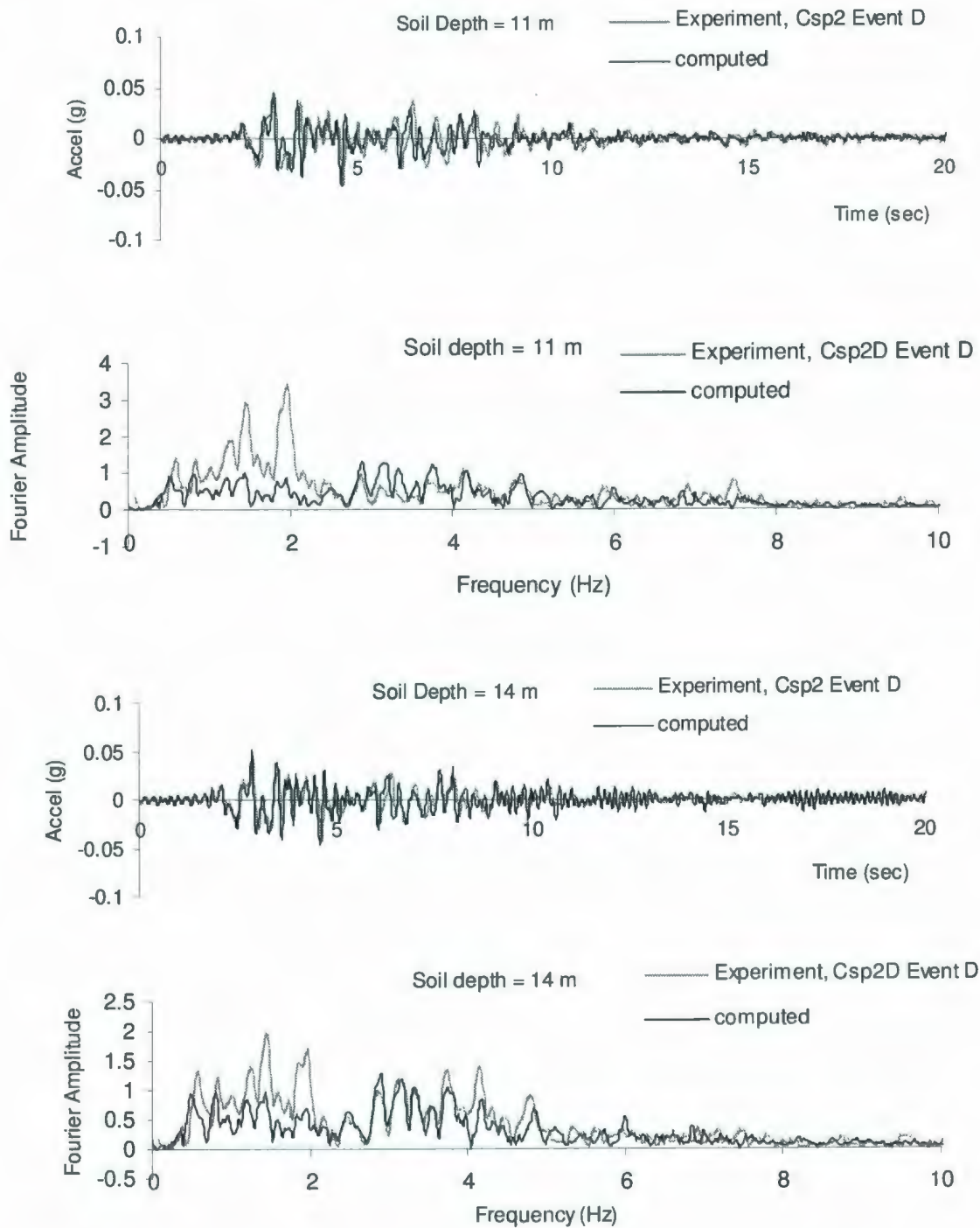


Figure 4.4: Horizontal acceleration time histories and corresponding Fast Fourier Transform for Event D of Csp2 Test (soil depths, 11 m to 14 m).

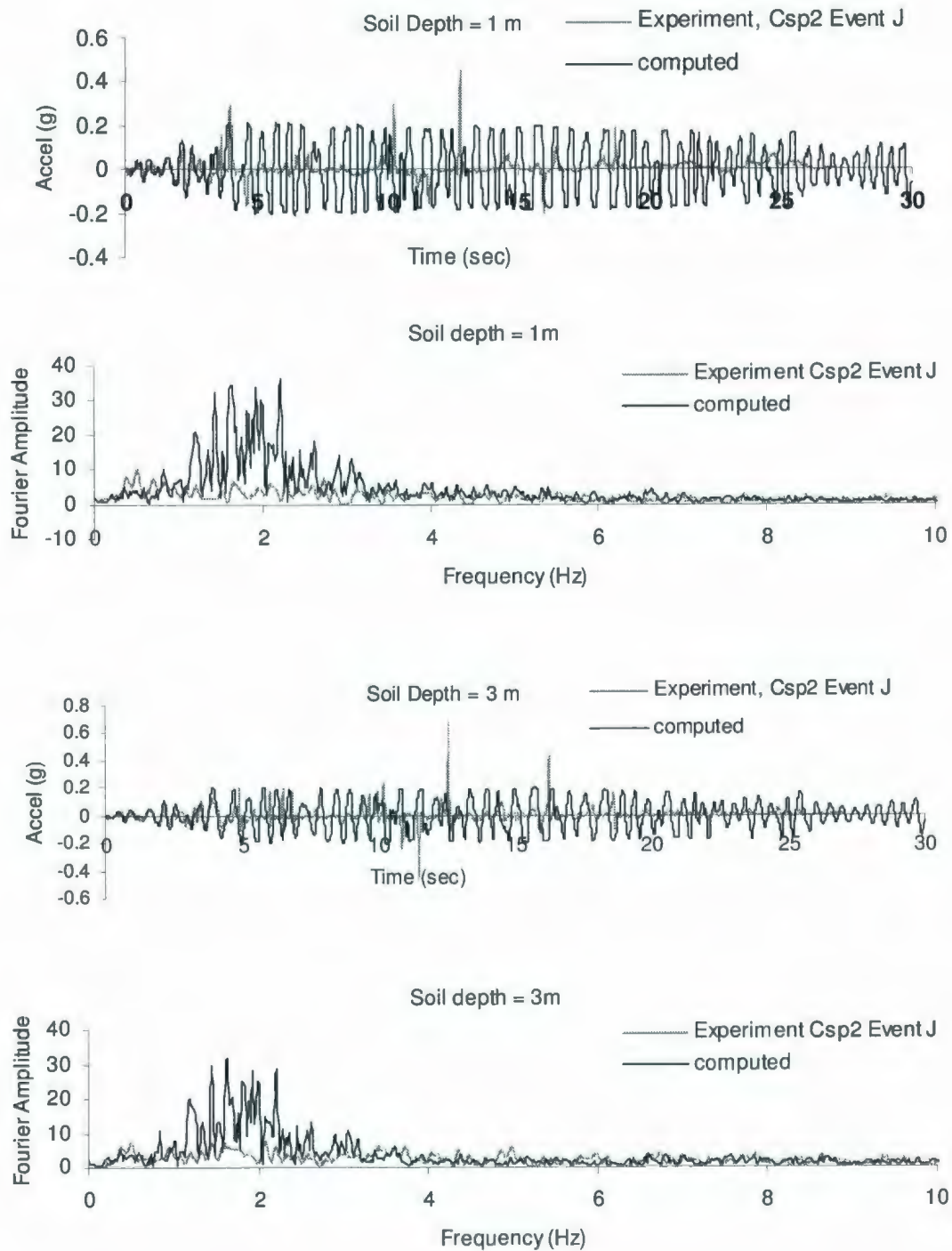


Figure 4.5: Horizontal Acceleration Time Histories and corresponding Fast Fourier Transform for Event J, Csp2 (soil depths, 1 m to 3 m).

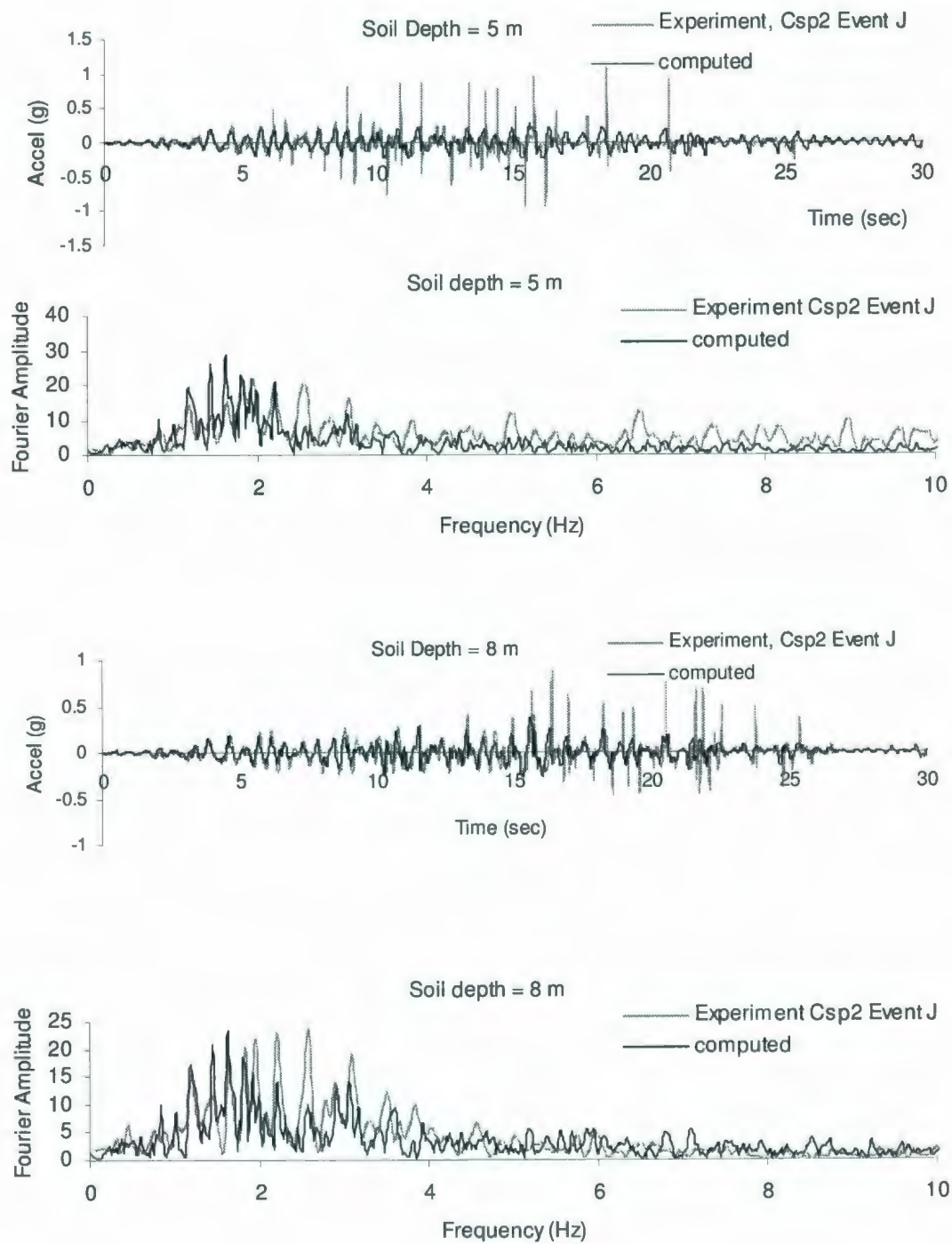


Figure 4.6: Horizontal Acceleration Time Histories and corresponding Fast Fourier Transform for Event J, Csp2 (soil depths, 5 m to 8 m).

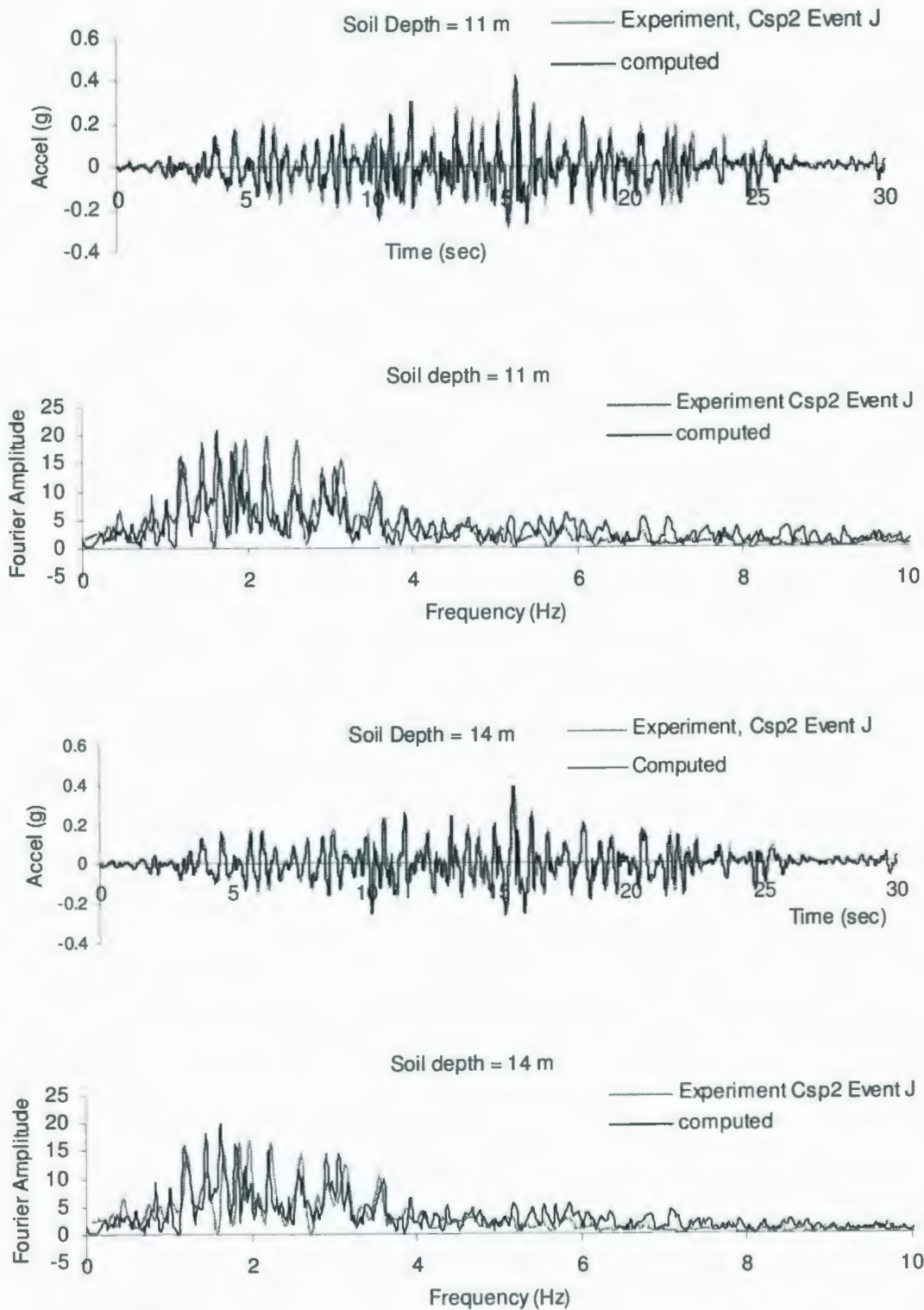


Figure 4.7: Horizontal Acceleration Time Histories and corresponding Fast Fourier Transform for Event J, Csp2 (soil depths, 11 m to 14 m).

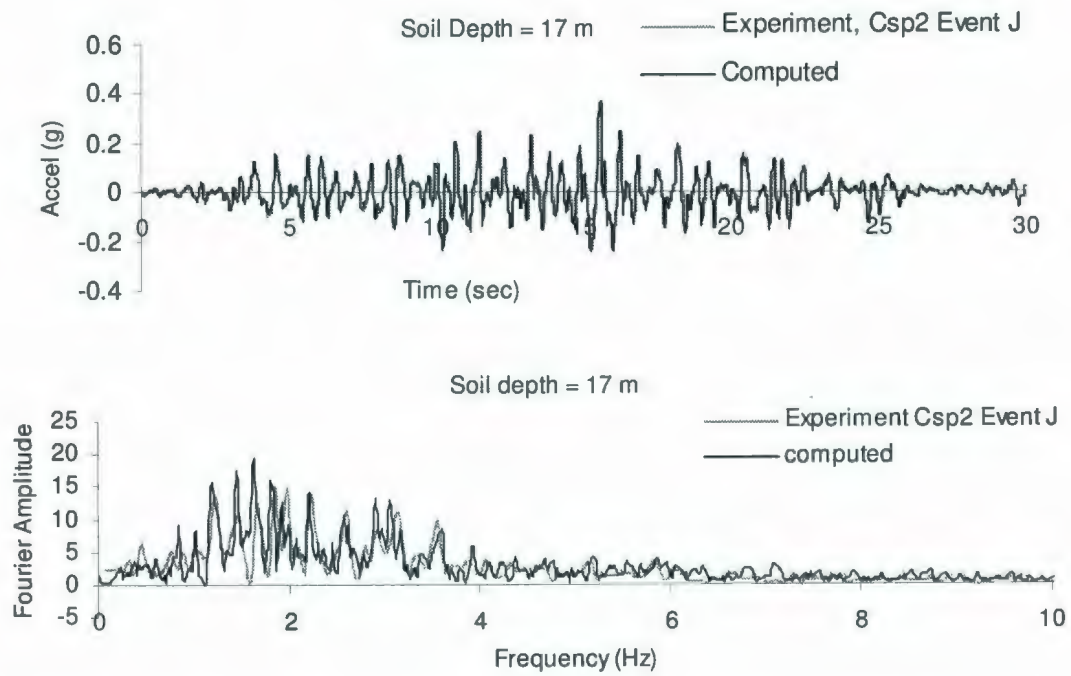


Figure 4.8: Horizontal Acceleration Time Histories and corresponding Fast Fourier Transform of Event J, Csp2 (soil depth, 17 m).

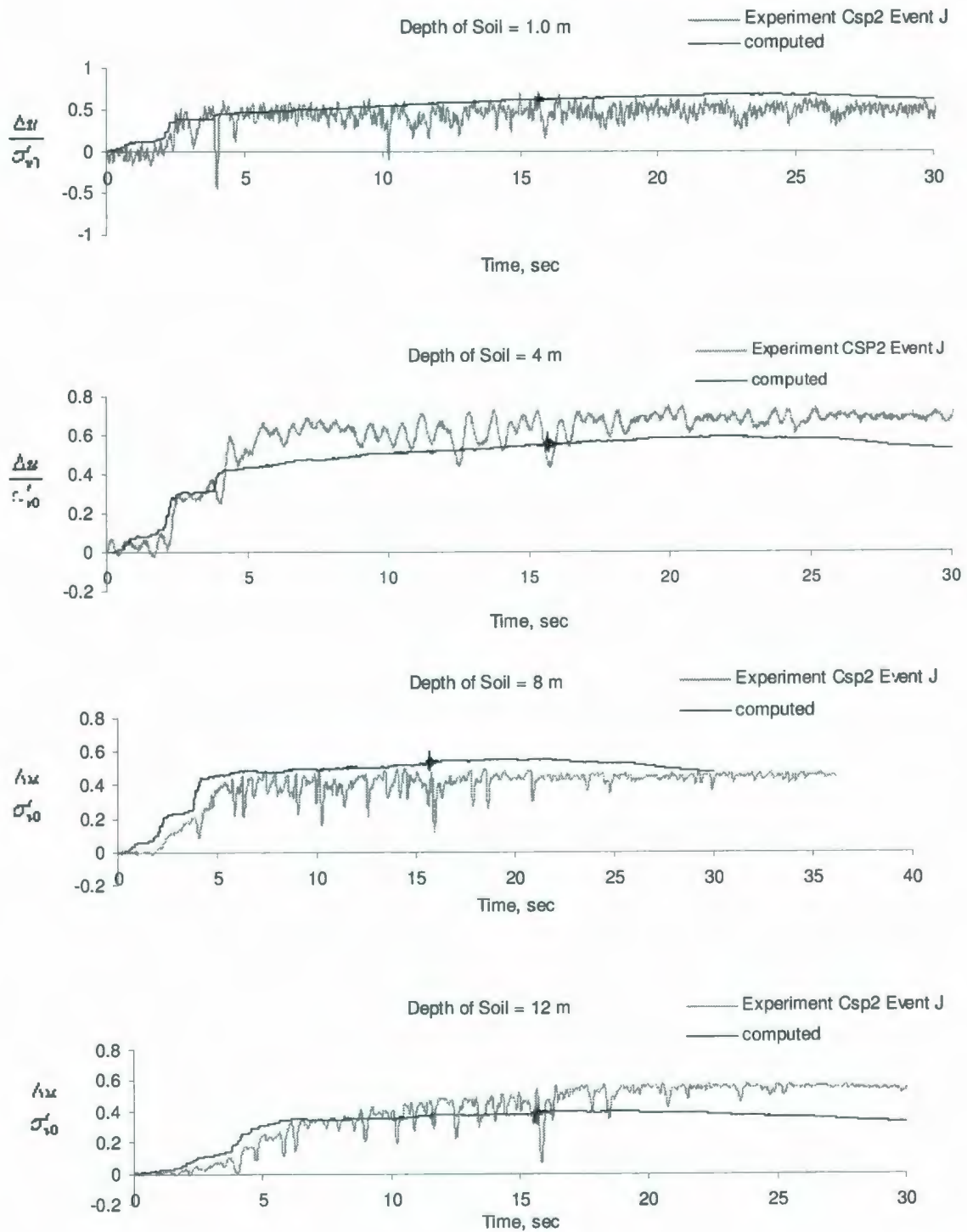


Figure 4.9: Excess Pore Water Pressure Time Histories for Event J, Csp2 (soil depths, 1 m to 12 m).

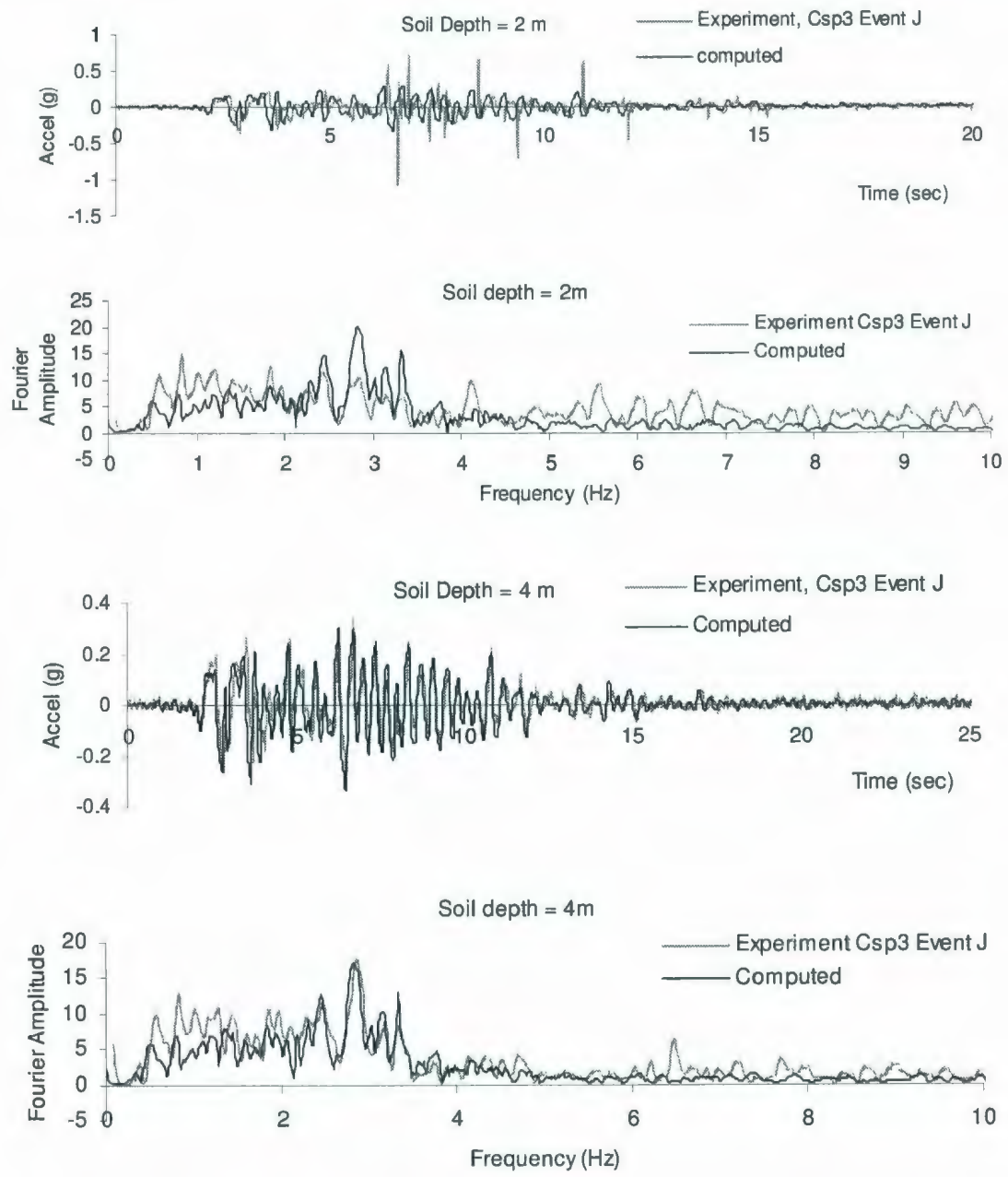


Figure 4.10: Horizontal Acceleration Time Histories and corresponding Fast Fourier Transform for Event J, Csp3 (soil depths, 2 m to 4 m).

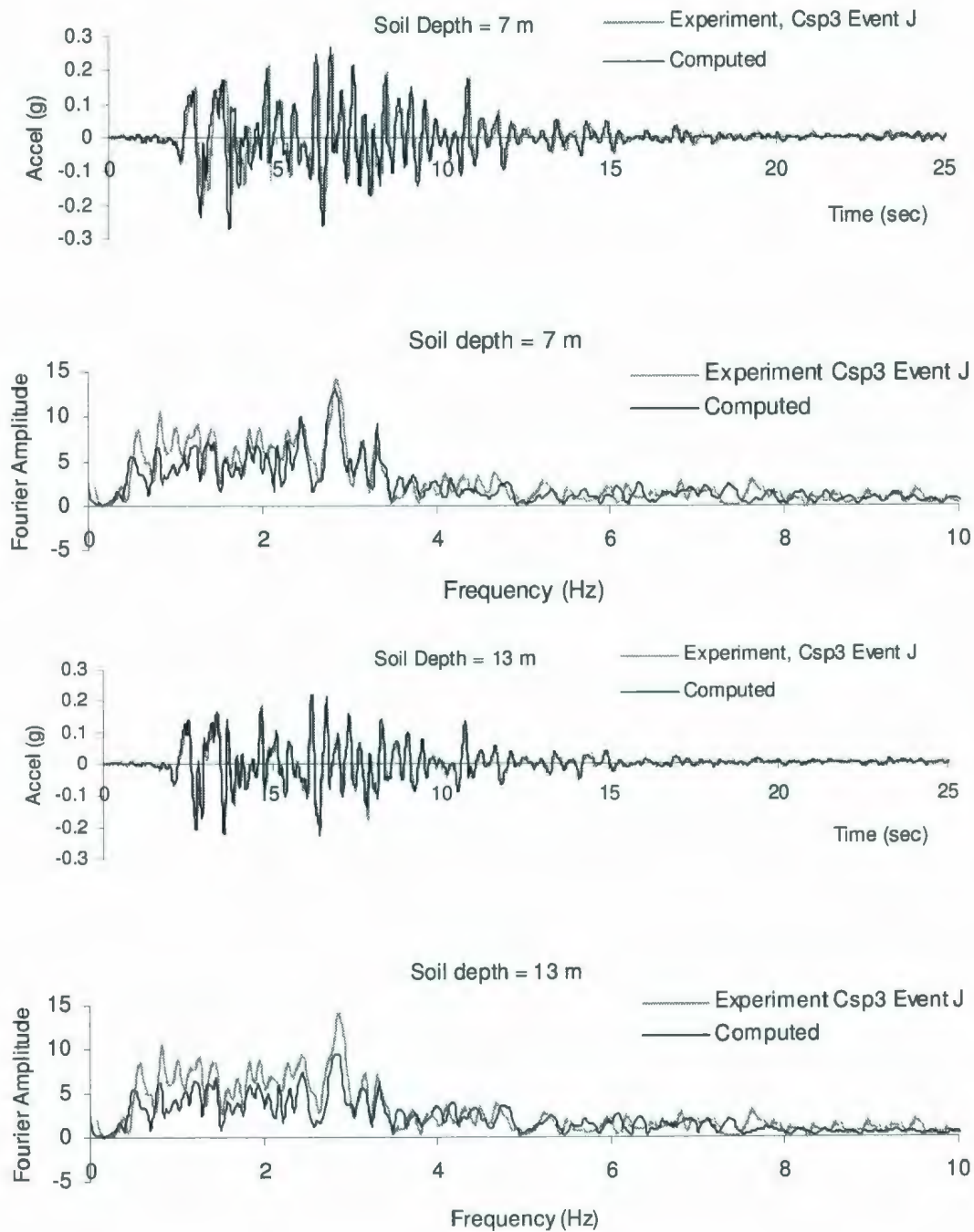


Figure 4.11: Horizontal Acceleration Time Histories and corresponding Fast Fourier Transform of Event J, Csp3 (soil depths, 7 m to 13 m).

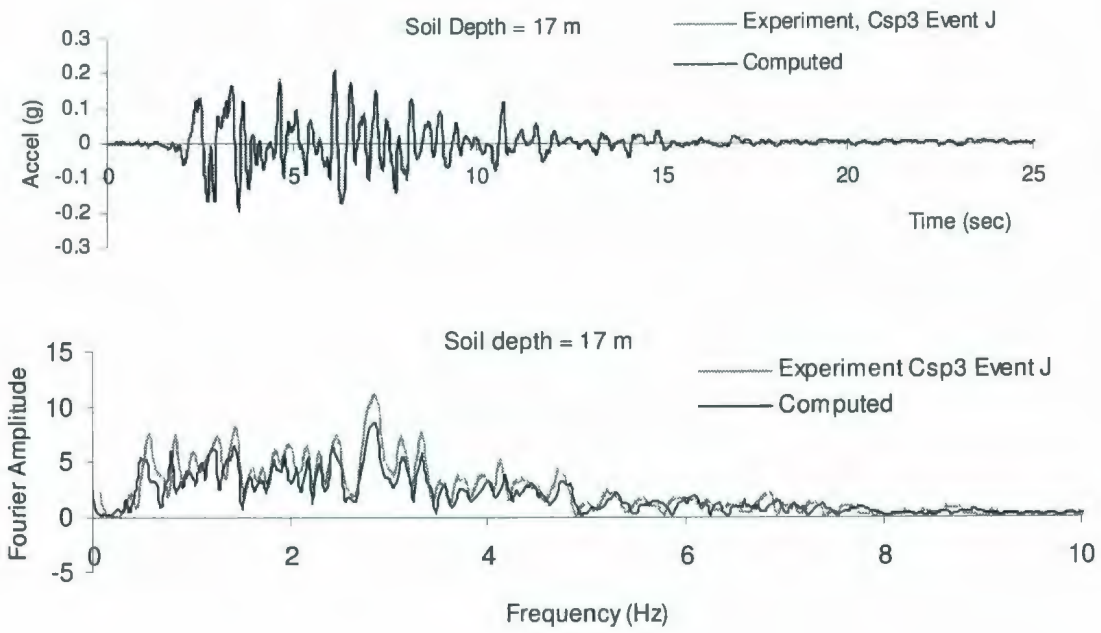


Figure 4.12: Horizontal Acceleration Time Histories and corresponding Fast Fourier Transform of Event J, Csp3 (soil depth, 17 m).

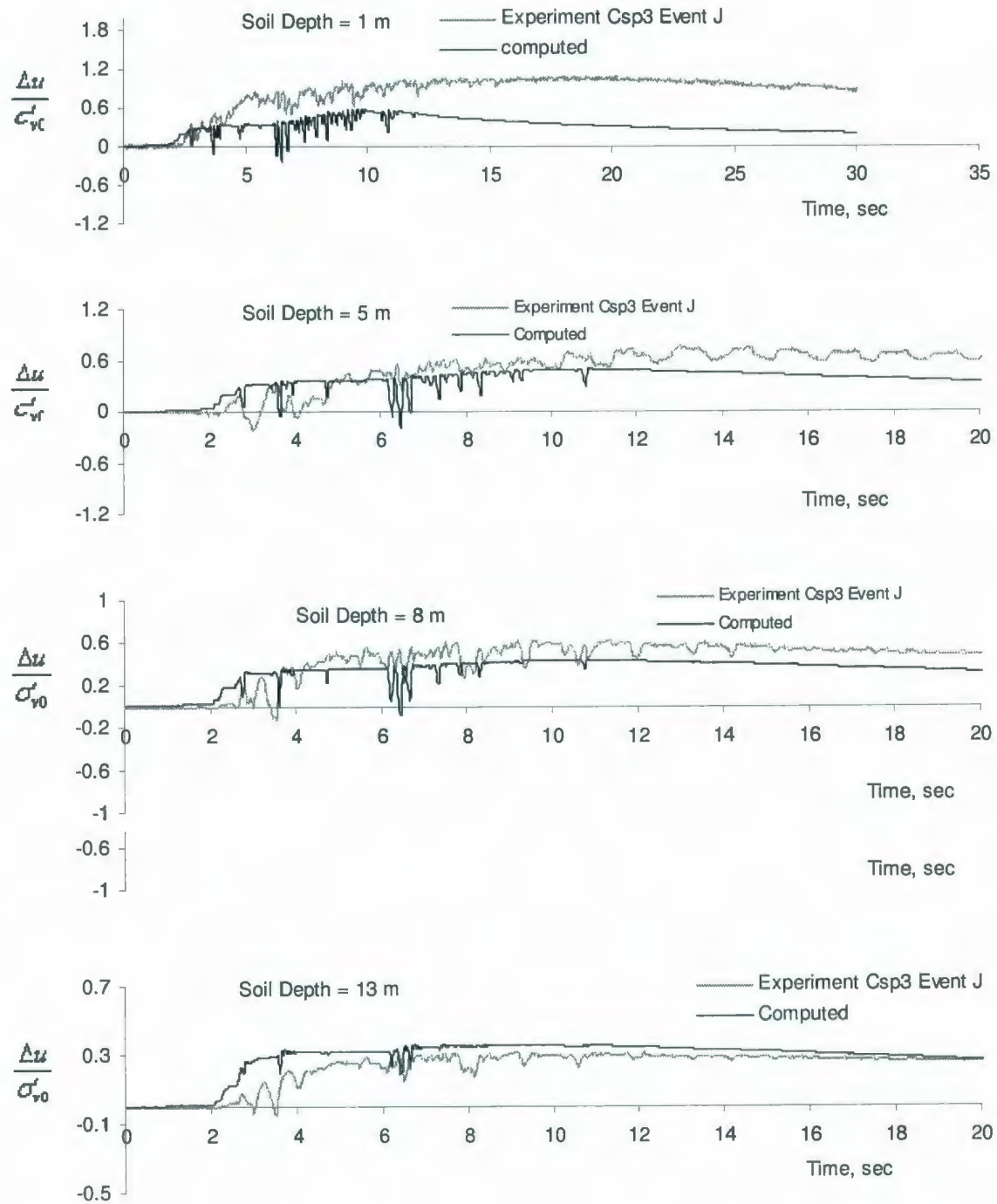


Figure 4.13: Excess Pore Water Pressure Time Histories of Event J, Csp3 (soil depths, 1 m to 13 m).

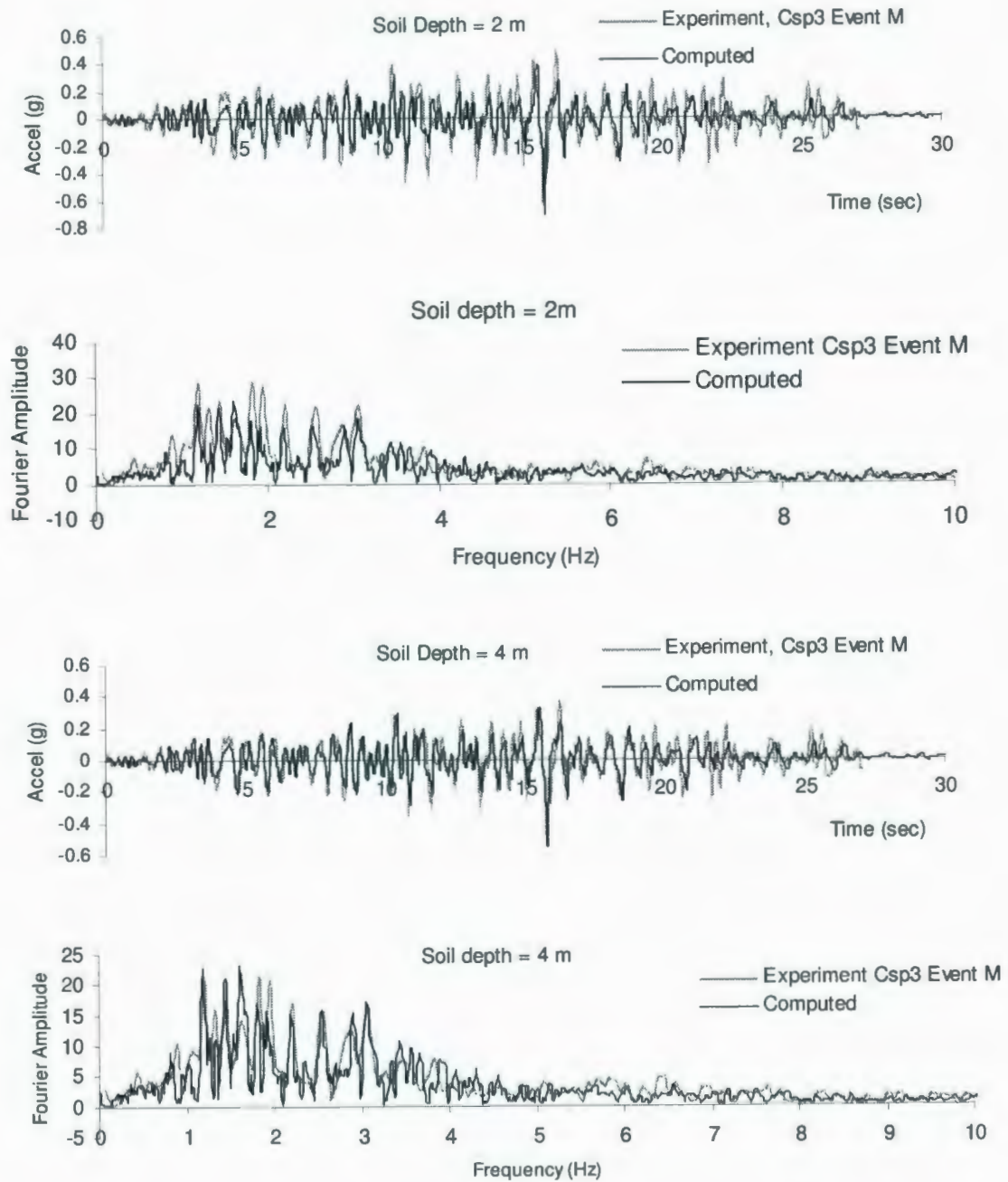


Figure 4.14: Horizontal Acceleration Time Histories and corresponding Fast Fourier Transform of Event M, Csp3 (soil depths, 2 m to 4 m).

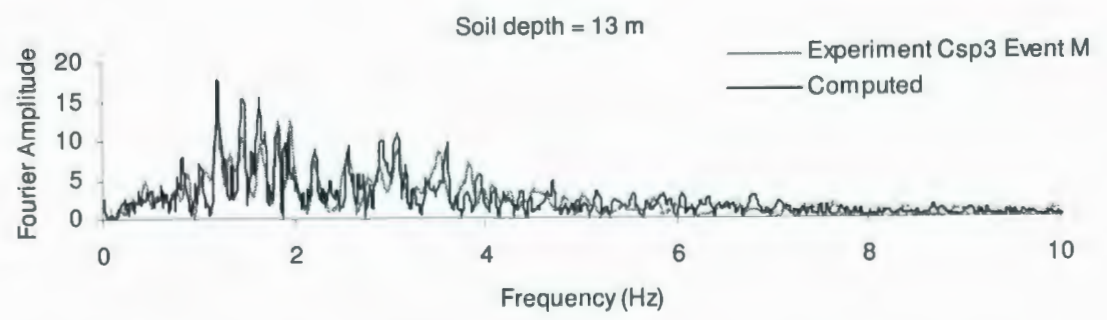
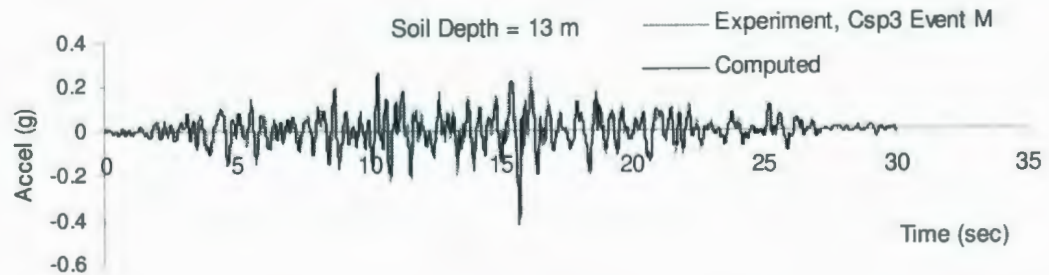
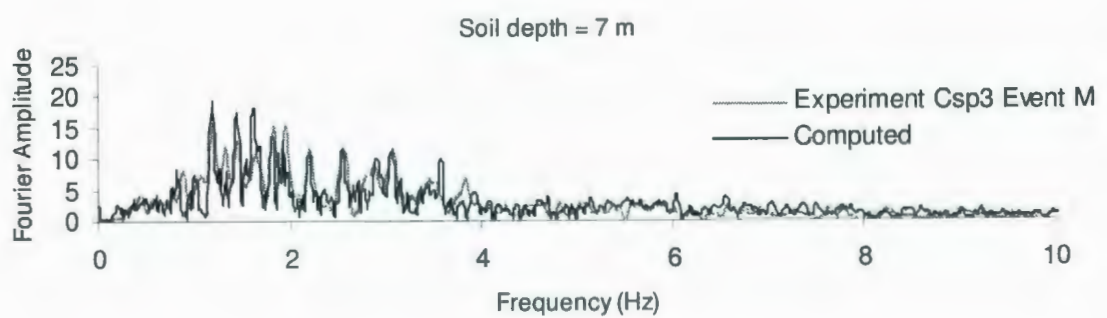
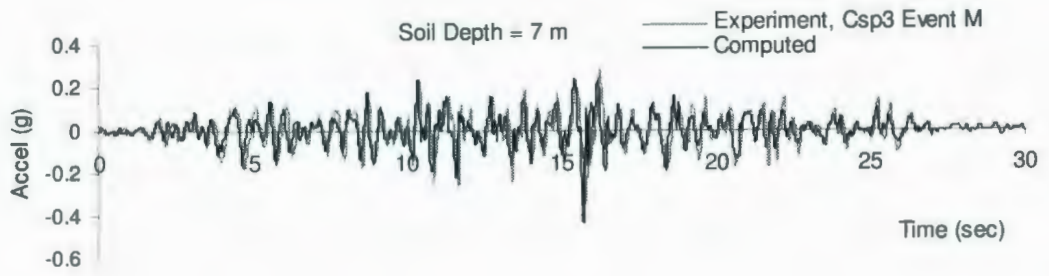


Figure 4.15: Horizontal Acceleration Time Histories and corresponding Fast Fourier Transform of Event M, Csp3 (soil depths, 7 m to 13 m).

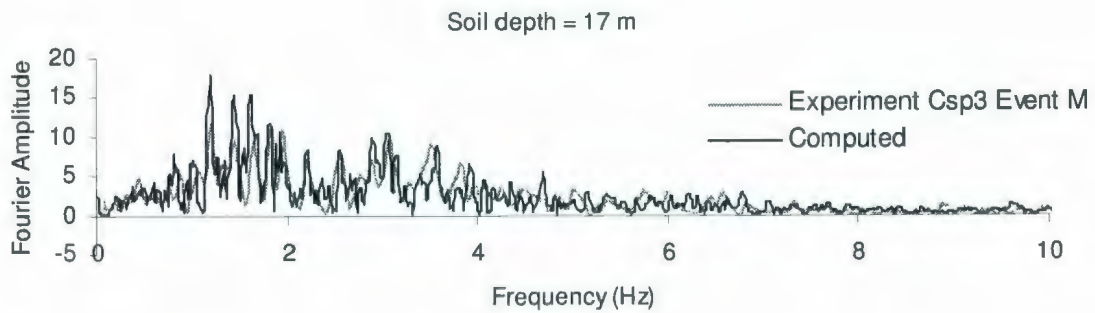
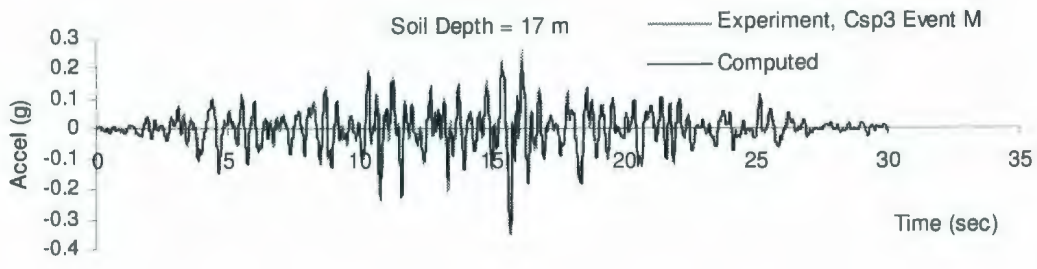


Figure 4.16: Horizontal Acceleration Time Histories and corresponding Fast Fourier Transform of Event M, Csp3 (soil depths 17 m).

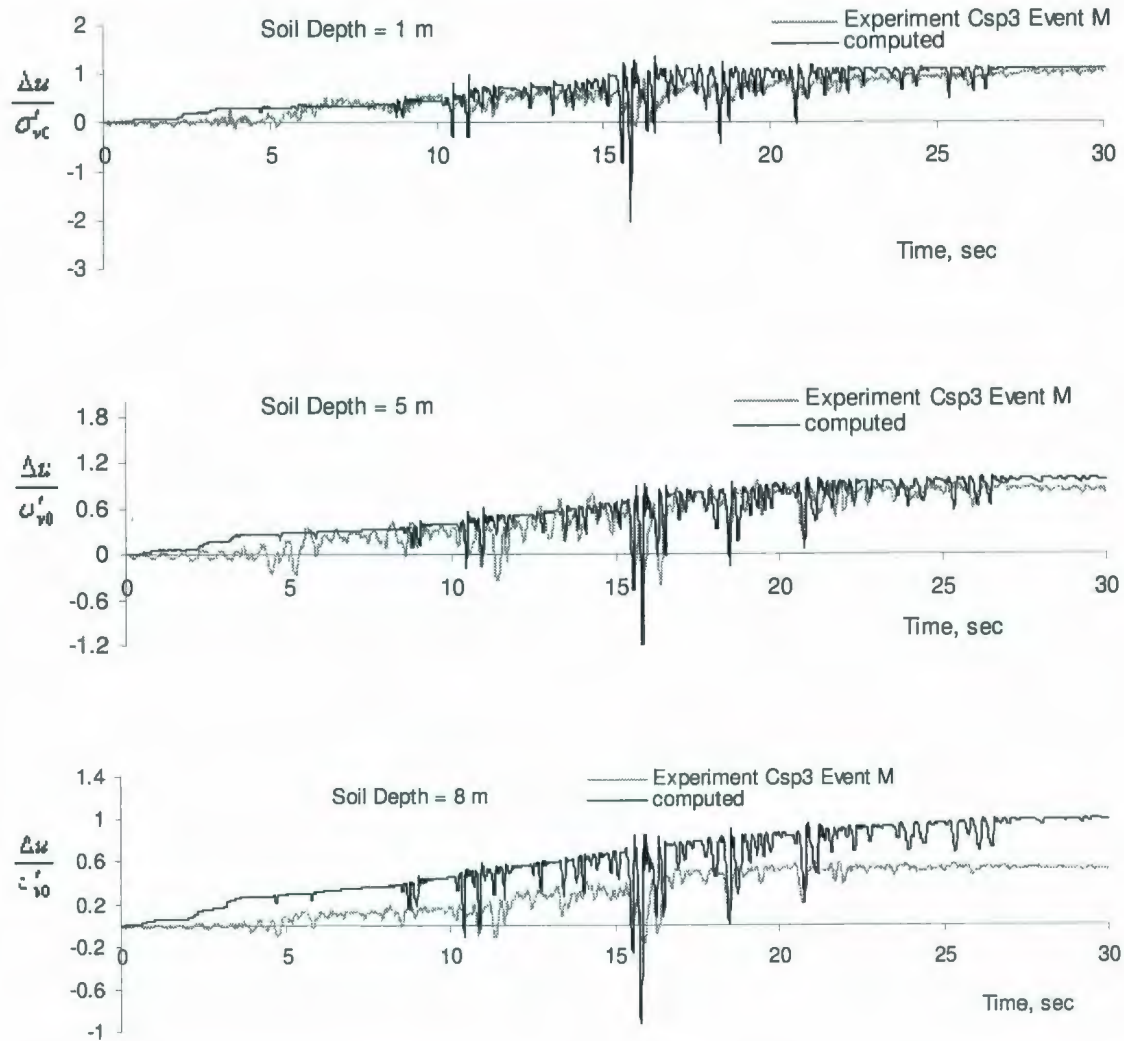


Figure 4.17: Excess Pore Water Pressure Time Histories of Event M, Csp3 (soil depths, 1 m to 8 m).

Figures 4.2-4.4 show the comparison of the recorded motions in event D of Csp2 tests with the motions computed by Cyclic1D software for soil layers with depths of 1-14 m. If we see FFTs (Fast Fourier Transform) of recorded acceleration time histories at soil layers with depths of 1-11 m (Figures 4.2-4.4), we find that the frequency components are concentrated between 1.5-2 Hz. The FFTs of computed motions at soil layers with depths of 1-8 m (Figures 4.2-4.3) also have major frequency components between 1.5-2 Hz and have amplitudes in good agreement with the experimental records. The

amplitudes of the Fourier spectra of the computed motions at soil layers with depths of 11-14 m (Figure 4.4) are in good agreement with recorded amplitudes in the range of 2.5-4 Hz. Low frequency components of the computed motions at soil layers with depths of 11-14 m fall between 0.5-2 Hz and are weaker in magnitude than those of recorded ones. The event D of Csp2 test was subjected to an acceleration record whose peak magnitude is 0.04 g. Non-linear stress-strain formula in Cyclic1D might have been unconservative in computing soil response to such a weak ground motion.

Figures 4.5-4.8 show the comparison of the recorded motions in event J of Csp2 tests with the motions computed by Cyclic1D software at soil layers with depths of 1-17 m. If we see FFTs of recorded acceleration time histories at soil layers with depths of 5-17 m (Figures 4.6 - 4.8), we find that the frequency components have ranged between 1.25-3 Hz. The FFTs of computed motions at soil layers with depths of 5-17 m (Figures 4.6-4.8) also have major frequency components between 1.25-3 Hz. The amplitudes of these frequencies are in good agreement with the experimental records. Although the FFTs of the computed motions at soil layers with depths of 1-3 m (Figure 4.5) have major frequency components between 1.5-2.5 Hz, the amplitudes are much higher than the recorded amplitudes. The recorded acceleration time histories in upper sections of the loose soil layer in event J of Csp2 test have experienced gradual de-amplification due to 100% liquefaction (Wilson et. al., 1998). This might have contributed to the differences between computed and recorded signals near in the ground surface.

Figures 4.10- 4.12 show the comparison of the recorded motions in event J of Csp3 tests with the motions computed by Cyclic1D software at soil layers with depths of 2-17 m. When FFTs of recorded and computed signals are compared along the soil profile, the frequency components of both recorded and computed signals have a predominant frequency in the range 2.25-3.5 Hz and are decreasing in magnitude at higher frequencies. Both the recorded and computed signals have peak energy at a frequency of 3 Hz.

Figures 4.14-4.16 show the comparison of the recorded motions in event M of Csp3 tests with the motions computed by Cyclic1D software at soil layers with depths of 2-17 m. When FFTs of recorded and computed signals are compared along the soil profile, the frequency components of both recorded and computed signals are concentrated between 1-3 Hz and decreasing in magnitude at higher frequencies.

Time histories of excess pore water pressure ratios at different layers of the soil profile of Csp2 for shaking event J are shown in Figures 4.9 and A-1. Agreement between predicted and experimental time histories of excess pore water pressure (EPWP) ratios is achieved very well for soil layers with depths of 1- 8 m (Figure 4.9). Agreement between predicted and experimental time histories of excess pore water pressure (EPWP) ratios is achieved reasonably well for the soil layer with a depth of 12 m (Figure 4.9). At 12 m depth (Figure 4.9), the computed response shows similar buildup of EPWP to those recorded during strong shaking phase of 1-16 s, but thereafter, the computed EPWP ratios have stayed at a ratio of 0.4 until the end of shaking phase whereas the recorded pore pressures has slowly increased up to 0.6 at the end of shaking phase. The coefficient of hydraulic conductivity for the lower dense sand in Cyclic1D model was 0.0001 m/s (Table 4.2) which might have been higher than the actual value of the centrifuge model. So, simulation shows a pattern of earlier dissipation immediately after strong shaking phase.

Time histories of EPWP ratios at different layers of the soil profile of Csp3 for shaking event J are shown in Figures 4.13 and A-2. All time histories reveal the same pattern; initial buildup of pore pressure, during strong shaking phase (2-8 s) and dissipation proceeding from the bottom up after strong shaking phase as the excess pore water pressure was expelled toward the ground surface. Agreement between predicted and experimental time histories of excess pore water pressure (EPWP) ratios is achieved reasonably well for soil layers with depths of 5-13 m. At 1 m depth of soil (Figure 4.13), simulation shows much lower EPWP ratios throughout the shaking phase. The computed responses all along the upper medium sand layer show a pattern of earlier dissipation than the experimental record indicating an overall higher input coefficient of hydraulic conductivity. Coefficient of hydraulic conductivity for the upper medium dense layer in

Cyclic1D model was 0.00015 m/s (Table 4.2) which might have been higher than the actual value of the centrifuge model. Another noticeable aspect of the computed responses is that, at soil layers with depths of 1-13 m (Figure 4.13), the computed responses show instantaneous drop in EPWP ratios similar to those recorded, denoting a tendency of dilation associated with corresponding negative spikes in the computed acceleration traces.

Time histories of EPWP ratios at different layers of the soil profile of Csp3 for shaking event M are shown in Figures 4.17 and A-3. In the upper sections of the soil layer (soil depths, 1-5 m), EPWP buildup in Cyclic1D is similar to the experimental record and gradually reaches 0.65 at the end of shaking phase. At the bottom of medium dense sand layer (soil depth, 8 m), simulation results show gradual buildup of EPWP almost exactly parallel to the experimental record throughout the shaking phase, reaching a ratio of 0.65 higher than the experimental counterpart as the shaking ends. Coefficient of hydraulic conductivity of the upper medium dense layer in Cyclic1D was 0.00015 m/s as compared to 0.0001 m/s for lower dense sand layer (Table 4.2). The difference between the coefficients of hydraulic conductivity of medium dense and dense sand layer as employed in Cyclic1D may not have been as high as it is in the experiment. This may be a reason of lower EPWP buildup in the recorded result at the interface between medium dense and dense sand layer (Figure 4.17).

Inspection of the computed time histories of EPWP ratios (Figures A-1, 2 and 3) reveals that the computed buildup in all three cases was higher than the recorded counterpart (especially in Figures A-2 and A-3). One possible explanation is based on an experimental fact that while the soil profile was assumed to be horizontal, the bucket of the centrifuge was actually inclined slightly resulting in permanent displacements of the soil profile (Wilson, 1998). This might be the reason for the lower recorded pore pressure below the dense sand layer. Unfortunately, this phenomenon can not occur in the Cyclic1D model as employed in the thesis since the magnitude of inclination was not reported in Wilson, (1998).

However, besides permeability coefficients, discrepancies between the computed and recorded pore pressures may also be due to the use of friction angles in Cyclic1D. Effective friction angles for loose and dense sand layers were reported in Wilson, (1998), but those were based on API, 1993 guidelines. The thesis used those values of effective friction angles for simulation purposes. Probably effective friction angles in Cyclic1D simulations may have been slightly higher than those present in the actual soil of Csp2 and Csp3 model resulting in slight higher rate of excess pore water pressure buildup in most Cyclic1D simulations relative to the experimental records.

4.7 Conclusion

In this paper, we have presented the efficient use of a computer program called Cyclic1D for performing one dimensional nonlinear seismic free field analyses of saturated sand deposits. The code Cyclic1D based on the multi yield soil plasticity model has shown to have the capability of generating seismic motions and excess pore water pressure at different layers of saturated sand with an acceptable degree of accuracy. It was concluded that the peak acceleration of the soil layers is predicted accurately by Cyclic1D for the events of moderate to strong excitations in Csp2 and Csp3 tests, where sand layers underwent liquefaction indicated by excess pore water pressures ratio approaching 1.0. For weak excitation, such as the event D of Csp2 test, where the generation of excess pore water pressure was not notable (Wilson et al., 1997 a), the effective stress based nonlinear Cyclic1D model underestimated free field all along the shallow soil profile. For strong motions, such as event J of csp2, Cyclic1D overestimated free filed motions near the surface of the soil profile. Despite such shortcomings, the Cyclic1D analysis method was found to be a computationally very inexpensive procedure for numerical prediction of seismic ground motion.

4.8 Acknowledgement

The authors are thankful to Dr. Elgamal, the University of California at San Diego for providing with Cyclic1D computer program. The authors gratefully acknowledge the receipt of centrifuge test data provided by Dr. Wilson, University of California at Davis.

Chapter 5

Evaluation of Seismic Lateral Response of a Pile in Saturated Sand

Co Authorship: Chapter 5 has been prepared in accordance with the regulations for a Manuscript format thesis stipulated by Faculty of Applied Science and Engineering at the Memorial University of Newfoundland, Canada and has been co-authored as:

Evaluation of Seismic Lateral Response of a Pile in Saturated sand, co-authored by Mohammad K. Talukder, Stephen D. Butt and Radu Popescu. A version of this paper is published in the refereed conference proceedings of the 1st International/1st Engineering Mechanics and Materials Specialty Conference, St John's, Newfoundland, May 28, 2009. Mohammad K. Talukder conducted the research and wrote the manuscript. Dr. Stephen D. Butt and Dr. Radu Popescu supervised the research, reviewed the manuscript.

5.1 Introduction

Earthquake design of pile supported infrastructure in seismic active areas is one of the most important parts of infrastructure design. Seismic soil pile interaction analysis is the main step in the evaluation of seismic behaviour of pile supported structures. Finite Element Methods provide powerful tools for conducting seismic nonlinear soil-pile interaction analyses. Continuum Finite Element Methods treat the soil as a continuum medium. The main advantage of this approach is the capability of performing the soil-pile interaction analysis in a coupled manner (El Naggar & Bentley, 2000), without resorting to separate site response analysis. However, this method is not commonly used in design offices mainly due to their excessive computational time and complicated formulation. The dynamic beam on Nonlinear Winkler Foundation (BNWF) method is a simplified approach that can account for nonlinearity in soil-pile interaction analysis. It is commonly used in professional engineering practices as it demands less computation time. El Naggar et al. (2005) used BNWF model for piles subjected to lateral seismic excitation. The p-y curves approach is a widely accepted method for predicting pile response under static loads because of its simplicity and practical accuracy. In BNWF models, soil stiffness is established using p-y curves while damping is established from analytical or empirical solutions to simulate energy dissipation through wave propagation

in the soil (El Naggar et al. 2005). El Naggar et al. (2005) implemented nonlinear springs based on p-y curves and dashpots in parallel to represent radiation damping in BNWF model. They chose soil conditions where both saturated clay and sand in the centrifuge box did not liquefy during seismic excitation. Boulanger et al. (1999) developed a BNWF model utilizing springs in series with dashpots representing radiation damping and used the model to analyze dynamic response of single-pile-supported structures in saturated clay overlying dense sand (relative density, 80%). The results computed by them were in good agreement with experimental centrifuge tests of carried out by Wilson et al. (1997a, b). However, the nonlinear p-y formulation in Boulanger et al. (1999) is complicated and heavily dependent on several parameters.

The main objective of this study is to introduce a simplified practical BNWF model using the general finite element code ABAQUS (version 6.7). This model can be readily used for capturing the soil-pile-interaction effects observed in saturated sand during dynamic centrifuge tests. This thesis gives special attention to the evaluation of free field excitation where saturated sand is concerned.

5.2 Pile-Soil Interaction Analysis with BNWF Models

BNWFs model in dynamic analysis should allow for the variation of soil properties with depth, nonlinear soil behavior and energy dissipation through damping mechanism. Therefore, proper analysis of the seismic response of piles involves modeling the pile and surrounding soil along with damping effects. While performing seismic response analysis, free field ground motion time histories are usually computed in a separate site response analysis (El Naggar et al. 2005). The computed ground motion at different depths of sand is then applied to the free nodes of spring-dashpot pairs of the BNWF model as support motions. Figures 5.1 and 5.2 show the schematic view of Dynamic BNWF model with its components for simulation of a single pile in saturated sand.

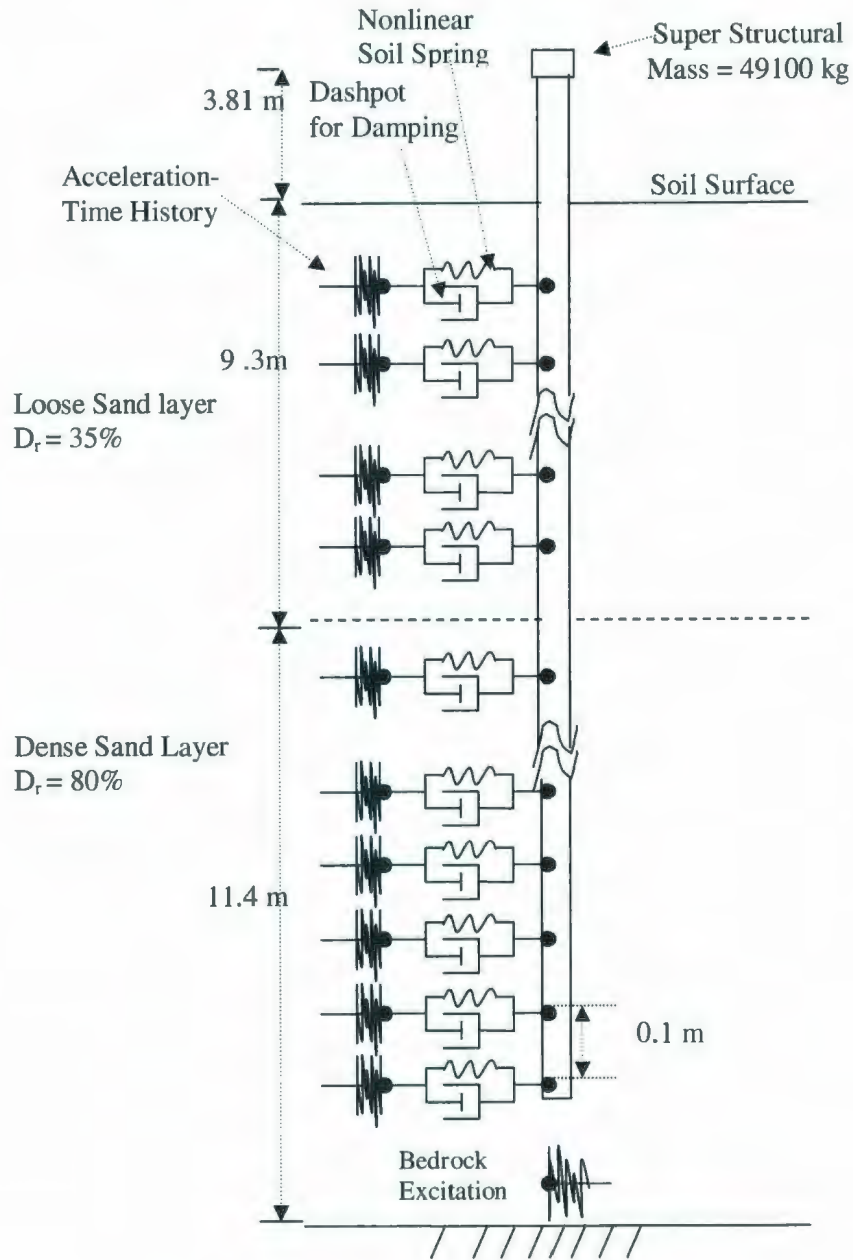


Figure 5.1: Schematic diagram of BNWF model for simulation of Csp2 using ABAQUS.

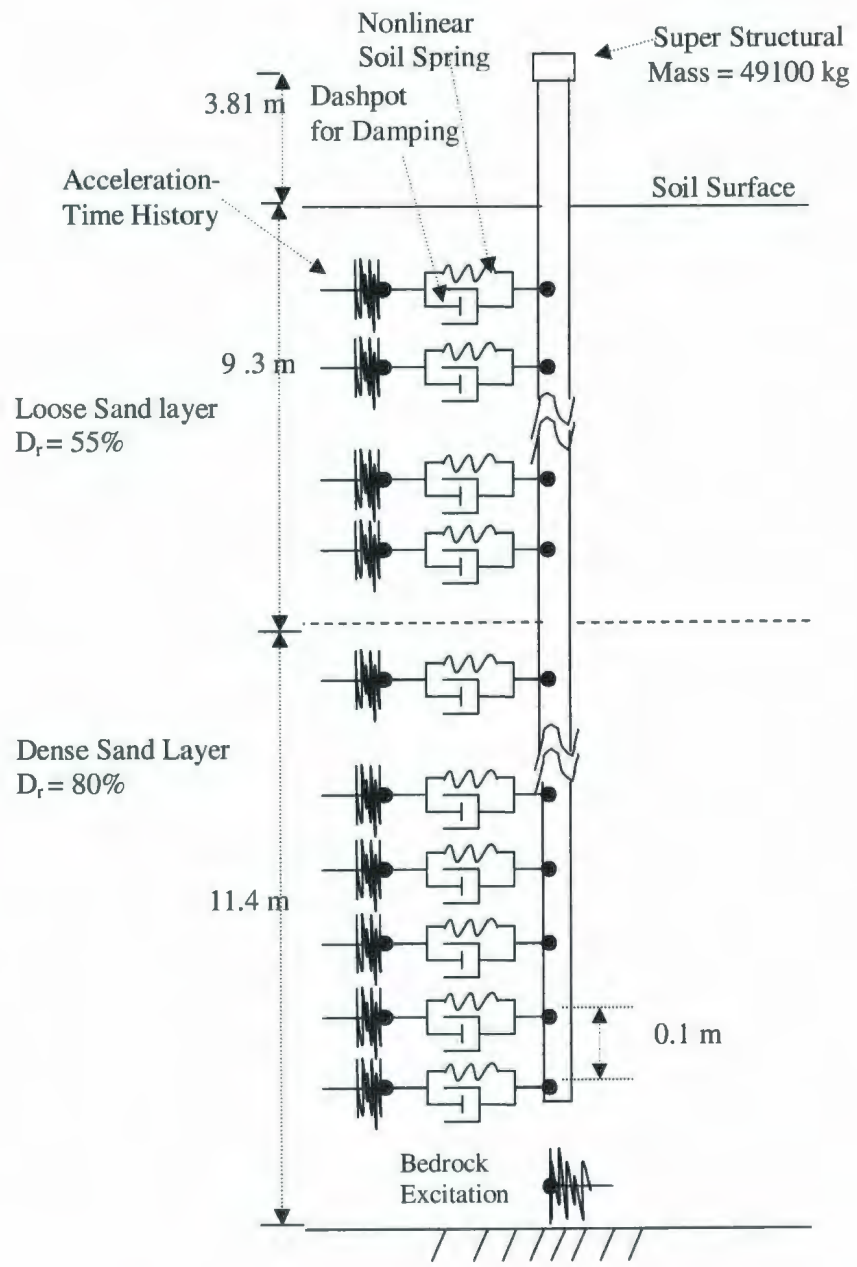


Figure 5.2: Schematic diagram of BNWF model for simulation of Csp3 using ABAQUS.

5.2.1 Pile Modeling

The single-pile-supported structure, SP1 was the most heavily instrumented of the structural models used in Csp2 and Csp3 tests (Wilson et al. 1997a, b) and is the only structure analyzed herein. The prototype steel pipe pile has an outer diameter of 0.67 m and a wall thickness of 19 mm. It supports a superstructure load 49,100 kg at about 3.81 m above soil surface. The pile and surrounding soil are subdivided into a number of discrete layers. Subdivision of a pile is done by defining a single pile into a number of elastic finite elements while subdivision of soil surrounding the pile was done by employing soil springs whose stiffness increases with depth. Pile response is traced independently at nodal points of the pile elements. In the present study, the pile was modeled by joining 206 elastic "PIPE21" elements of ABAQUS element library at nodal points. Length of each element in the present BNWF model is 0.10 m. The Finite Element model of the pile has 207 nodes. 165 nodes are below ground surface. Pile nodes below ground surface are connected to spring-dashpot pairs on one side of the pile (Figure 5.1). Elastic young's modulus and density of steel pile material was of 200 GPa and 7800 kg/m³ respectively.

5.2.2 Soil Stiffness Modeling

The soil profile in centrifuge models (Wilson et al., 1997a, b) consisted of two horizontal layers of saturated fine graded Nevada sand (Wilson et al. 1998). In the present study, stiffness of soil spring is modeled by employing API (2000) recommended static p-y curves. Currently available p-y curve recommendations are based on static and cyclic lateral load tests, and are not necessarily applicable to seismic loading conditions as the tests did not necessarily excite the mechanisms involved in seismic loading. Equation 5.1 below represents p-y curves computed for soil profile of Csp2 and Csp3:

$$p = AP_u \tanh\left(\frac{kz}{AP_u} y\right) \quad (5.1)$$

where A is 0.9 for pile under cyclic loading, p is unit soil reaction (kPa), P_u is ultimate soil strength (kPa), z is depth of soil (m) from ground surface, y is pile displacement (m) and k is initial modulus of subgrade reaction (kN/m³). Equation 5.1 is modified version of Equation 2.3. P-y curves for sand layers begin from the origin of axes (Figure 5.3) and

hence the slope of the curve up to the point of first yield is considered initial stiffness of the soil layer.

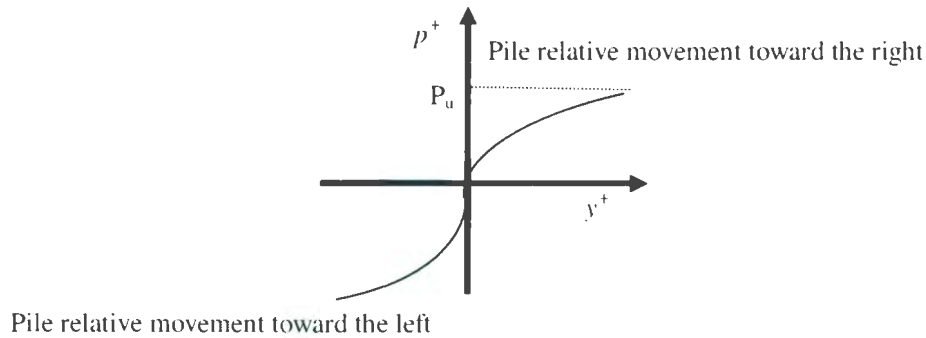


Figure 5.3: Schematic p-y curve for calibration of soil springs of BNWF model.

Soil characteristics used for generation of p-y curves are shown in Table 3.3. API p-y model does not take into consideration the possible shear stresses between the soil and the sides of the pile. In this study it is assumed that each pile element is acted upon by a uniform horizontal stress p , which is constant across the width of the pile. It is also assumed that the soil at the back of the pile adheres to the pile when it moves from one direction to the other due to seismic excitation.

5.2.3 Calibration of Soil Stiffness Model

In API (2000); the ultimate soil resistance is taken as minimum of the values given by Equation 5.3 and 5.4:

$$P_u = A(C_1 z + C_2 B) \gamma' z \quad (5.3)$$

$$P_u = AC_3 B \gamma' z \quad (5.4)$$

where C_1, C_2 and C_3 are coefficients dependent on the soil angle of internal friction, z is depth of soil from ground surface (m); γ' is effective unit weight of soil (kN/m^3); B is

pile diameter (m). The parameters C_1, C_2 and C_3 depend on the soil angle of internal friction. Values of C_1, C_2 and C_3 can be determined from the chart shown in Figure B-1 of appendix B. Initial modulus of subgrade reaction k is calibrated from the chart shown in Figure B-2 of Appendix B.

Representative p-y curves computed by following API (2000) are shown for Csp2 and Csp3 soil profile in B-1 and 5.7. It can be noted from Figures B-3 and B-4 of appendix B that API based monotonic p-y curve is continuous and differentiable at all points. The curve has an initial gradient at very small displacements and has zero gradients at ultimate stress. Therefore, it satisfies basic properties of monotonic nonlinear force displacement curve.

5.2.4 Pile Material Damping

The Raleigh approach is used to evaluate the material damping of pile elements:

$$[C] = \alpha[M] + \beta[K] \quad (5.4)$$

where $[C]$ is the material damping matrix of the pile foundation system; $[M]$ is the mass matrix of the pile foundation system; $[K]$ is the stiffness matrix of the pile foundation system; and α and β are damping coefficients.

The damping coefficients α and β are determined from unique specified damping ratio ξ for both i th and j th modes of vibrations, as follows:

$$\alpha = \xi \frac{2\omega_i\omega_j}{\omega_i + \omega_j} \quad (5.5)$$

$$\beta = \xi \frac{2}{\omega_i + \omega_j} \quad (5.6)$$

In Equations 5.5 and 5.6, ω_i and ω_j are the natural frequencies (rad/sec) of the i th and j th modes of vibrations respectively, and ξ is the material damping ratio assumed for all modes of vibration of the pile. Different values of ξ has been chosen for this study to better estimate the pile peak bending moments.

5.2.5 Modeling Radiation Damping of Soil

El Naggar et al. 2005 modeled the damping force generated in saturated clay and Nevada sand during seismic event by a coefficient established as shown below:

$$c = 4B\rho_s V_s \quad (5.7)$$

where B is pile diameter, ρ_s is the mass density of soil and V_s is the shear wave velocity in soil. Equation 5.7 is first proposed by Berger et al. (1977). Shear wave velocity needs to be determined for modeling radiation damping in dynamic analysis. Radiation damping that occurs as dynamic forces in the pile cause the soil to deform, producing stress waves that travel away from the foundation. Hardin and Drnevitch (1972) related small strain shear stress modulus G_{\max} (psi) to confining pressure σ'_m (psi) as shown below:

$$G_{\max} = \rho V_s^2 \quad (5.8)$$

where G_{\max} is low strain shear modulus of sand (psi) and ρ is the bulk density of soil. Equation 5.8 can be modified for sand with the help of Equation 2.3 as shown below:

$$1230 \frac{(2.973 + e_0)^2}{1 + e_0} (\sigma'_m)^{0.5} = \rho V_s^2 \quad (5.9)$$

where e_0 is initial void ratio of sand. Equation 5.9 was used to calculate shear wave velocity of sand layers. Shear wave velocity calculated for different layers of Csp2 and Csp3 models are shown in Figures B-5 and B-6 of appendix B. Dashpot coefficients based on Equation 5.7 are assigned to linear dashpots of “CONN2D2” element for modeling radiation damping of sand.

5.3 ABAQUS Methodology in BNWF Model

A “CONN2D2” element of the ABAQUS library adjoins nonlinear springs and linear dashpots in parallel (Figures 5.1 and 5.2) and is a unidirectional two noded connector element. One end of each “CONN2D2” element connects a pile node and the other node is assigned with acceleration time histories. Only axial capacity of this element was used for current analysis. P-y curves are assigned to nonlinear springs of “CONN2D2” elements (Figure 5.3). El Naggar et al. (2005) used a similar approach in nonlinear pile-

soil interaction analyses and the calculated response of the pile was in good agreement with centrifuge test results. Horizontal seismic acceleration causes the pile to move back and forth in horizontal direction creating tension in sand on one side of the pile while creating compression in sand on the other side. As gap formation does not occur in the vicinity of pile, so no interface element was used between the pile node and soil spring. Lumped mass of the superstructure is modeled using element type "MASS" from ABAQUS element library. "MASS" is a point element that is attached to the top of pile in ABAQUS model. In the present study, two dimensional dynamic response analyses of the pile have been carried out and hence all element capabilities are set to two dimensional modeling only. A modal superposition method is used to implement a transient dynamic analysis procedure. Transient modal dynamic analysis gives the response of the pile as a function of time based on a given time-dependent loading. As vibration of a single vertical pile is dominated by the first few modes of the total modes of vibration so the first 100 modes of vibrations are extracted. Each of these modes is assigned with the same pile material damping ratio in any analysis. Forcing function in the centrifuge tests performed by Wilson et al. (1997a, b) is a seismic record in which acceleration values are given every 0.015 s. In the present study, it is assumed that the acceleration varies linearly between any two consecutive time increments of experimental record. The time increment used for seismic loading in the modal dynamic procedure is 0.015 s which is the same one used in the experimental base acceleration. Influence of time increment on the prediction of dynamic pile behavior was verified by considering three different time steps such as 0.005, 0.01 and 0.02 s. Superstructure lateral deflections of the pile due to seismic motion in Event D of Csp3 for these three different time steps are shown in Figures B-7 to B-9 of Appendix B. The result of the analysis with time increment 0.005 s was close to the other two analyses involving 0.01 and 0.02 s as can be noted in Table 5.1.

Table 5.1: Verification of effect of time step used in ABAQUS analyses.

Centrifuge Test	Shaking Event	Time step used for ABAQUS analyses	Predicted Superstructure displacement (mm)
Csp3	D (0.04g)	0.005	3.315
		0.01	3.306
		0.02	3.271

Following this comparison, all analyses in this study have been performed with time step 0.015 s. For a 35 s earthquake with 0.015 s time increment, the modal dynamic analysis of current BNWF model would last approximately 20 minutes on an Intel Pentium 1.66 GHz computer.

5.4 Free Field Excitation

Computer codes SHAKE and NERA are widely used for free field ground motion analyses. SHAKE is an equivalent linear while NERA is a nonlinear time domain approach to predict seismic ground response. Boulanger et al. (1999) and El Naggar et al. (2005) used SHAKE and NERA respectively for free field analyses. The results of such free field analyses are then used as the input excitations to the free end of “CONN2D2” elements placed in different layers of soil. However, results from these two well known softwares often do not agree well with the recorded motions since they are capable of performing total stress based analysis. Especially in a case, where cohesionless saturated soil is concerned, one must use effective stress based free field analysis methods that can generate both pore pressure and acceleration time histories.

In this study, a fully coupled finite element code called Cyclic1D (Elgamal et al. 2006) is used for prediction of unknown acceleration time histories at any depth in sand of Csp2 and Csp3 models (Talukder and Butt, 2009). Cyclic1D being based on soil plasticity constitutive model (Elgamal et al., 2002), can compute ground motions at any depth of soil due to earthquake excitations at the bed rock level of two dimensional Finite Element Models of soil strata. Seismic motion induces shear strain in sand. This model considers

energy dissipation through material and stiffness proportional damping of soil by controlling the accumulated cycle by cycle shear deformations in sand during earthquake (Elgamal et al., 2002). Recorded acceleration time histories in Events D, J of Csp2 and J, M of Csp3 were compared with motions predicted by Cyclic1D Finite Element model. Further details regarding prediction of input motions with Cyclic1D are given in Chapter 4. The acceleration time histories obtained from Cyclic1D analyses were applied to the free nodes of "CONN2D2" elements as input motions (Figures 5.1 and 5.2).

5.5 Comparison of Numerical and Experimental Results

Performance of superstructure segment of the BNWF finite element model developed in this study are presented by showing computed response parameters of the model in terms of time histories of superstructure displacement, super structure acceleration, pile head acceleration and bending moments. The response of the present BNWF model was computed for all 11 earthquake events listed in Table 3.1 and 3.2. Comparisons of the calculated and recorded responses for the structural model for $\xi = 5\%$ are shown in Figures 5.4 to 5.39 and B-10 to B-72.

Coincidence factor denoted by CF in all figures is a ratio of experimental magnitude of response quantity (superstructure displacement, acceleration or bending moments) at any time step to those of the BNWF model. If any average of five values of CF over five consecutive time steps falls in a range of 0.75 and 1.25, it was plotted to show good correlation between the computed and experimental response quantities.

It is notable in Figures 5.4 to 5.39 that the occurrence of computed peak values of response quantities (peak pile head accelerations, peak superstructure accelerations, peak superstructure displacements and peak pile bending moment) is at about the same time of the occurrence of experimental peak responses. Chapter 6 compares the computed peak responses of the BNWF model with experimental peak responses of the pile.

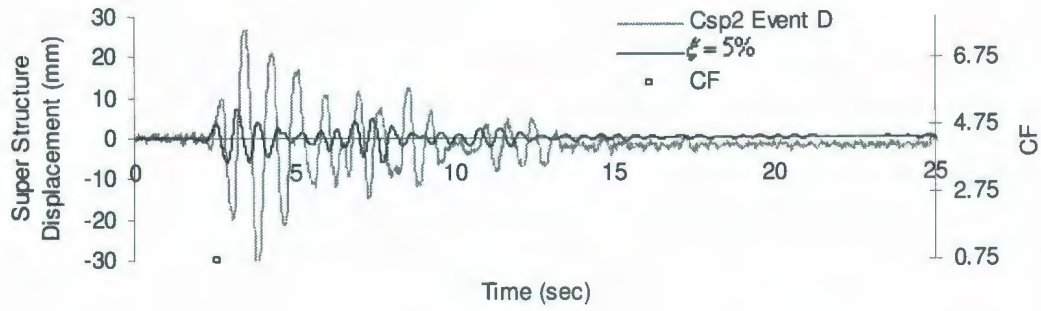


Figure 5.4: Comparison of Superstructure Displacement Time History for Event D, Csp2.

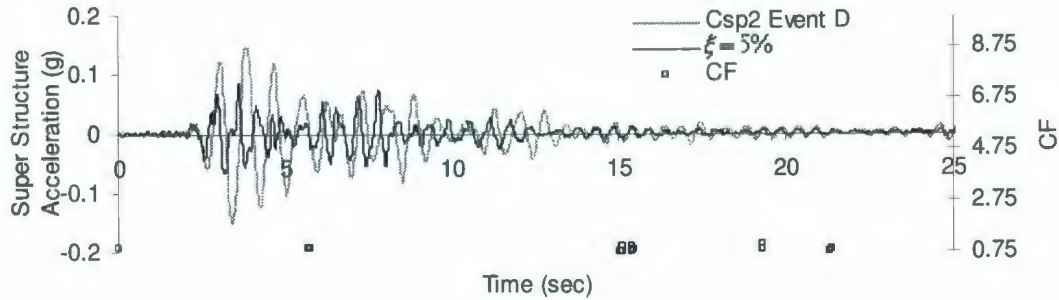


Figure 5.5: Comparison of Superstructure Acceleration Time History for Event D, Csp2.

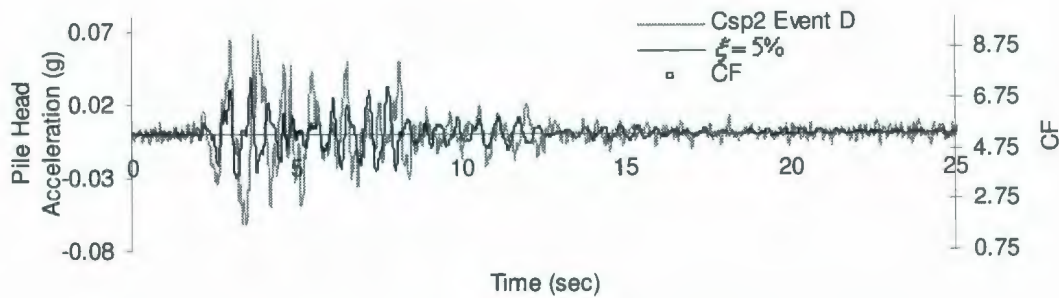


Figure 5.6: Comparison of Pile Head Acceleration Time History for Event D, Csp2.

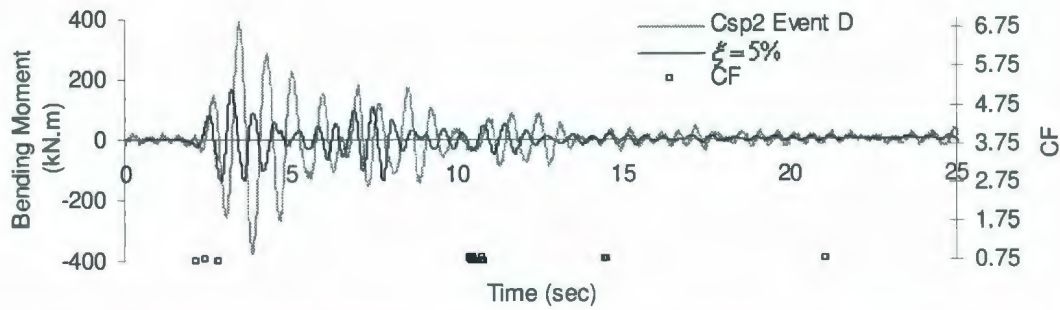


Figure 5.7: Comparison of Bending Moment Time History for Event D, Csp2 at soil depth 0.5 m.

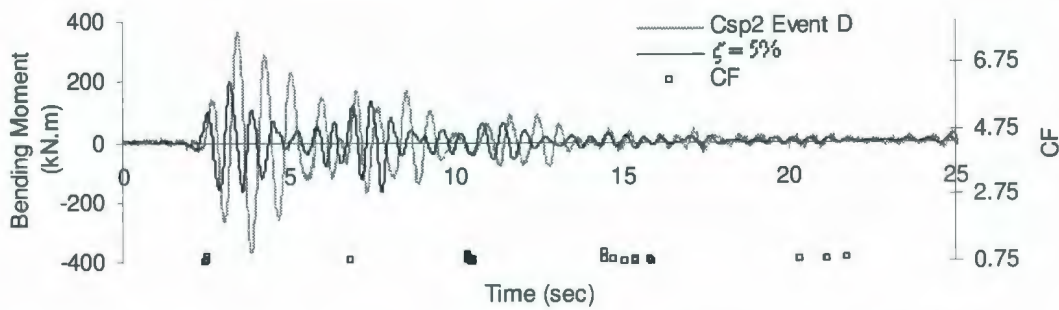


Figure 5.8: Comparison of Bending Moment Time History for Event D, Csp2 at soil depth 1.5 m.

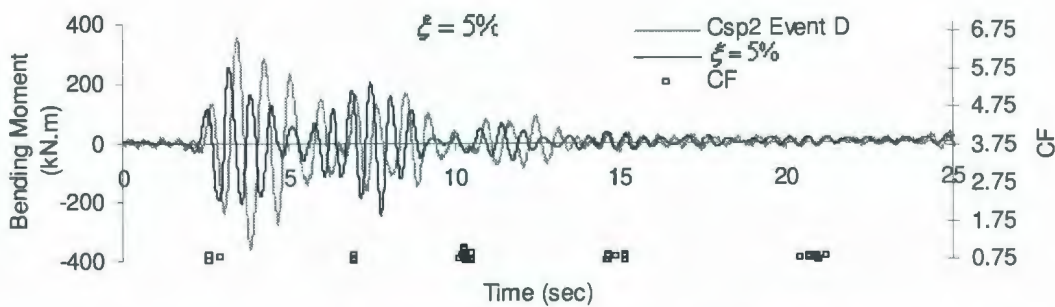


Figure 5.9: Comparison of Bending Moment Time History for Event D, Csp2 at soil depth 2.5 m.

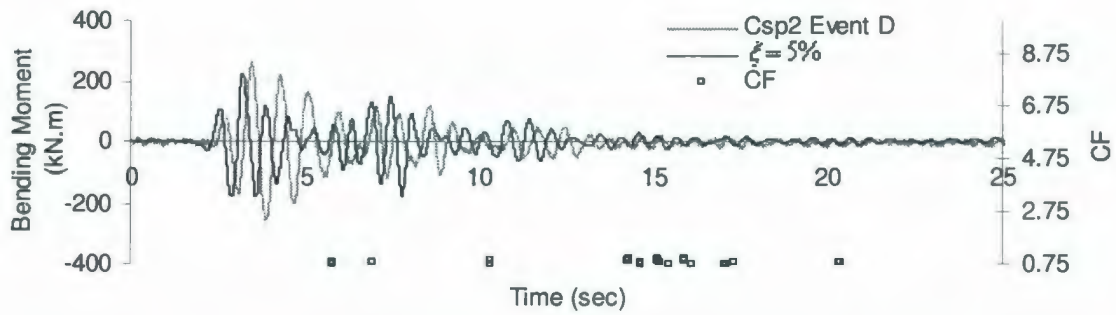


Figure 5.10: Comparison of Bending Moment Time History for Event D, Csp2 at soil depth 4.0 m.

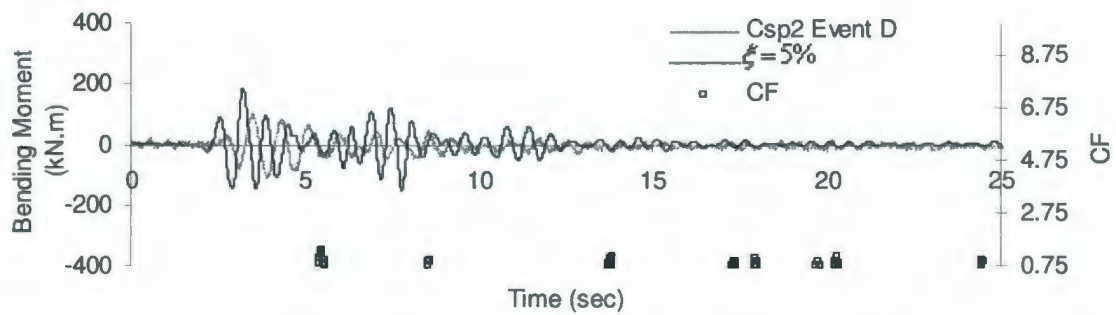


Figure 5.11: Comparison of Bending Moment Time History for Event D, Csp2 at soil depth 5.5 m.

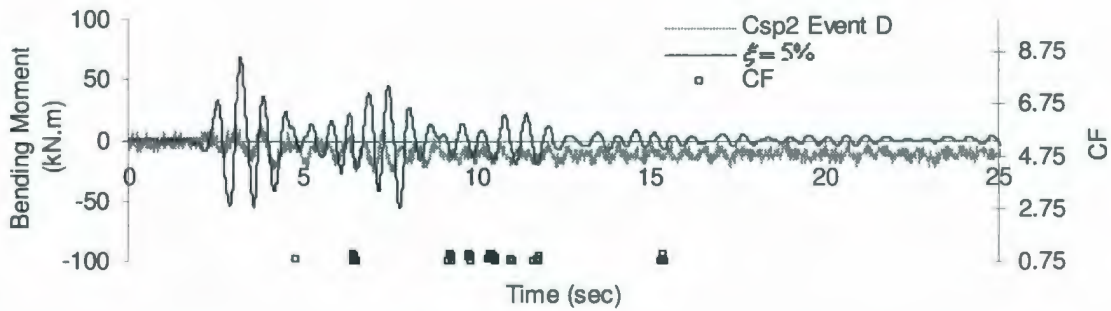


Figure 5.12: Comparison of Bending Moment Time History for Event D, Csp2 at soil depth 8.5 m.

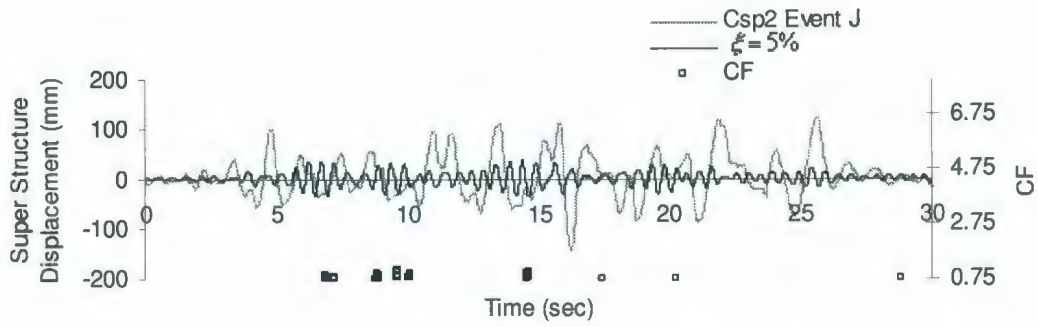


Figure 5.13: Comparison of Superstructure Displacement Time History for Event J, Csp2.

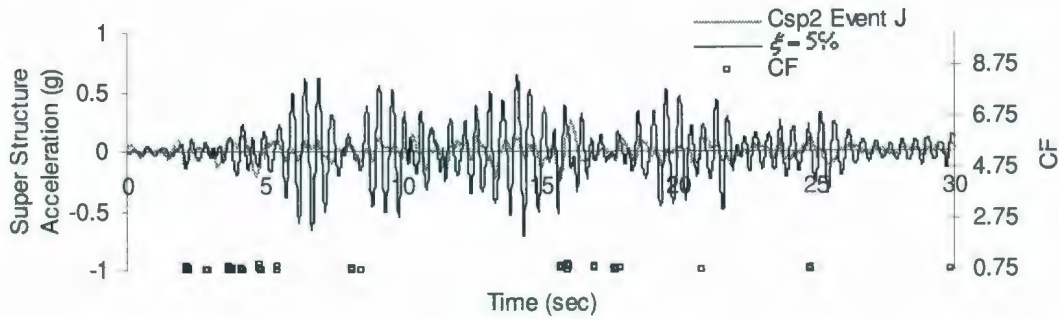


Figure 5.14: Comparison of Superstructure Acceleration Time History for Event J, Csp2.

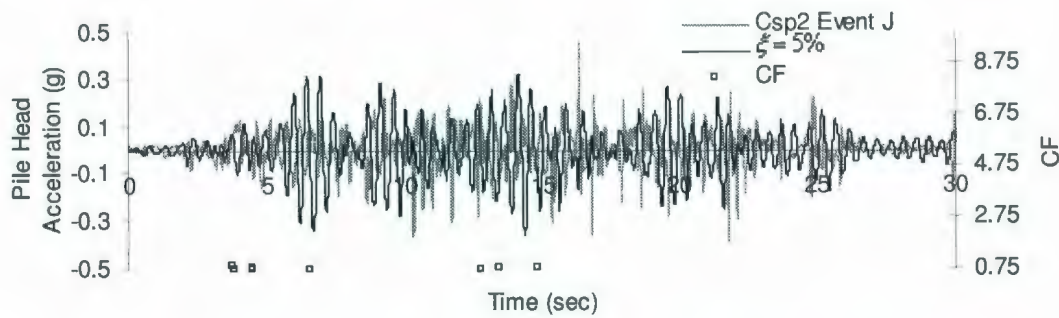


Figure 5.15: Comparison of Pile Head Acceleration Time History for Event J, Csp2.

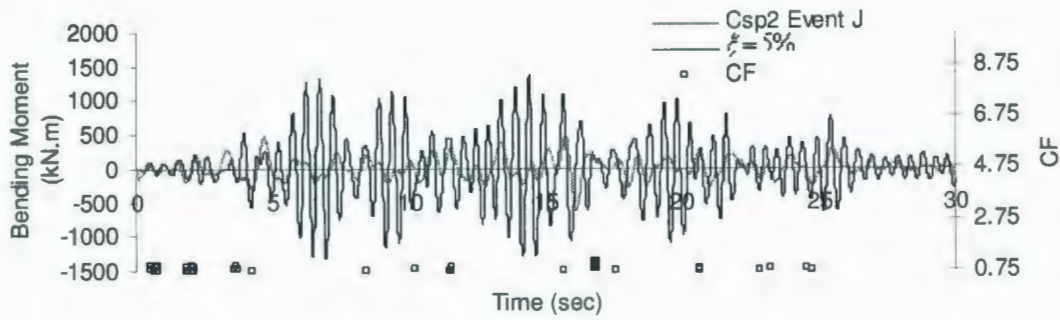


Figure 5.16: Comparison of Bending Moment Time History for Event J, Csp2 at soil depth 0.5 m.

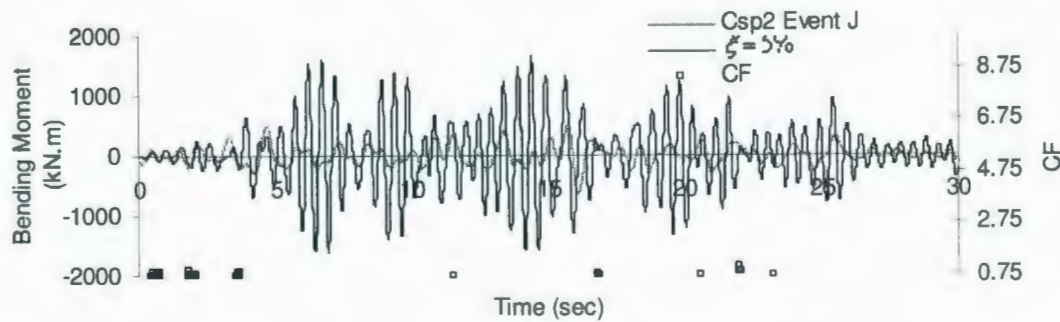


Figure 5.17: Comparison of Bending Moment Time History for Event J, Csp2 at soil depth 1.5 m.

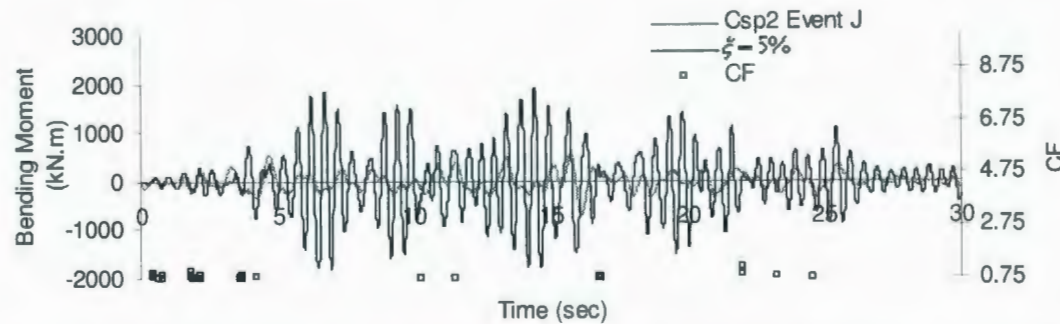


Figure 5.18: Comparison of Bending Moment Time History for Event J, Csp2 at soil depth 2.5 m.

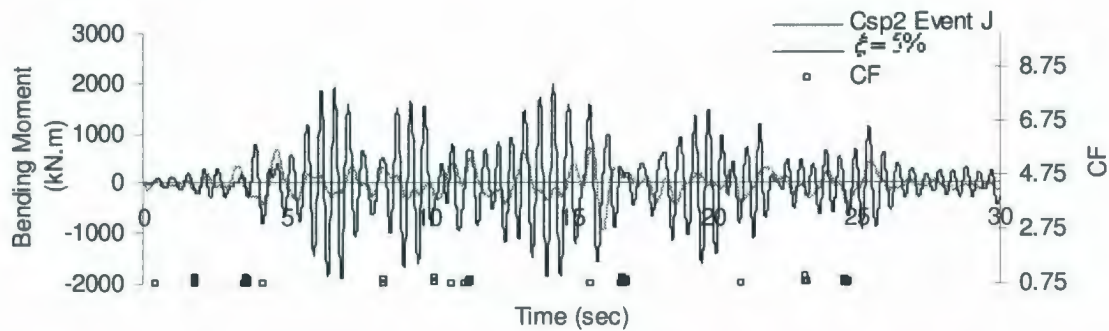


Figure 5.19: Comparison of Bending Moment Time History for Event J, Csp2 at soil depth 4.0 m.

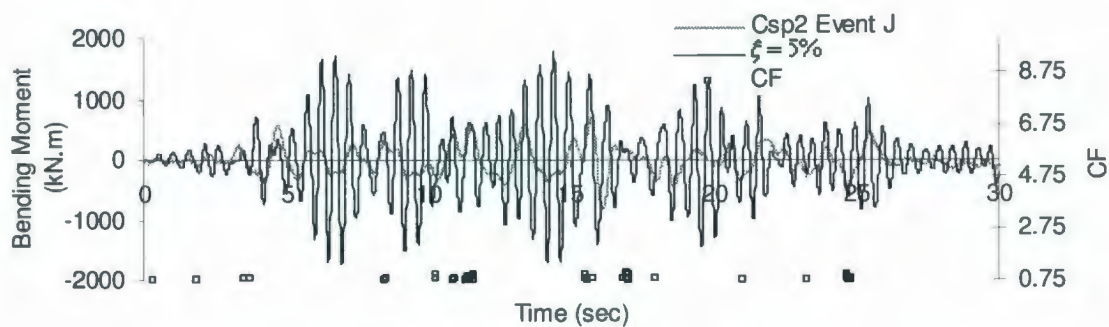


Figure 5.20: Comparison of Bending Moment Time History for Event J, Csp2 at soil depth 5.5 m.

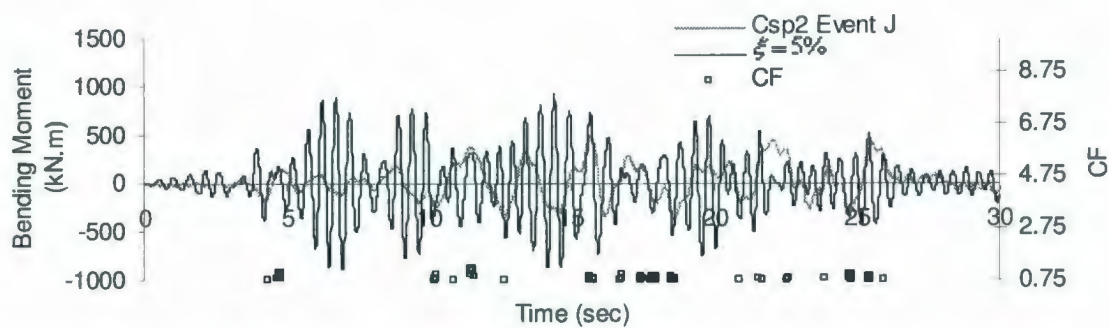


Figure 5.21: Comparison of Bending Moment Time History for Event J, Csp2 at soil depth 8.5 m.

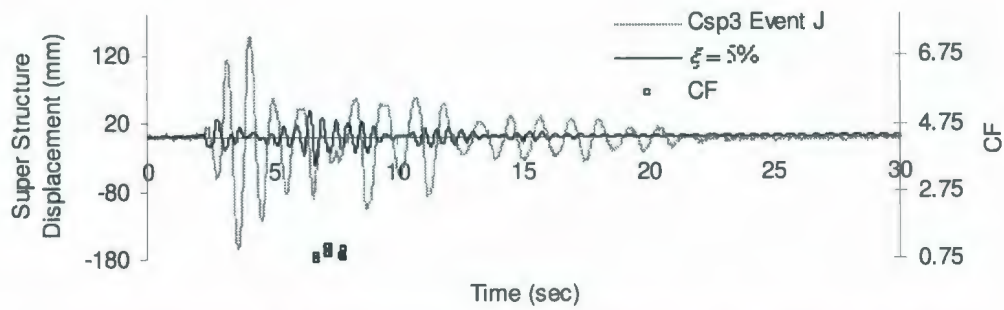


Figure 5.22: Comparison of Superstructure Displacement Time History for Event J, Csp3.

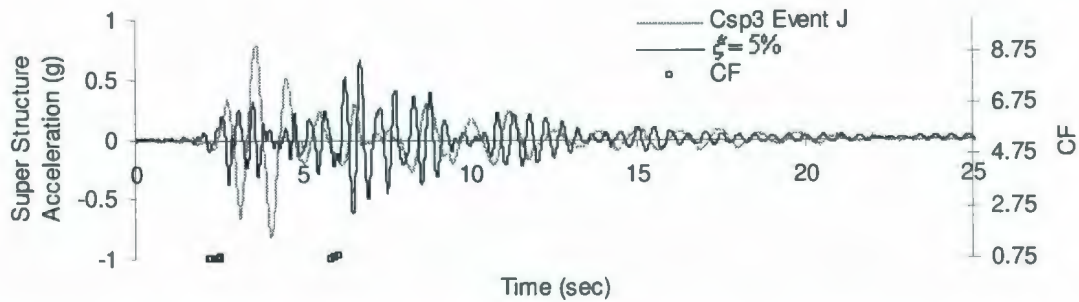


Figure 5.23: Comparison of Superstructure Acceleration Time History for Event J, Csp3.

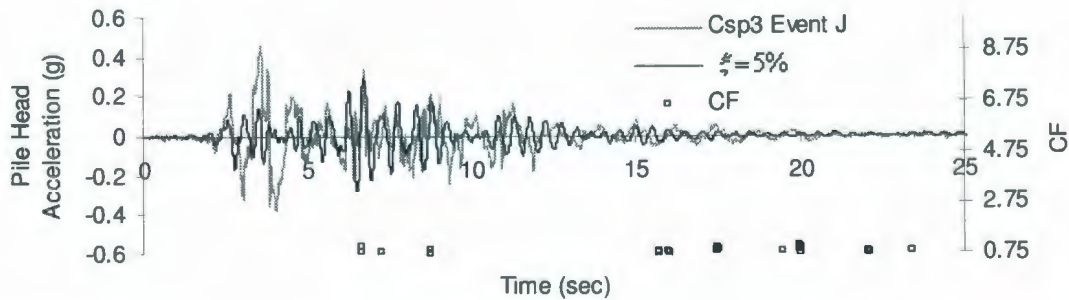


Figure 5.24: Comparison of Pile Head Acceleration Time History for Event J, Csp3.

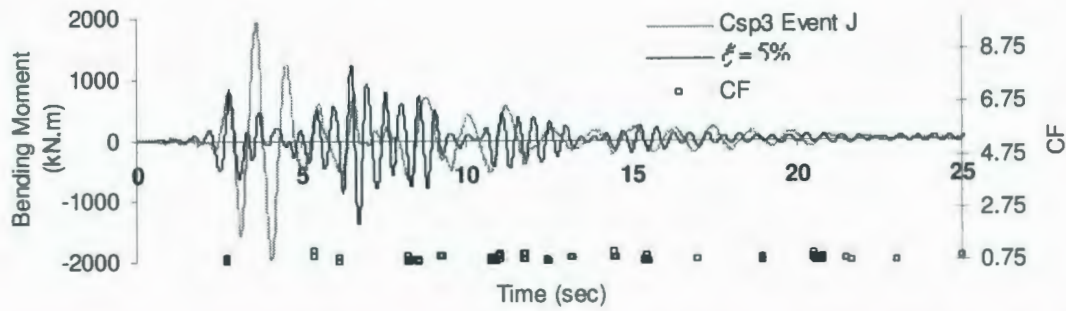


Figure 5.25: Comparison of Bending Moment Time History for Event J, Csp3 at soil depth 0.5 m.

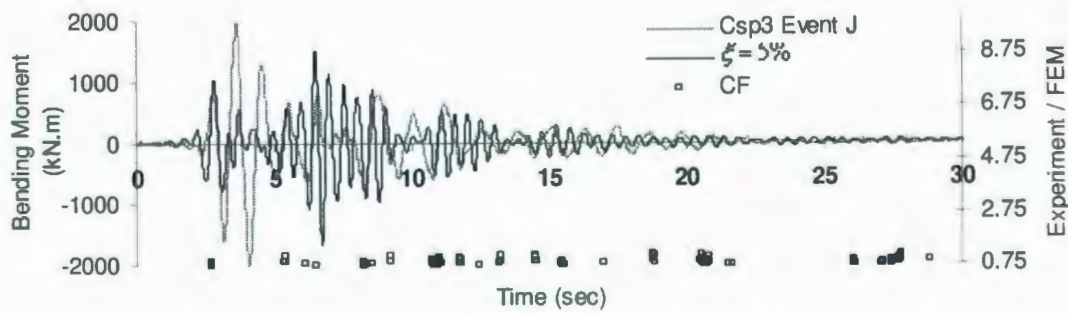


Figure 5.26: Comparison of Bending Moment Time History for Event J, Csp3 at soil depth 1.5 m.

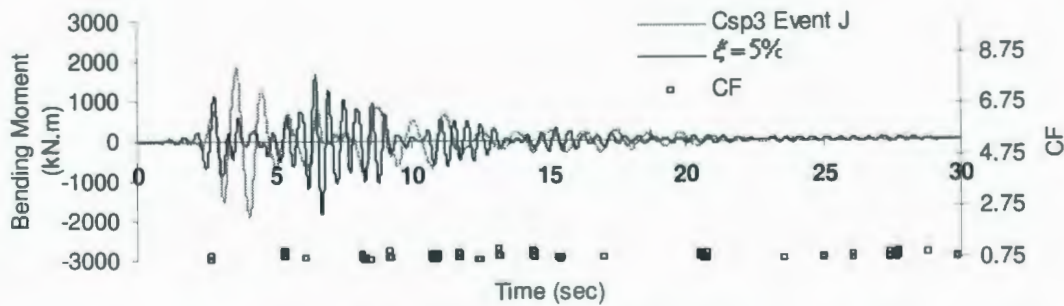


Figure 5.27: Comparison of Bending Moment Time History for Event J, Csp3 at soil depth 2.5 m.

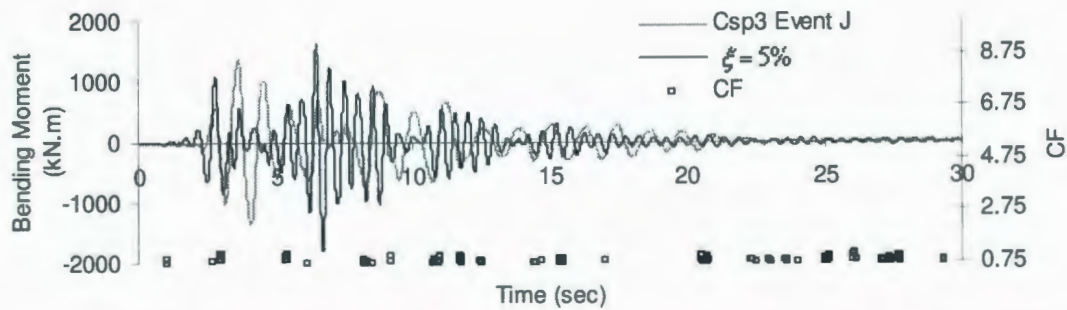


Figure 5.28: Comparison of Bending Moment Time History for Event J, Csp3 at soil depth 4.0 m.

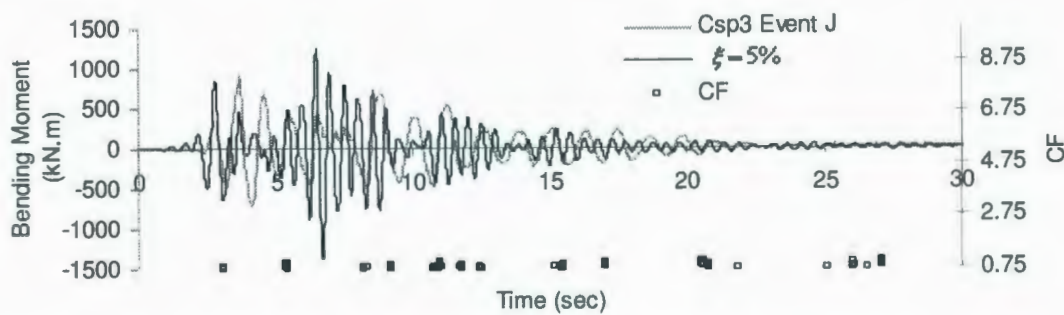


Figure 5.29: Comparison of Bending Moment Time History for Event J, Csp3 at soil depth 5.5 m.

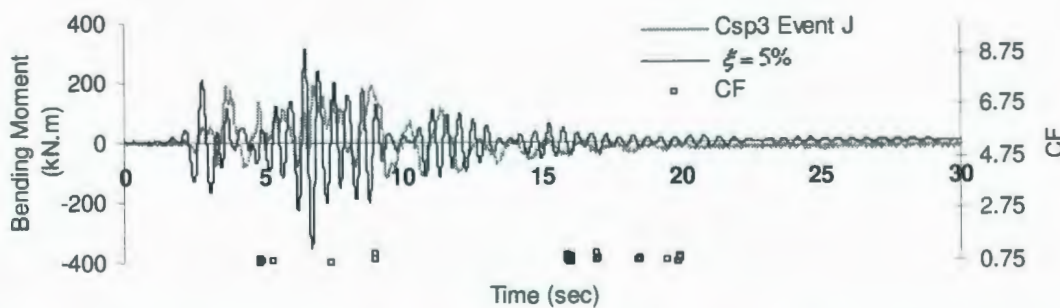


Figure 5.30: Comparison of Bending Moment Time History for Event J, Csp3 at soil depth 8.5 m.

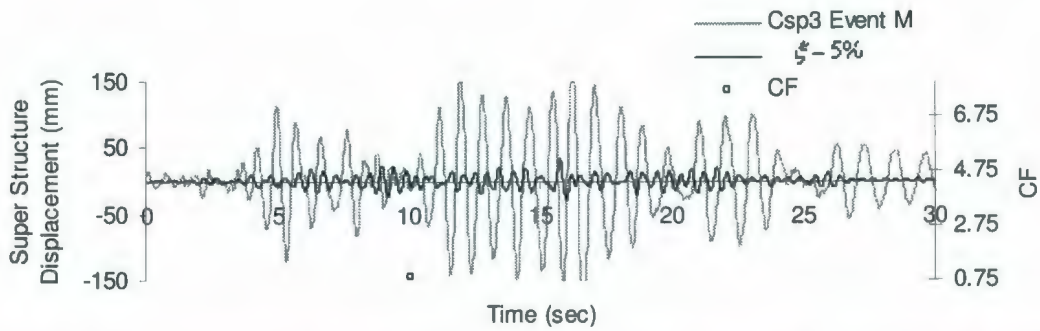


Figure 5.31: Comparison of Superstructure Displacement Time History for Event M, Csp3.

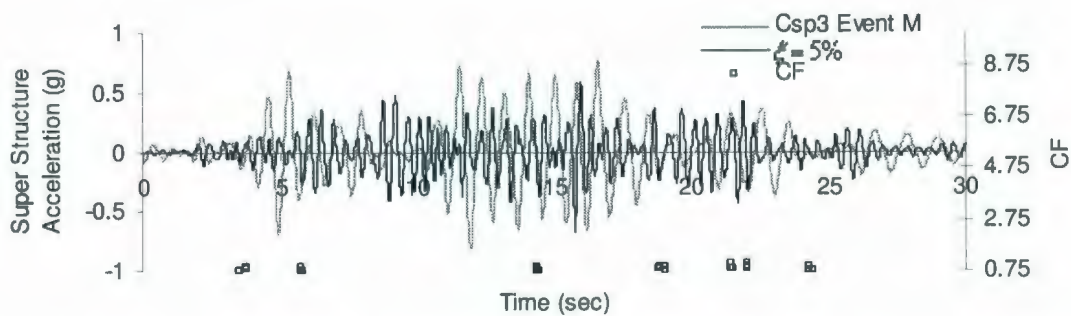


Figure 5.32: Comparison of Superstructure Acceleration Time History for Event M, Csp3.

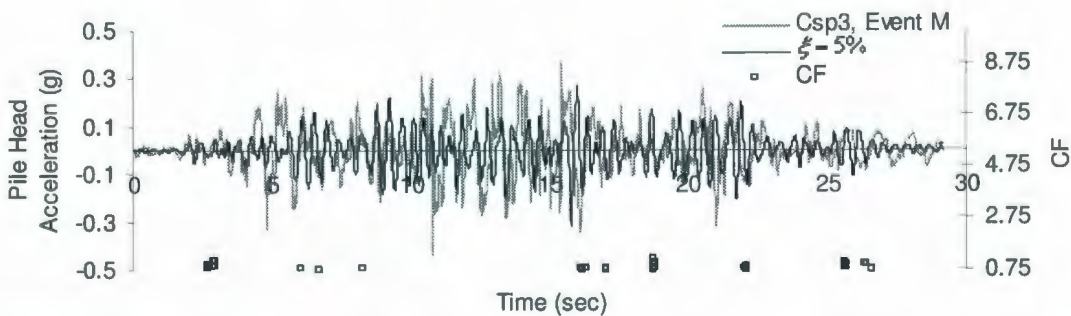


Figure 5.33: Comparison of Pile Head Acceleration Time History for Event M, Csp3.

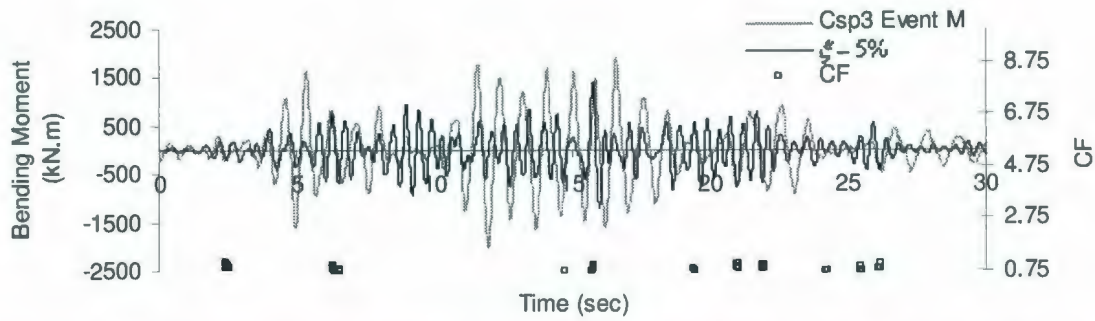


Figure 5.34: Comparison of Bending Moment Time History for Event M, Csp3 at soil depth 0.5 m.

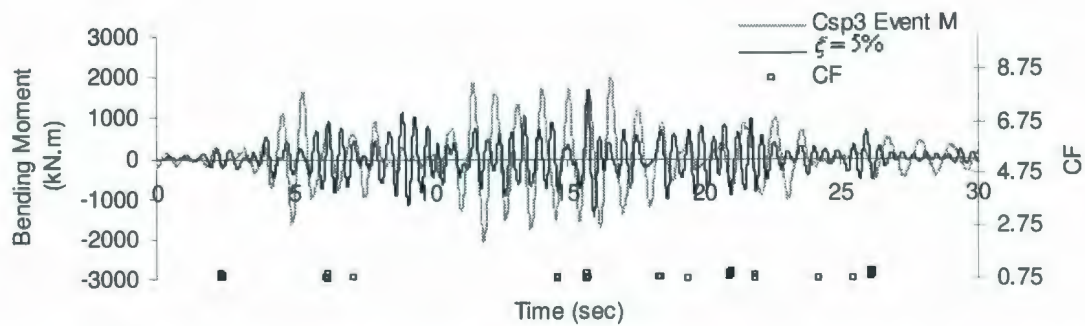


Figure 5.35: Comparison of Bending Moment Time History for Event M, Csp3 at soil depth 1.5 m.

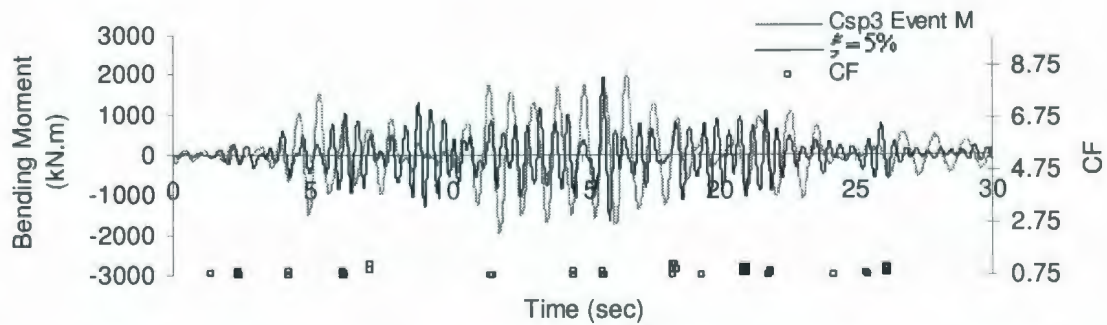


Figure 5.36: Comparison of Bending Moment Time History for Event M, Csp3 at soil depth 2.5 m.

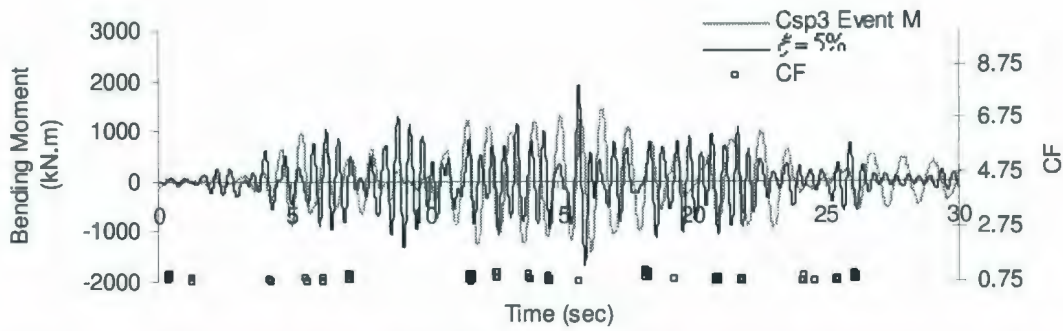


Figure 5.37: Comparison of Bending Moment Time History for Event M, Csp3 at soil depth 4.0 m.

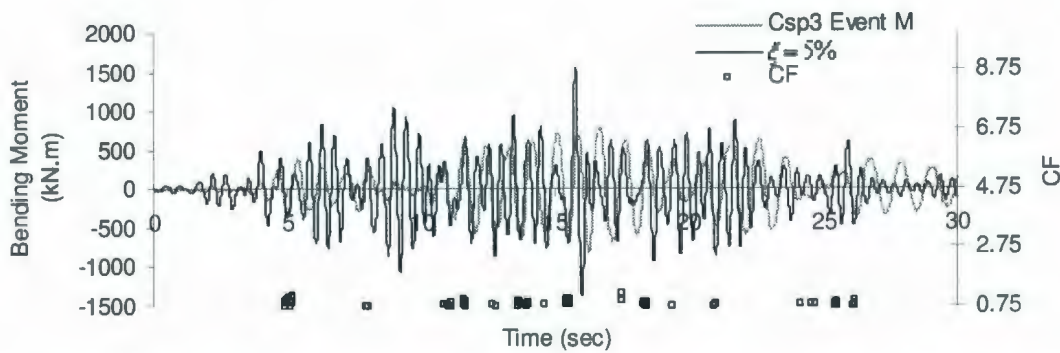


Figure 5.38: Comparison of Bending Moment Time History for Event M, Csp3 at soil depth 5.5 m.



Figure 5.39: Comparison of Bending Moment Time History for Event M, Csp3 at soil depth 8.5 m.

Calculated responses for Csp3 tests are in reasonably good correlation with recorded structural responses, with exceptions for events F, J and E of Csp2 tests. Predicted superstructure responses (superstructure displacements and superstructure accelerations time histories) for both Csp2 and Csp3 have highly underestimated the recorded superstructure responses at $\xi = 5\%$.

According to the pile head acceleration distribution shown in Figures 5.6, 5.15, 5.24, 5.33, B-12, B-21, B-30, B-39, B-48, B-57 and B-66, results obtained from the numerical model agree well with Csp2 and Csp3 tests.

As can be noted from Figures 5.5, 5.14, 5.23, 5.32, B-11, B-20, B-29, B-38, B-47, B-56 and B-65 accelerations of the superstructure achieved from numerical analyses are in better agreement with the recorded accelerations during Csp3 tests. However, the results of predicted superstructure accelerations do not agree with those of Csp2 tests.

Figures 5.7 to 5.12, 5.16 to 5.21, 5.25 to 5.30, 5.34 to 5.39, B-13 to B-18, B-22 to B-27, B-31 to B-36, B-40 to B-45, B-49 to B-54, B-58 to B-63, B-67 to B-72 show that bending moment time histories obtained from numerical analyses are in good agreement with that recorded at different layers of soil during Csp3 tests if $\xi = 5\%$. However, time histories of pile bending moment recorded during Csp2 tests are lower than that obtained from the numerical model, which does not take into account the effect of pore water pressure of soil.

5.6 Discussion on the Numerical Results

A computationally inexpensive ABAQUS model based on the BNWF approach was presented to simulate dynamic pile performance in saturated sand. First an effective stress based ground response analysis is carried out using Cyclic1D a nonlinear earthquake ground response analysis model. Second, the resulting ground accelerations are applied to the BNWF model to obtain dynamic response of the pile.

The performance of the BNWF was evaluated against a set of centrifuge model tests involving a profile of saturated loose sand overlying dense saturated sand. Spring constants were derived from API recommendations and dashpots constants were derived from Berger et al. (1977) to represent radiation damping (El Naggar et al., 2005). It was found that apart from some events F, J, E of Csp2 and I of Csp3 in which higher EPWP ratios (Wilson et al., 1997a, b) were induced, the comparisons of computed and experimental responses yielded reasonable agreement with recorded pile responses. Event D of Csp2 and events G, D, J, M of Csp3 correspond to relatively small pore pressure ratios (Wilson et al., 1997a, b). Hence, results of numerical analyses for these shaking events were in good agreement with experiments. In this study, API based p-y curves were not modified to account for the effect of excess pore water pressure ratios. In addition to this, differences between calculated and recorded free field accelerations might have contributed to the discrepancies between calculated and recorded superstructure responses (superstructure acceleration and displacement) of the pile. Boulanger et al. (1999) suggested bypassing the site response calculations by using the recorded free field motions as input motion to the dynamic BNWF model. Boulanger et al. (1999) mentioned that the use of recorded input motions produced better agreement between calculated and recorded superstructure responses compared to site response analysis used to calculate the free-field motions.

5.7 Acknowledgement

The authors are thankful to Dr. Elgamal, the University of California at San Diego for providing with Cyclic1D computer program. The authors gratefully acknowledge the receipt of centrifuge test data provided by Dr. Wilson, University of California at Davis.

Chapter 6

Pile Peak Response Curves for Seismic Analysis of Piles in Saturated Sand

Co Authorship: Chapter 6 has been prepared in accordance with the regulations for a Manuscript format thesis stipulated by Faculty of Applied Science and Engineering at The Memorial University of Newfoundland. Abstract of this paper is published in the refereed conference proceedings of Canadian Geotechnical Society Conference, Halifax, September, 2009. Mohammad K. Talukder conducted the research and will write the manuscript. Dr. Stephen D. Butt and Dr. Radu Popescu supervised the research.

6.1 Introduction

In the preceding chapter, the calculated and recorded time histories of the current BNWF model were compared for eleven shaking events listed in Table 3.1 and 3.2 by keeping pile material damping ratio, ξ at 5%. The results of recorded and computed time histories were not in good agreement for some shaking events of Csp2 tests. This chapter shows that by varying pile material damping ratio ξ , we can achieve good agreement between recorded and computed peak superstructure acceleration, as well as peak pile head acceleration for any shaking event of Csp2 and Csp3 tests. Superstructure displacements vs. peak ground input acceleration curves for different values of ξ are plotted to show the extent of differences between calculated and recorded superstructure displacements. It is also shown that by plotting pile peak bending moment (PPBM) vs. peak ground input acceleration curves for different values of ξ , predicted PPBMs can lead to better estimation of experimental PPBMs observed over a wide range of shaking events of Csp2 and Csp3 with reasonable accuracy.

6.2 Analysis of Predicted Pile Head Accelerations

Pile head acceleration time histories of the BNWF model were computed for all earthquake events listed in Table 3.1 and 3.2 for ξ of 1%, 2.5% and 5%. These time histories were compared with experimental pile head acceleration time histories. These

comparisons are summarized in Figures 6.1 and 6.2 which show both calculated and recorded peak pile head accelerations versus peak ground input acceleration curves. The calculated responses are in good agreement with the recorded responses for all events of Csp3, with exceptions for events D, F and E of the Csp2 test.

6.3 Analysis of Predicted Superstructure Accelerations

Pile superstructure acceleration time histories of the BNWF model were computed for all earthquake events listed in Table 3.1 and 3.2 for ξ of 1%, 2.5% and 5%. These time histories were compared with experimental superstructure acceleration time histories. These comparisons are summarized in Figures 6.3 and 6.4 which show both calculated and recorded peak superstructure accelerations versus peak ground input acceleration. The calculated responses are in excellent agreement with the recorded responses for all events of the Csp3 tests, but approximately 250% higher than the recorded responses of events F, J and E of Csp2 tests.

6.4 Analysis of Predicted Superstructure Displacements

Pile superstructure displacement time histories of the BNWF model were computed for all earthquake events listed in Table 3.1 and 3.2 for ξ of 1%, 2.5% and 5%. These time histories were compared with experimental superstructure displacement time histories. These comparisons are summarized in Figures 6.5 and 6.6 which show both calculated and recorded peak superstructure displacements versus peak ground input acceleration curves. The calculated responses resulted in an underestimation (on an average of approximately 400%) of the recorded responses for all events of Csp2 and Csp3 tests.

Figures 6.5 and 6.6 show that superstructure displacements were heavily underestimated by the predictions of the current BNWF model. API recommendations assume that initial p-y stiffness increases linearly with depth. It defines the initial stiffness as the product of depth, z and the initial modulus of subgrade reaction coefficient, k . API recommendations for k were derived from lateral loading tests that were controlled by drained soil behavior at relatively shallow depths. A constant k value overestimates the p-y stiffness at depths greater than a few pile diameters, because the stiffness of sand generally increases in

proportion to the square root of confinement, not in proportion to confinement (Boulanger et al., 1999). Therefore, the initial stiffness of soil springs at all depths along the BNWF model were stiffer than that of measured p-y curves in saturated sand of Csp2 or Csp3 centrifuge models (Wilson et al., 2000). For the shaking events of Csp2 covered in this study, the current BNWF model underestimated peak superstructure motions (displacements and accelerations) on an average of 400%.

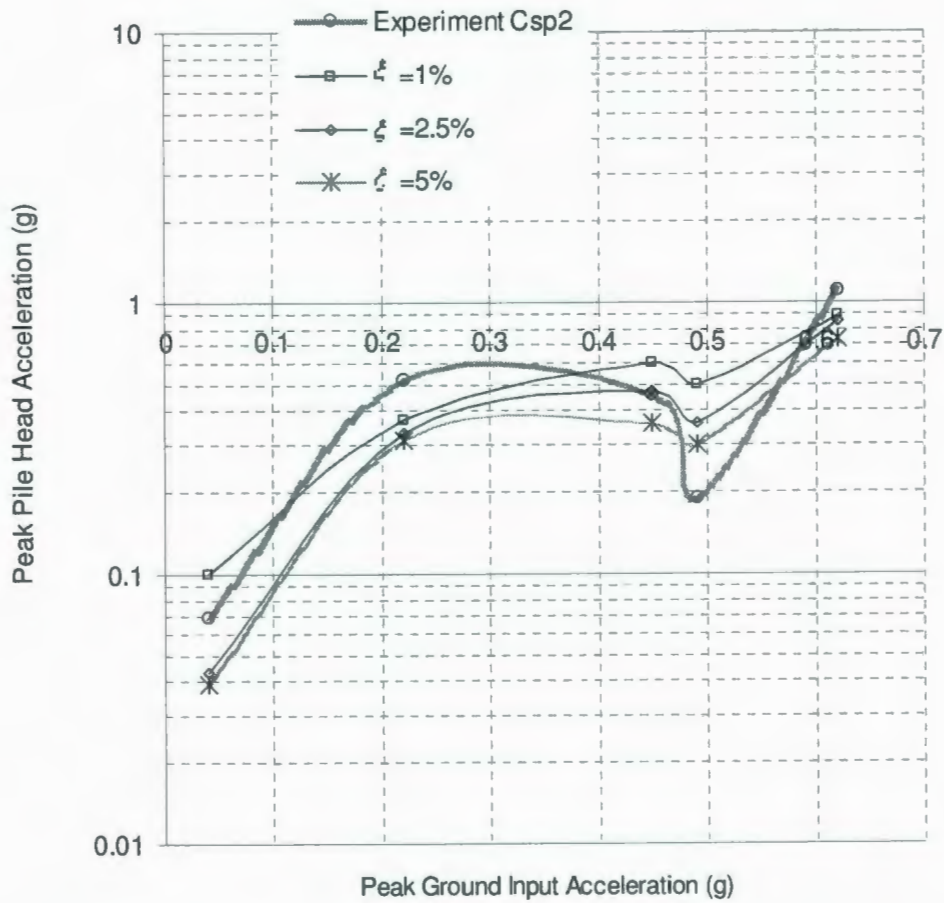


Figure 6.1: Calculated and Recorded Peak Pile Head Accelerations for Csp2 tests.

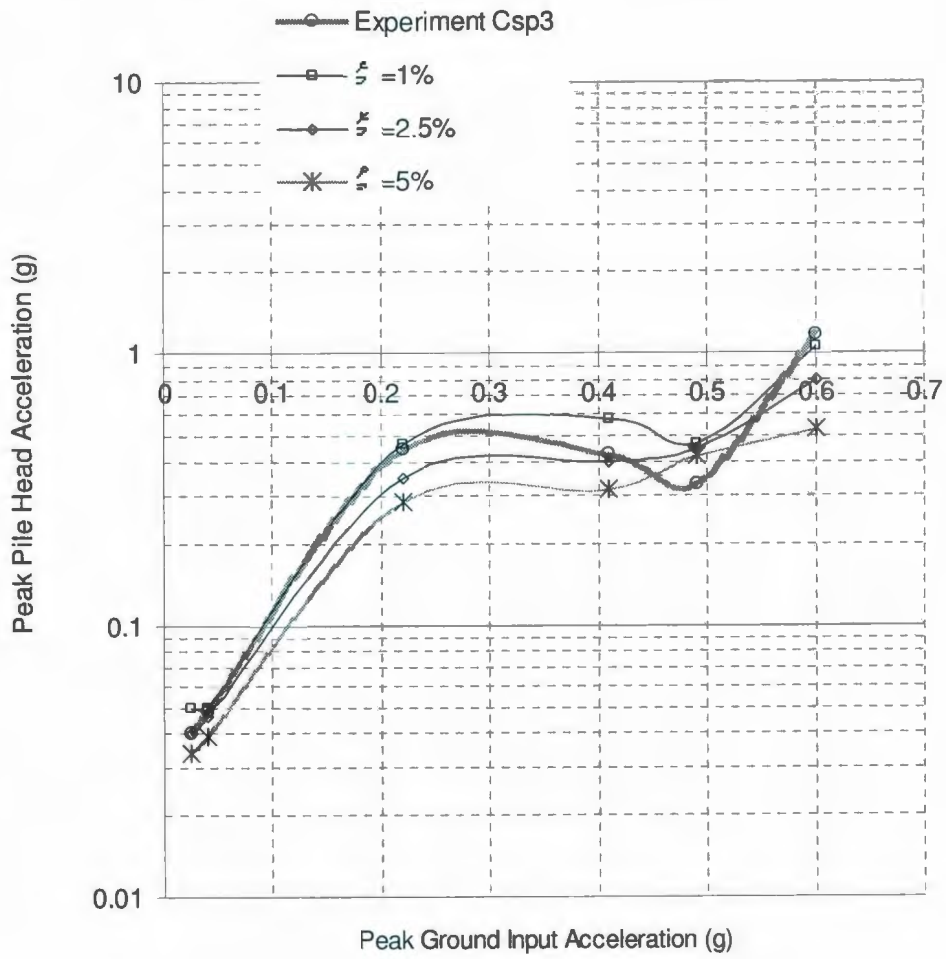


Figure 6.2: Calculated and Recorded Peak Pile Head Accelerations for Csp3 tests.

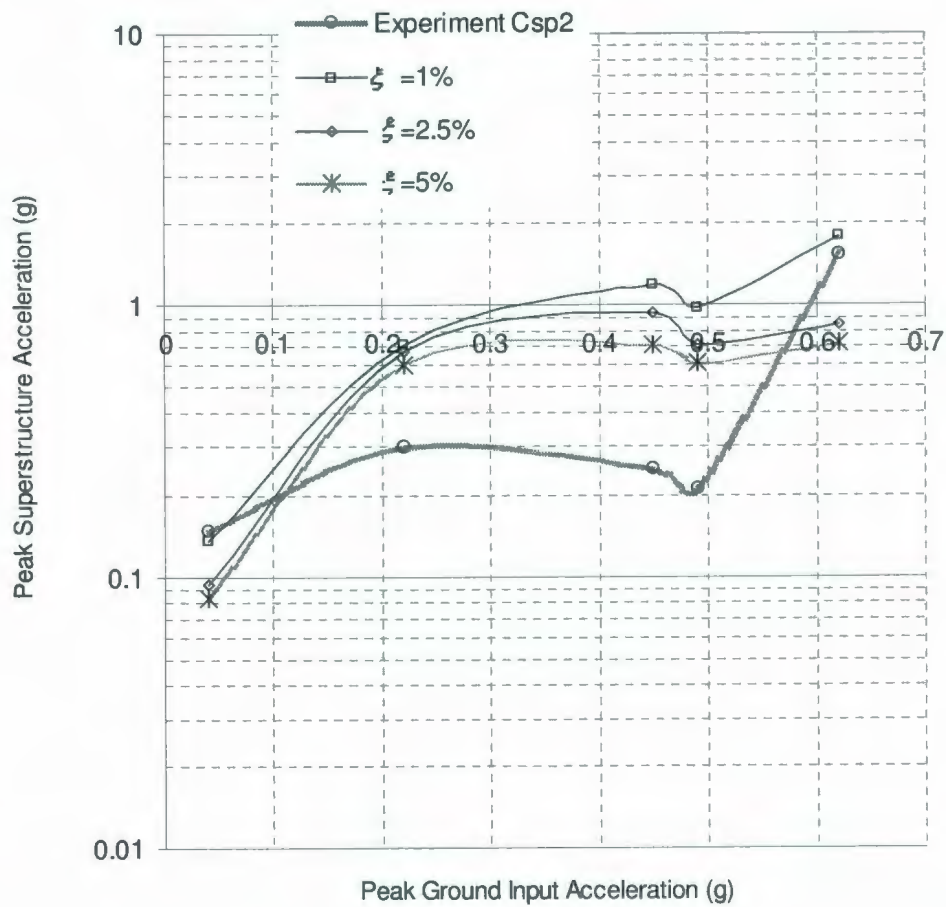


Figure 6.3: Calculated and Recorded Peak Superstructure Accelerations for Csp2 tests.

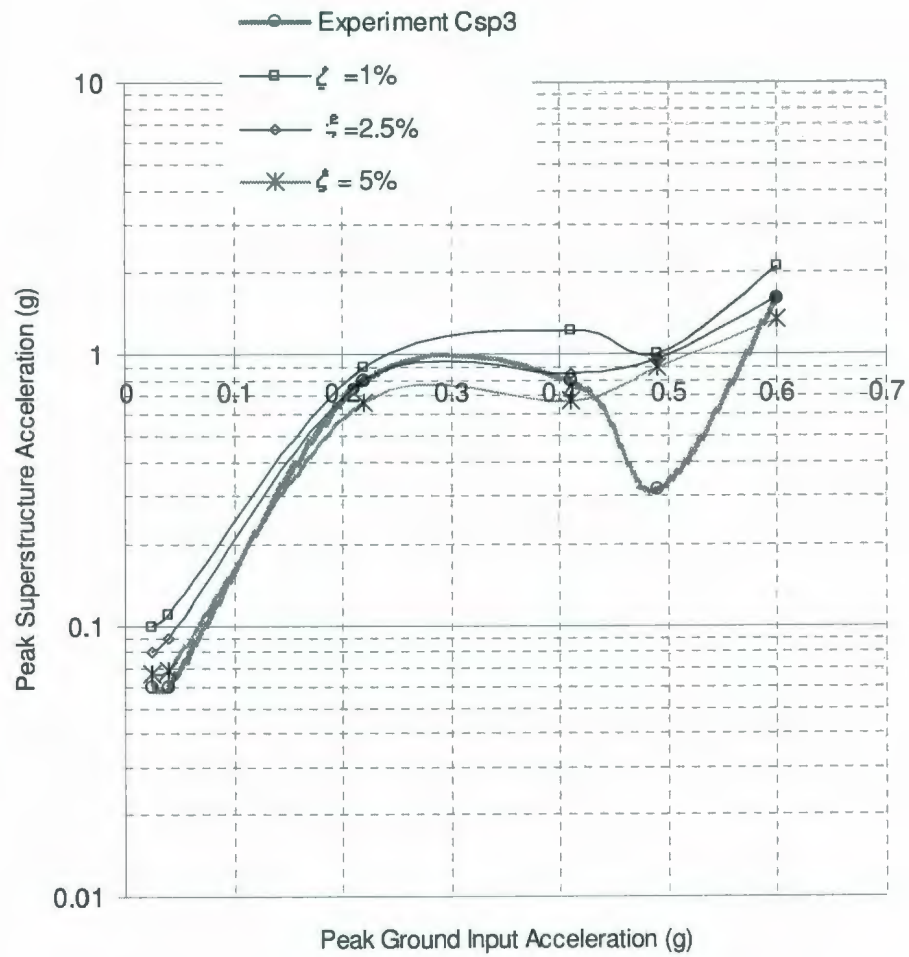


Figure 6.4: Calculated and Recorded Peak Superstructure Accelerations for Csp3 tests.

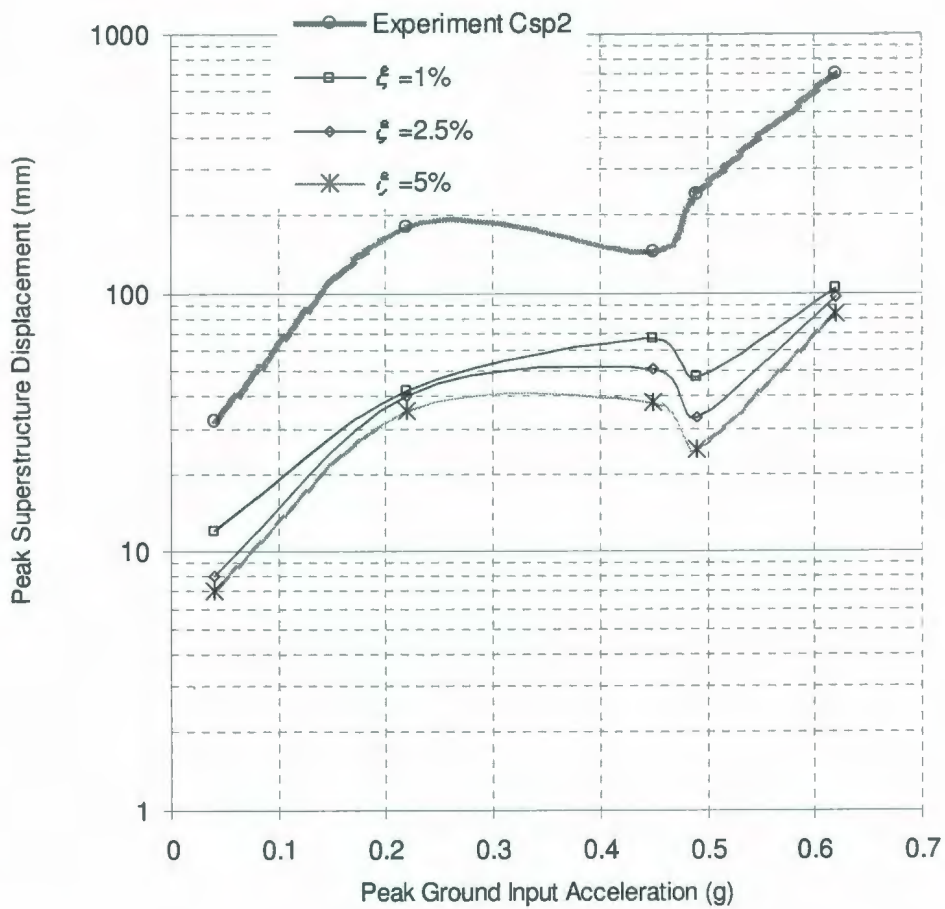


Figure 6.5: Calculated and Recorded Peak Superstructure Displacements for Csp2 tests.

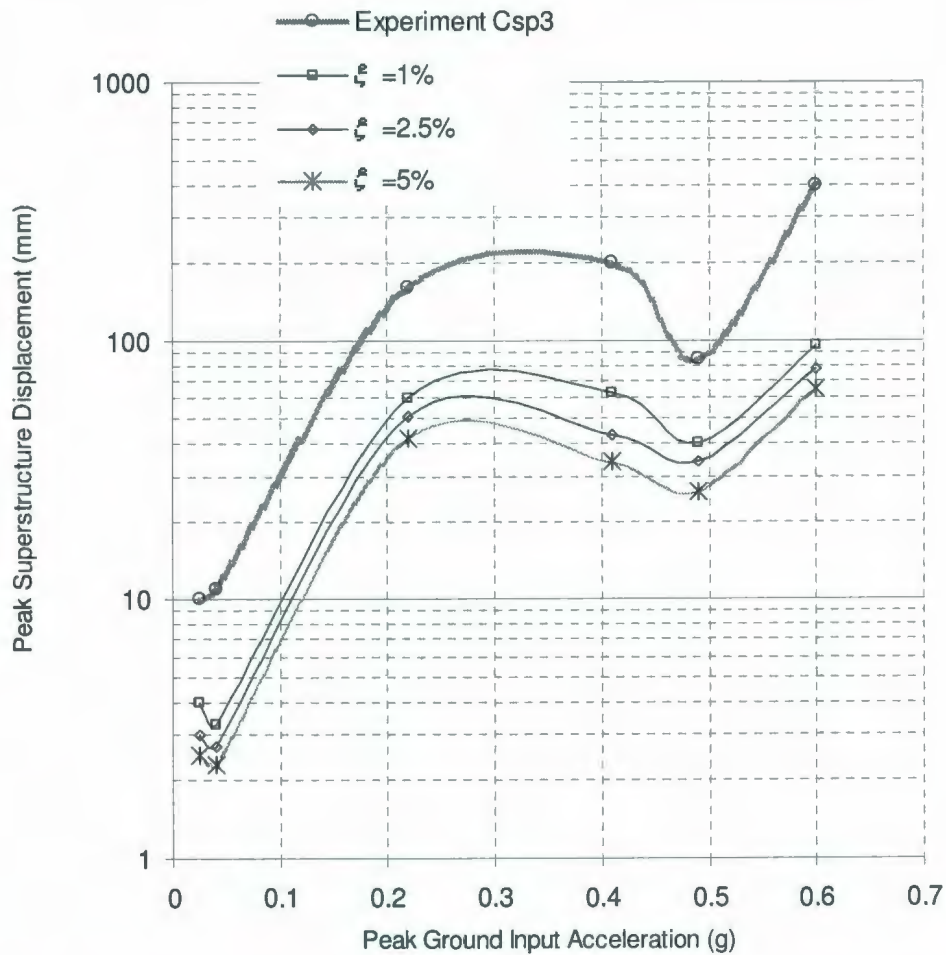


Figure 6.6: Calculated and Recorded Peak Superstructure Displacements for Csp3 tests.

6.5 Analysis of Predicted Bending Moments

Pile peak bending moments (PPBM) within different soil layers could be considered as the main parameter to evaluate the ABAQUS model's ability to conduct seismic response analyses of piles (Liyanapathirana and Poulos, 2005). The calculated and experimental PPBM along the pile shaft for the seismic events listed in Table 3.1 and 3.2 are shown in Figures C-1 to C-11 of Appendix C. Talukder et al. (2009b) and El Naggar et al. (2005) used a wide range of pile material damping ratios for achieving good agreement between computed and recorded PPBMs. In line with this approach, different material damping ratios for pile elements were used in the analyses of the present ABAQUS model. It can be seen from Figures C-1 to C-11 of Appendix C that an increase in the pile material

damping ratio, ξ leads to a decrease in the computed PPBM. For events D and L of Csp2 (PGA, 0.04g and 0.62g respectively), good agreement between the calculated and experimental results can be obtained by using ξ of 1.0% to 5.0%. For other events of Csp2 such as F, J and E, no reasonable agreement between the experimental and predicted PPBM could be obtained (Figures C-2 to C-4). A reasonable range of material damping ratio (between 2.5% and 5 %) could yield satisfactory agreement between experimental and calculated peak bending moments for all events of Csp3 with the exception for event I of Csp3 test (Figures C-6 to C-11). Findings of Figures C-1 to C-11 are summarized in Figures 6.7 and 6.8 respectively.

Figure 6.7 shows the maximum calculated and recorded experimental Pile Peak Bending Moment (PPBM) along the pile shaft for soil profile Csp2 versus peak ground input accelerations. It is observed that for a wide range of PGAs (between 0.040g and 0.62g) and by using various pile material damping ratio, ξ (between 1% and 15 %), there would be an overestimation of PPBMs in the range of PGAs between 0.20g and 0.5g. This study proposes that by opting ξ between 5% and 12.5%, a foundation engineer can have a safe estimate of PPBM from Figure 6.7 in response to PGAs in the range 0.04g-0.25g and 0.5 g to 0.62 g. For example, the recorded PPBM in event H (0.11g) of Csp2 was 600 kN.m. This result may be predicted from Figure 6.7 with ξ of 5 %.

Figure 6.8 shows the maximum calculated and recorded experimental Pile Peak Bending Moments (PPBM) along the pile shaft versus peak ground input accelerations for soil profile in Csp3. It is observed that for a wide range of PGAs (between .025g and 0.62g) while opting ξ between 2.5% and 5%, a foundation engineer can have a safe estimate of PPBM from Figure 6.8 in response to PGAs between 0.025g and 0.62g. For example, recorded PPBM in event L (0.11g) of Csp3 was 1200 kN.m. This result can be estimated from Figure 6.8 with ξ of 2.5 %.

Based on the performance of the present BNWF model, Table 6.1 summarizes range of ξ values that may be used by design engineers for the estimation of pile peak responses in saturated sand during seismic hits.

Table 6.1: Design Pile Material Damping Ratios, ξ input to the current BNWF model.

Soil Condition	Range of PGA	Pile Response parameters of interest	Design values of ξ
Csp2 (Wilson, 1998)	$0.04g \leq PGA \leq 0.62g$	Peak Pile Head Acceleration (g)	$1\% \leq \xi \leq 5\%$
	$0.11g \geq PGA \geq 0.6g$	Peak Pile Superstructure Acceleration (g)	$1\% \leq \xi \leq 5\%$
	$0.11g \geq PGA \geq 0.6g$	Peak Pile Bending Moment (kN.m)	$1\% \leq \xi \leq 5\%$
Csp3 (Wilson, 1998)	$0.02g \leq PGA \leq 0.6g$	Peak Pile Head Acceleration (g)	$1\% \leq \xi \leq 2.5\%$
	$0.02g \leq PGA \leq 0.6g$	Peak Pile Superstructure Acceleration (g)	$1\% \leq \xi \leq 2.5\%$
	$0.02g \leq PGA \leq 0.6g$	Peak Pile Bending Moment (kN.m)	$2.5\% \leq \xi \leq 5\%$

It can be seen from Table 6.2 that liquefaction did not occur under the low shaking levels of event D of Csp2, event G of Csp3, and event D of Csp3. Thus, computed PPBMs for these events are closer to experimental ones in both Csp3 and Csp2. It is also notable in Table 6.2 that at the time of occurrence of PPBMs, EPWP ratios were 80 to 100% throughout the upper soil profile in events F, J and E of Csp2 (Wilson et al., 1997a, b). On the other hand, EPWP ratios were 50% to 65% throughout the upper soil profile in events J, and M of Csp3 (Wilson et al., 1997 a, b) at the time of occurrence of PPBMs. Hence, computed PPBMs for event J and M of Csp3 are in good agreement with experimental ones with pile material damping ratio falling between 2.5% and 5% (Figure 6.8). Since in this study, the effect of pore water pressure was not considered in modeling

spring stiffness, no agreement between computed and recorded PPBM versus PGA curves was achieved for events F, J and E of Csp2 with pile material damping ratio exceeding 15% (Figure 6.7).

Wilson, (1998) reported that in event L of Csp2 (PGA, 0.62g) and event O of Csp3 (PGA, 0.60 g), EPWP time histories induced dilation in the soil. This dilation occurred in early shaking resulting in the largest lateral resistance from soil to the pile. Consequently, recorded responses of the pile for these two events were at their maximum. Numerical PPBMs for these two events were in good agreement for ξ between 2.5% and 5% (Figures 6.7 and 6.8). The author also reported that the recorded acceleration on the pile head and superstructure were questionable, resulting in complications in the interpretation of data for event O of Csp3. Thus, uncertainties in centrifuge data were obvious. However, the author did not report on whether the normal performance of data acquisition systems during shaking events E of Csp2 and I of Csp3 suffered badly from heavy liquefaction while registering comparatively lower PPBMs.

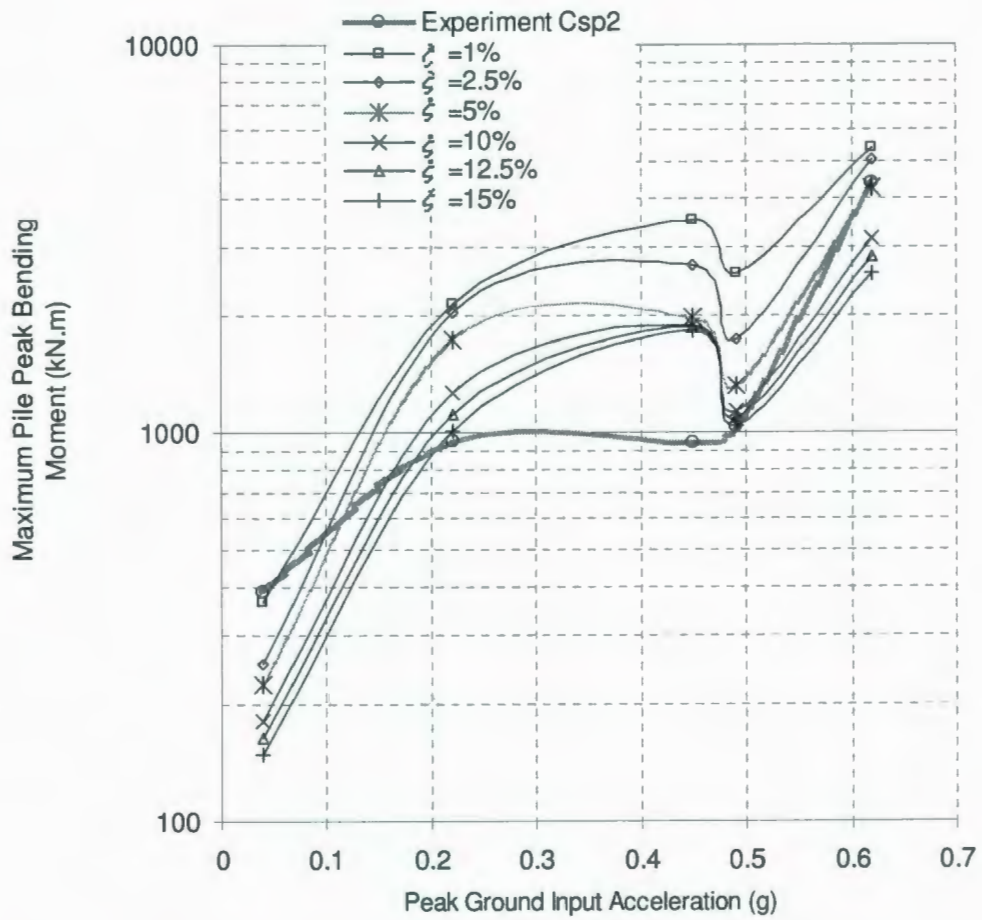


Figure 6.7: Maximum Pile Peak Bending Moment vs. Peak Ground Input Acceleration curves for Csp2 Tests.

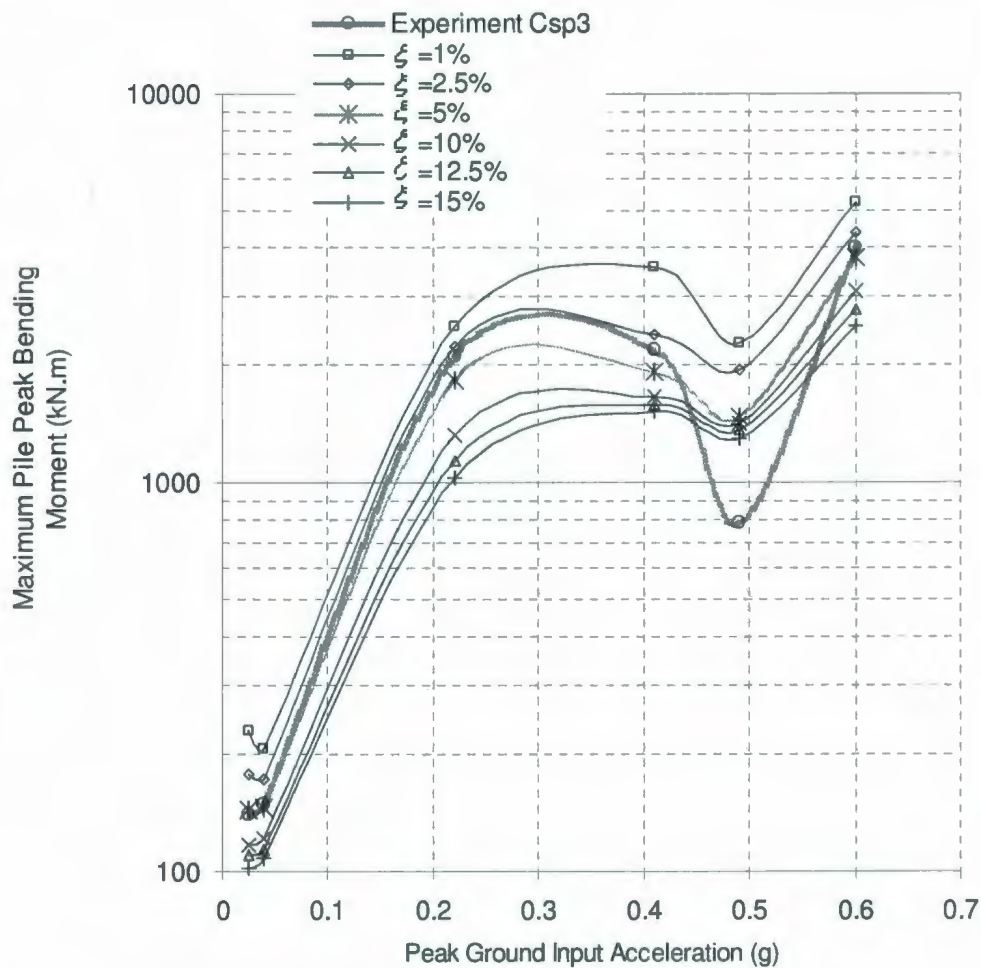


Figure 6.8: Maximum Pile Peak Bending Moment vs. Peak Ground Input Acceleration curves for Csp3 Tests.

6.6 Discussion on the pattern of PPBM vs. PGA curves

It could easily be noticed that all the experimental peak response curves have a valley near PGA, 0.50g by going through all peak pile response curves (Figures 6.1 to 6.8). The remarkable feature of Figures 6.1 to 6.8 is that the numerical peak response curves also capture discontinuity of experimental curves at PGA, 0.50g. Recurrence of discontinuity in the numerical peak response curves is observed at PGA, 0.50g for all values of ξ . Spectral acceleration vs. periods curves of the ground input motions of Csp2 and Csp3 tests (Table 3.1 and 3.2) are shown in Figure 6.9 and 6.10. Spectral acceleration of a

ground input motion near the fundamental period of the pile foundation system indicates the amount of energy content of the ground input motion to which the structure was subjected (Wilson, 1998). In this study, by performing a frequency analysis, the fundamental period of the Finite Element model of BNWF system was obtained to be 0.49 s. The magnitude of spectral accelerations of ground input motions at 0.49 sec are obtained from Figures 6.9 and 6.10 and arranged in Table 6.2. We can attempt to analyze the recurrent of discontinuity in numerical PPBM vs. PGA curves near PGA, 0.50g by referring to Table 6.2.

Table 6.2 Analyses of Spectral Acceleration of Ground Input Motions

Test	Event	Input	PGA (g)	Approx. time of occurrence of PPBM in experiment (Wilson et al. 1997a, b)	Approx. EPWP ratio in loose upper sand layer at the time of occurrence of PPBM (Wilson et al., 1997a, b)	Spectral Acceleration, SA of base input motion at fundamental period (0.49 s) of the BNWF model. (Wilson et al., 1997a, b)
Csp2	D	Kobe	0.04	at 3.5 s	0 %	0.065 g
	F	Kobe	0.22	at 3.5 s	100%	0.425 g
	J	Santa Cruz	0.45	at 16.5 s	100%	0.85 g
	E	Santa Cruz	0.49	at 6 s	80 %	0.35 g
	L	Kobe	0.62	at 5 s	Negative	0.90 g
Csp3	G	Santa Cruz	0.025	10 s	0%	0.025 g
	D	Santa Cruz	0.04	15 s	0%	0.035 g
	J	Kobe	0.22	at 5 s	50 %	0.45 g
	M	Santa Cruz	0.41	at 11 s	65 %	0.85 g
	I	Santa Cruz	0.49	at 10 s	80 %	0.30 g
	O	Kobe	0.60	at 3.50 s	Negative	0.85 g

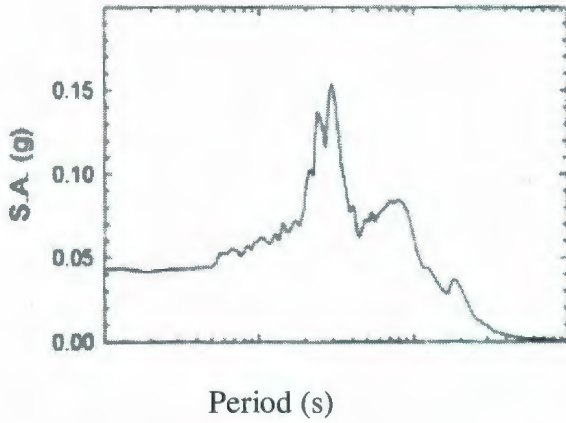


Figure 6.9a: Event D with PGA, 0.04 g

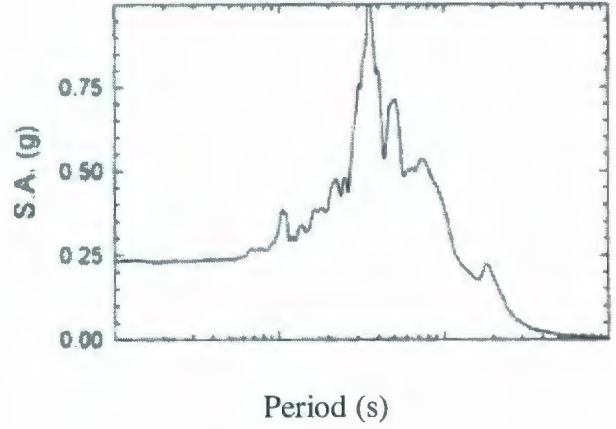


Figure 6.9b: Event F with PGA, 0.22 g.

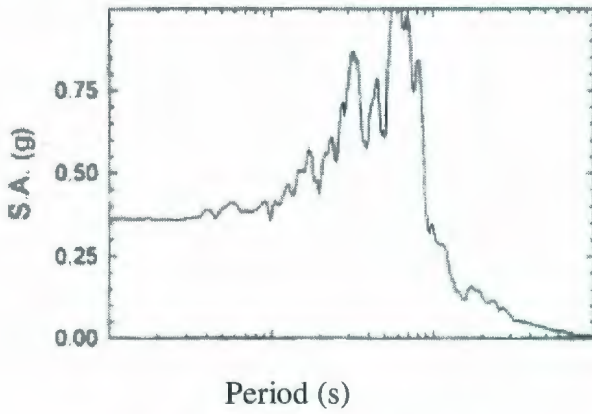


Figure 6.9c: Event J with PGA, 0.45 g.

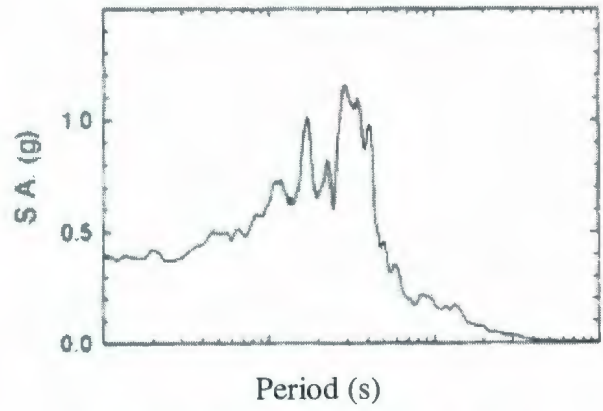


Figure 6.9d: Event E with PGA, 0.49 g.

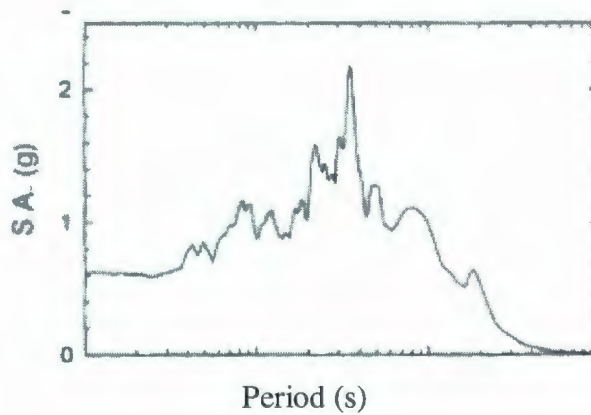


Figure 6.9c: Event L with PGA, 0.62 g.

Figure 6.9: Spectral acceleration vs. Period curves for the Ground Input Motions of Csp2 Tests (after, Wilson et al. 1997a).

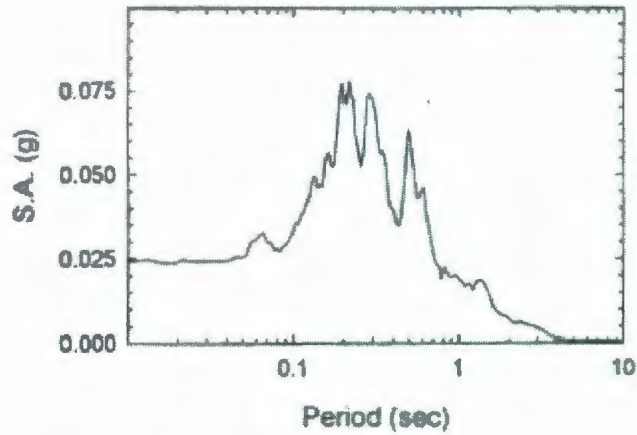


Fig 6.10a: Event G with PGA, 0.025 g

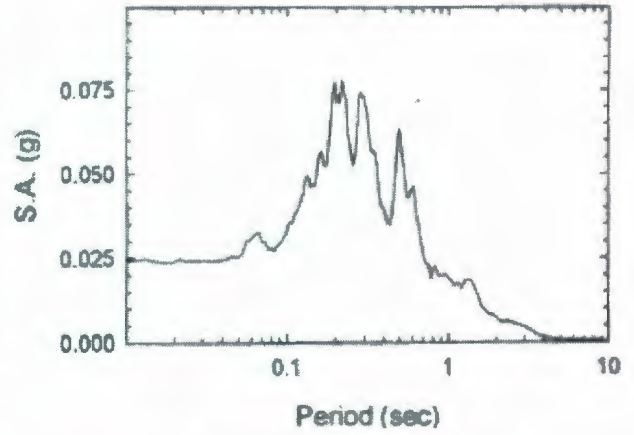


Fig 6.10b: Event D with PGA, 0.04 g.

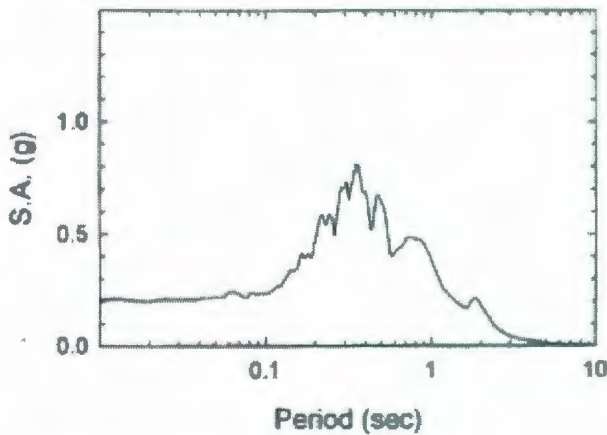


Fig 6.10c: Event J with PGA, 0.22 g.

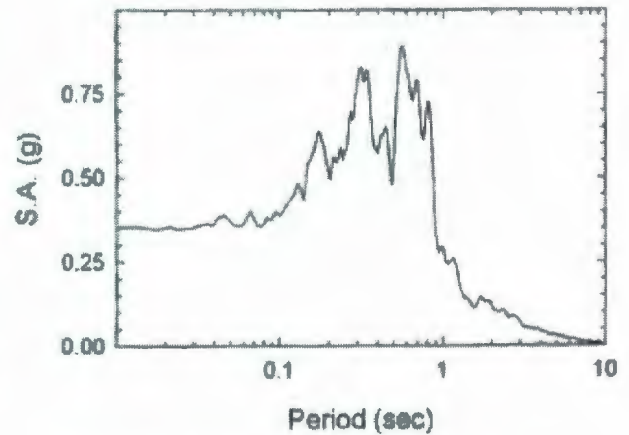


Fig 6.10d: Event M with PGA, 0.41 g.

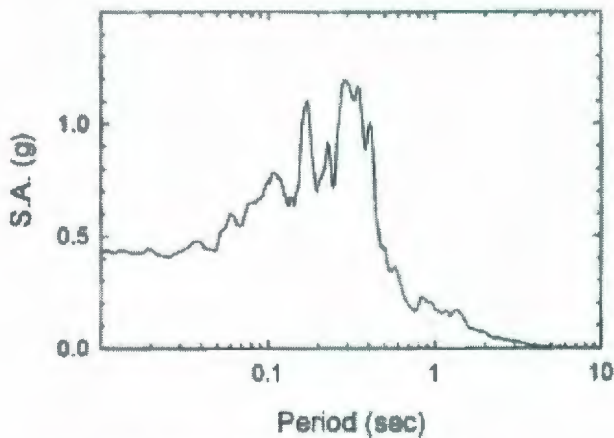


Fig 6.10e: Event I with PGA, 0.49 g.

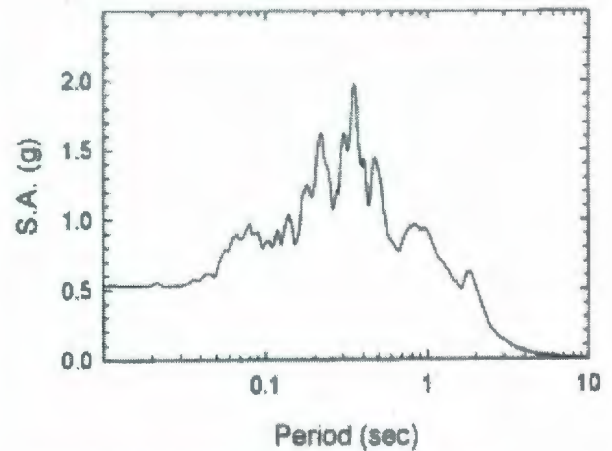


Fig 6.10f: Event O with PGA, 0.60 g.

Figure 6.10: Spectral acceleration vs. Period curves for the Ground Input Motions of Csp3 Tests (after, Wilson et al. 1997b).

It is notable in Table 6.2 that at the time of occurrence of PPBMs, excess pore pressure ratios were 80 % to 100% throughout the upper soil profile in events F (0.22 g), J (0.45 g) and E (0.49 g) of Csp2 tests. On the other hand, EPWP ratios were 50% to 65% throughout the upper soil profile in events J (0.22 g), and M (0.41 g) of Csp3 tests at the time of occurrence of PPBMs. Wilson (1998) reported that in event L of Csp2 (PGA, 0.62g) and event O of Csp3 (PGA, 0.60 g). EPWP time histories induced dilation in the soil. This dilation occurred in early shaking resulting in the largest lateral resistance from soil to the pile. Consequently, recorded responses of the pile for these two events were at their maximum as can be seen from Figures 6.7 and 6.8.

In the Csp2 test, the sand was loose ($D_r \approx 35\%$), while in Csp3 the sand was medium dense ($D_r \approx 55\%$). Wilson (1998) observed that liquefaction was more extensive in Csp2 than in Csp3, as evidenced by EPWP time histories showing that pore water pressures increased much more quickly and dissipated more slowly in the relative density $D_r \approx 35\%$ sand layer of Csp2 than in the $D_r \approx 55\%$ sand layer of Csp3. It is reported in Wilson et al. (1997a, b) that excess pore water pressure ratios were 80 to 100% throughout the upper soil profile in events F (PGA, 0.2g), J (PGA, 0.45g) and E (PGA, 0.49g) of Csp2. Wilson (1998) reported that the looser condition of the upper layer in Csp2, relative to Csp3, resulted in generally lower ground surface accelerations and lower peak superstructure accelerations. As a result pile peak bending moments (PPBMs) were larger in Csp3 than in Csp2 for nearly similar ground input motions (Wilson et al., 1997a, b). Since in this study, the effect of pore water pressure was not considered in modeling spring stiffness, no agreement between computed and recorded PPBM versus PGA curves was achieved for Csp2 tests in the range of PGAs 0.2g-0.5g with pile material damping ratio exceeding 15% (Figure 6.7).

For simulation of Csp3 event I, the BNWF model was excited by peak ground input motion 0.49 g (Table 6.2). Spectral acceleration of this ground input motion near fundamental period of the BNWF model (0.49 s) was 0.30g. Csp3 event M was shaken by peak ground input motion 0.41g which was lower than that of Csp3 event I. Nevertheless, spectral acceleration of the ground input motion for Csp3 event M was

0.85g (Table 6.2) which is higher than the spectral acceleration of the ground input motion for Csp3 event I. Therefore, the ground input motion applied to event I of Csp3 had lower energy content near the fundamental period of the structure than Event M of the Csp3 test. Thus, the predicted PPBM for event I of Csp3 may have dropped below the predicted PPBM of event M of Csp3 (Figure 6.8).

Similarly, the calculated PPBM for 0.49 g event E of the Csp2 test may have fallen below the PPBMs of significant shaking events of Csp2 tests (Figure 6.7). For simulation of event E (0.49 g) of the Csp2, the BNWF model was excited by peak ground motion 0.49g (Table 6.2). Spectral acceleration of this ground input motion near the fundamental period of the BNWF model (0.49 s) was 0.35g. At the fundamental period of the BNWF model, spectral acceleration of ground input motions in 0.22 g, 0.45 g and 0.62 g events of the Csp2 test are 0.425 g, 0.85 g and 0.90 g (Table 6.2) respectively. Hence, the ground input motion applied to event E of Csp2 had lower energy content near the fundamental period of the structure than 0.22 g, 0.45 g and 0.62 g events of the Csp2 tests.

Similar explanation may be drawn for the discontinuity in numerical peak superstructure accelerations and displacements vs. PGA curves.

Chapter 7

Conclusion and Recommendation for Future Research

7.1 Conclusions

Various approaches have been developed for the dynamic response analysis of single piles. One such method which was used throughout this thesis is the Beam on Nonlinear Winkler Foundation (BNWF) method. A simplified ABAQUS model based on BNWF method of analysis was used to numerically simulate the results of Csp2 and Csp3 centrifuge model data over the wide range of shaking events covered in this study.

The analyses in Chapter 4 consisted of performing 1D nonlinear ground response analyses to calculate the dynamic response of the free-field soil profile and then dynamic p-y analyses to calculate the dynamic response of the structural models. A well known computer code called Cyclic1D was used for computation of free field input motions as input to the BNWF model. Cyclic1D being based on soil plasticity constitutive model (Elgamal et al., 2002), can account for liquefaction in cohesionless soil and compute ground motions at any depth of soil due to earthquake excitations at the bed rock level of Finite Element Models of soil strata. Time histories of free field accelerations and excess pore water pressure ratios computed by Cyclic1D were compared with those obtained from centrifuge experiments Csp2 and Csp3. In a situation where ground input motion to Cyclic 1D soil model was weak (0.04g), Cyclic1D appeared to show slight underestimation of the experimental results. The comparisons yielded good agreement with experimental evidence, if the ground input motions were moderately strong, 0.20 g to 0.50 g. As a whole, prediction of Cyclic1D proved that an effective stress based analysis is capable of representing dynamic behavior of saturated sand under seismic excitation with an acceptable level of accuracy.

In Chapter 5 the BNWF model, together with nonlinear earthquake site response analysis for free field analyses, was evaluated against dynamic centrifuge tests Csp2 and Csp3 involving a pile supported structure in a profile of loose saturated sand overlying

saturated dense sand. Important features of the model included: the use of API recommended p-y curves to model soil stiffness, viscous damper to represent radiation damping of soil, and variation in pile material damping ratios (ξ) to provide design engineers with a variable mechanism of energy dissipation during seismic analysis of long flexible pile. By employing monotonic p-y curves for dynamic analyses of pile in saturated sand, this study did not consider degradation of initial stiffness of p-y curves due to pore water pressure effects. All simulations in this thesis were conducted in time domain. Time histories of different response parameters including pile superstructure displacements, superstructure accelerations, pile head accelerations, and bending moments for ξ of 5% were predicted by the ABAQUS model and compared with the results of Csp2 and Csp3. Comparison yielded good agreement for Csp3 simulations.

Talukder et al. (2009b) and El Naggar et al. (2005) used a wide range of pile material damping ratios for achieving good agreement between computed and recorded PPBMs. In line with this approach, in Chapter 6, different material damping ratios for pile elements were used for producing practical design recommendations in the form of peak response (maximum moments in piles and peak displacements and accelerations of superstructure) for piles in saturated sand subjected to seismic motions. In a second phase of modeling (Chapter 6), time histories of pile response parameters were computed for a wide range of ξ values and peak ground input accelerations (PGA). Peak values of pile response parameters (maximum moments in piles and peak displacements and accelerations of superstructure) were then plotted against peak ground input accelerations (PGA) to provide peak pile response curves for seismic analyses of piles. This provides design engineers with a preliminary rough estimation of peak pile responses to earthquake motions in saturated sand.

Peak pile response curves were compared with experimental response curves and summarized in Figures 6.1 to 6.8. Comparisons of calculated peak pile head accelerations, peak superstructure accelerations and peak pile bending moments with those of Csp3 tests were found to closely agree. It can be noted in Figures 6.7 and 6.8 that the BNWF model developed in this study produced close predictions for Csp3 tests, but

poor prediction for Csp2 tests. However, overestimation of PPBMs as compared to PPBMs measured in Csp2 tests was similar to the underestimation of superstructure displacements for all shaking events of Csp2 and Csp3 tests. Differences between calculated and recorded peak bending moments in the piles were similar to the differences between calculated and recorded peak superstructure displacements shown in Figures 6.5 and 6.6.

Peak pile bending moments along the pile length were overestimated by about 250% while simulating various shaking events of Csp2. However, peak bending moments predicted for very weak (0.04g) or very strong (0.62g) ground input motion of Csp2 tests were in good agreement with the experimental results. A range of design values for ξ were tabulated in Table 6.1 for use in the preliminary estimation of peak pile response parameters through BNWF analyses of piles embedded in saturated sand during seismic events. Based on the results of this thesis, the following conclusions may be drawn:

- Free field ground motions for saturated sand can be calculated by using Cyclic1D model (Elgamal et al. 2006) with a satisfactory level of accuracy.
- Results of the BNWF model developed in this study were compared with recorded responses of the single pile supported systems of Csp2 and Csp3. The presented approach predicts peak pile bending moments recorded in Csp3 tests with reasonable accuracy for a wide range of peak ground input accelerations and pile material damping ratios. Nevertheless, predictions of peak pile bending moment observed in Csp2 tests were highly overestimated.
- The present BNWF model does not consider pore pressure effect on soil stiffness. The current BNWF model underestimated peak superstructure displacements observed in Csp2 and Csp3 soil profile. Thus, initial stiffness of API recommended static p-y curves need to be modified to account for the effects of soil degradation found in saturated sand during seismic events.

- Achieving better simulation of Csp3 tests suggests that the presented BNWF model may be used to predict dynamic behavior of pile foundation observed in dry sand profile more successfully.
- The uncertainties in experimental data resulting from signal processing (Wilson, 1998) may have affected the comparison of predicted results with experimental results.
- The presented approach is a computationally effective two dimensional approach of representing 3D soil pile interaction problems. This approximation may have affected the performance of the BNWF model.
- In a 3D continuum Finite Element approach, seismic soil-pile interaction is more realistically analyzed in a coupled way, unlike the present BNWF approach where uncoupling of the free field, soil and pile is the way of approach to predict dynamic pile behavior. This simplification may have affected the performance of the BNWF model.

7.2 Recommendation for future research

API based p-y model used in the current BNWF model need to be validated against test results other than the data it has been calibrated on in the thesis.

Reliable dynamic p-y curves for piles are being developed for incorporating degradation of stiffness and strength of soil under seismic loading (Boulanger et al., 1999). After employing such p-y curves into the present BNWF model, an extensive parametric study on soil-pile interaction should be conducted involving different pile and soil profile to assess how variations in p-y model parameters affect the response quantities of interest.

References

- ABAQUS Version 6.7-1. ABAQUS Inc. Rising Sun Mills: RI. USA.
- ANSYS Inc. 2000. User's manual for ANSYS 5.7. ANSYS Inc., Canonsburg, Pa.
- American Petroleum Institute (API). 2000. Recommended practice for planning, designing and constructing fixed offshore platforms. 21st ed. American Petroleum Institute. Washington D.C. API Recommended Practice 2A (RP-2A).
- Bardet, J. P., and Tobita, T. 2001. NERA: Nonlinear earthquake site response analysis of layered soil deposits. Univ. of California, [_http://geoinfo.usc.edu/gees](http://geoinfo.usc.edu/gees).
- Berger, E., Mahin, S.A. and Pyke R. 1977. Simplified method for evaluating soil-pile-structure interaction effects. Proceedings of the 9th Offshore Technology Conference, OTC paper 2954, Huston, Texas, 589-598.
- Boulanger, R.W., Curras, C.J., Kutter, B.L., Wilson, D.W. and Abghari, A. 1999. Seismic soil pile structure interaction and experiments. J. of Geotechnical and Geoenvironmental Engineering, ASCE, Vol. 125, No. 9, pp. 750-759.
- Elgamal, A., Yang, Z., and Lu, J. 2006. CYCLIC 1D: A computer program for seismic ground response. Report No. SSRP-06/05, Department of Structural Engineering, University of California, San Diego, la Jolla, CA.
- Elgamal, A., Yang, Z., and Parra, E. 2003. Modeling of cyclic mobility in saturated cohesionless soils. International Journal of Plasticity, Vol 19, pp. 883-905
- Elgamal, A., Yang, Z., and Parra, E. 2002. Computational modeling of cyclic mobility and post-liquefaction site response. Soil Dynamics and Earthquake Engineering, Vol 22, pp 259-271.
- El Naggar, M.H. & Bentley, K. J. 2000. Dynamic analysis for laterally loaded piles and dynamic p-y curves. Canadian Geotechnical Journal, Vol. 37. Issue. 6. pp 1166-1183.
- El Naggar, M.H., Shayanfar, M. A., Kimiaei, M. and Aghakouchak, A. A. 2005. Simplified BNWF model for nonlinear seismic response analysis of offshore piles with nonlinear input ground motion analysis. Canadian Geotechnical Journal, Vol. 42, pp. 365-380.
- Hardin, O.B. and Drnevitch, P.V. 1972. Shear modulus and damping in soils: design equations and curves. Journal of Soil Mechanics and Foundations Divisions, ASCE, Vol. 98, No.SM7, pp. 667-692.
- Hazen, A. 1930. Water supply. American Civil Engineers Hand Book. Wiley, Newyork.

Idriss, I. M., and Sun, J. I. 1991. SHAKE91: A computer program for conducting equivalent linear seismic response analyses of horizontally layered soil deposits. Center for Geotechnical Modeling, Dept. of Civil and Environmental Engineering, Univ. of California, Davis, Calif.

Kimiaei, M., El Naggar, M.H., Shayanfar, M. A. and Aghakouchak, A. A. 2004. Non linear seismic pile soil structure interaction analysis of piles in offshore platforms. Proc. of 23rd International Conference on Offshore Mechanics and Arctic Engineering, Vancouver, Canada.

Kramer, S. L. 1996. Geotechnical earthquake engineering. Prentice-Hall, Upper Saddle River, N.J.

Liyanapathirana, D.S. and Poulos, H.G. (2005), " Seismic lateral response of piles in liquefying soil," J. of Geotechnical and Geoenvironmental Engineering, ASCE, Vol. 131, No. 12., pp.1466-1479.

Lo Presti, Diego C. F., Lai, Carlo G. and Puci, Ignazio. 2006. ONDA: Computer Code for Nonlinear Seismic Response Analyses of Soil Deposits. Journal of Geotechnical and Geoenvironmental Engineering, Vol. 132, No. 2, February 1, 2006, pp. 223-236

Murchison, Jack M., and O'Neill, Michael W. 1984. Evaluation of p-y relationships in cohesionless soils. (Texas Dep of Highways & Public Transportation, Bridge Div, Austin, TX, USA). Source: ASCE, pp. 174-191.

Reese, L.C. Cox, W.R. and Koop, F.D. 1974. Analysis of laterally loaded piles in sand. Offshore Technology Conference, paper No. OTC 2080, pp. 473-483

Reese, L.C. and Van Ampe, W.F. 2001. Single piles and pile groups under Lateral Loading. © 2001 A.A. Balkema, Rotterdam, ISBN 90 5809 3409.

Talukder, M. K., and Butt, S.D. 2009a. Nonlinear seismic Free field response of saturated sand. 1st International/1st Engineering Mechanics and Material Specialty Conference (IEMM), St. John's, Newfoundland and Labrador, May 27-30, 2009, pp. IEMM-06(1-10)

Talukder, M. K., Butt, S. D., and Popescu, R. 2009b. Evaluation of Seismic Lateral Response of a Pile in Saturated Sand. 1st International/1st Engineering Mechanics and Materials Specialty Conference, St John's, Newfoundland, May 28, 2009. pp. IEMM-07(1-10)

Wilson, D. W., Boulanger, R. W., & Kutter, B. L. 1997a. Soil-pile superstructure interaction at soft or liquefiable soil sites. Centrifuge Data Rep. for Csp2. UCD/CGMDR-97/03. University of California at Davis. Davis: Calif.

Wilson, D. W., Boulanger, R. W., and Kutter, B. L. 1997b. Soil-pile superstructure interaction at soft or liquefiable soil sites. Centrifuge Data Rep. for Csp3. UCD/CGMDR-97/04, Ctr. Geotech. Modeling, University of California at Davis, Davis, Calif.

Wilson, D. W. 1998. Soil-Pile-Superstructure interaction in Liquefying sand soft clay, Ph.D. Dissertation, Department of Civil and Environmental Engineering, University of California, Davis.

Wilson, D. W., Boulanger, R. W. and Kutter, B. 2000. Observed seismic lateral resistance of liquefying sand. J. of Geotechnical and Geoenvironmental Engineering, ASCE, Vol. 126, No. 10, pp. 898-906.

Wu, G. and Finn, W.D. 1997. Dynamic nonlinear analysis of pile foundations using finite element method in the time domain. Canadian Geotechnical Journal Vol. 34, No. 1, pp. 44-52

Appendix A: Excess Pore Water Pressure Time Histories

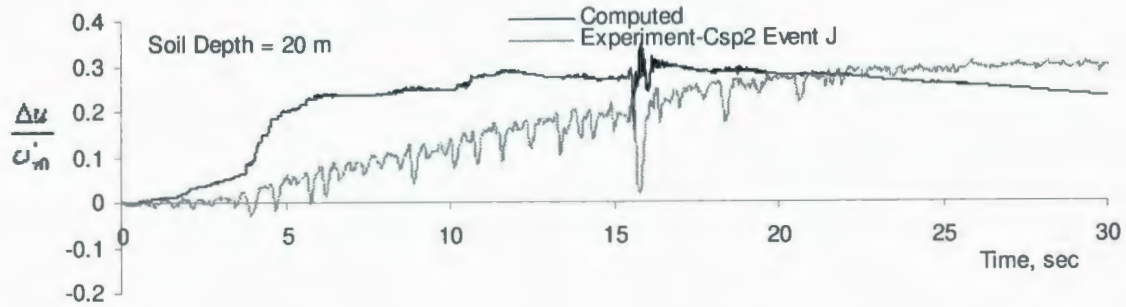


Figure A-1: Excess Pore Water Pressure Time Histories of Event J, Csp2 (soil depth 20 m).

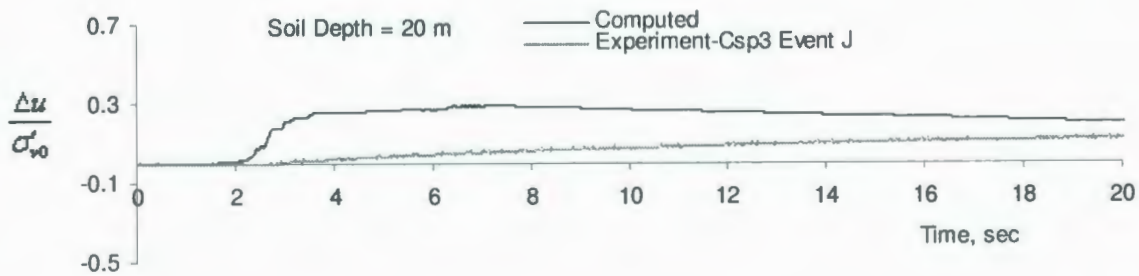


Figure A-2: Excess Pore Pressure Time Histories of Event J, Csp3 (soil depth 20 m).

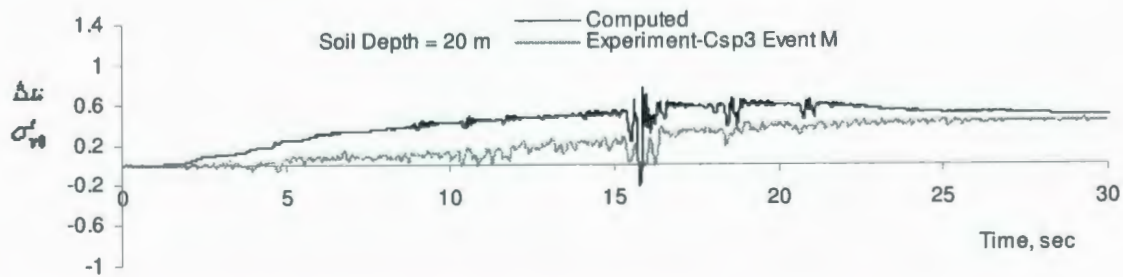


Figure A-3 : Excess Pore Pressure Time Histories of Event M, Csp3 (soil depth 20 m).

Appendix B: Pile Response Time Histories

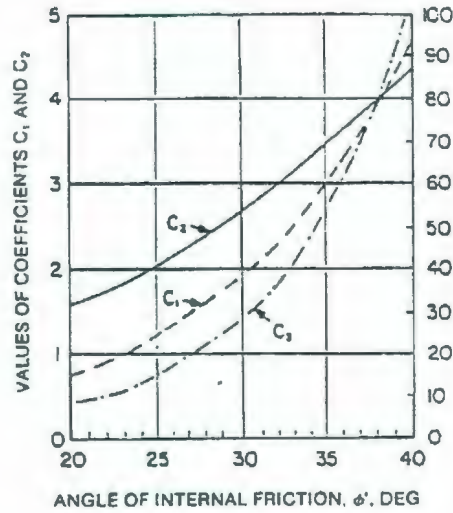


Figure B-1: Parameters C_1 , C_2 and C_3 (API, 2000).

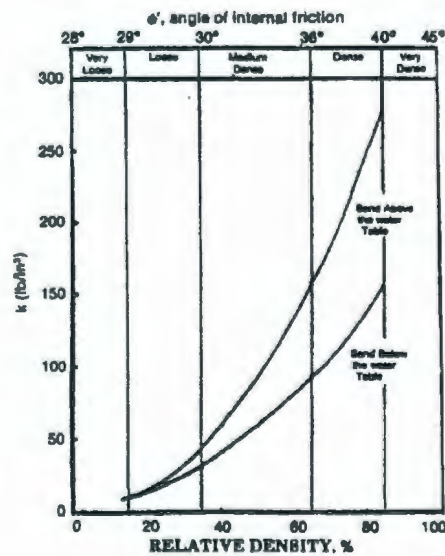


Figure B-2: Initial modulus of subgrade reaction for sands (API, 2000).

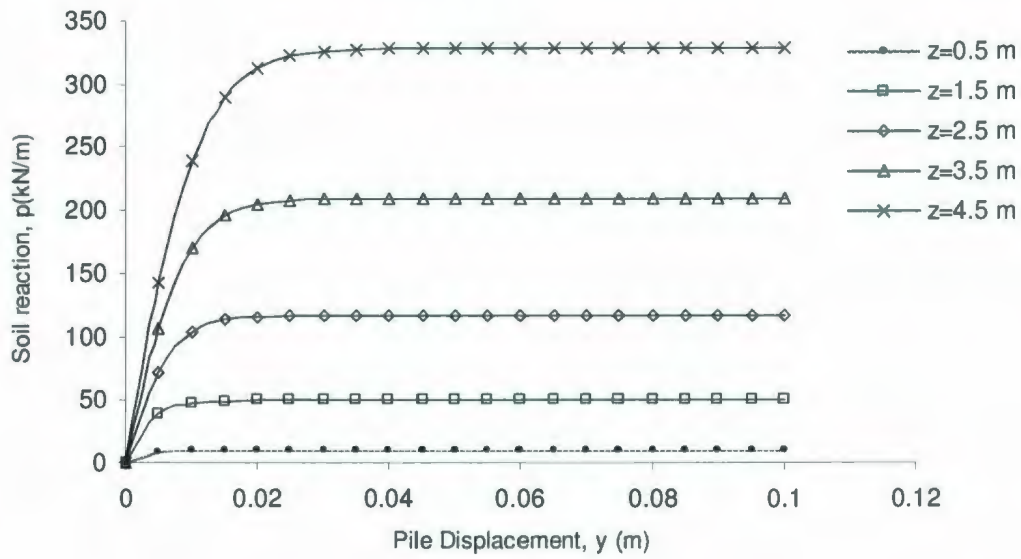


Figure B-3: Typical p-y curves for loose sand layer ($D_r = 35\%$) in Csp2 centrifuge model using API, 2000.

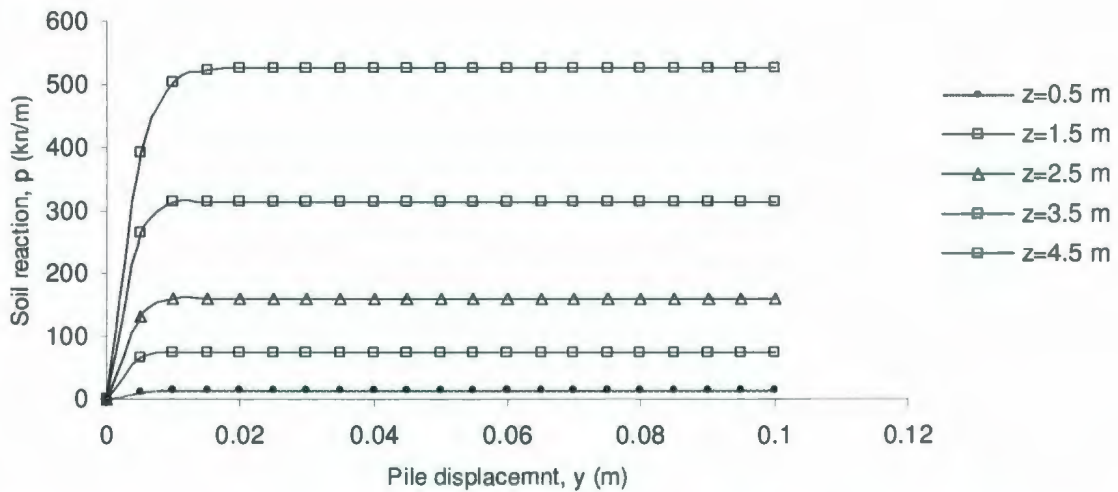


Figure B-4: Typical p-y curves for loose sand layer ($D_r = 55\%$) in Csp3 centrifuge model using API, 2000.

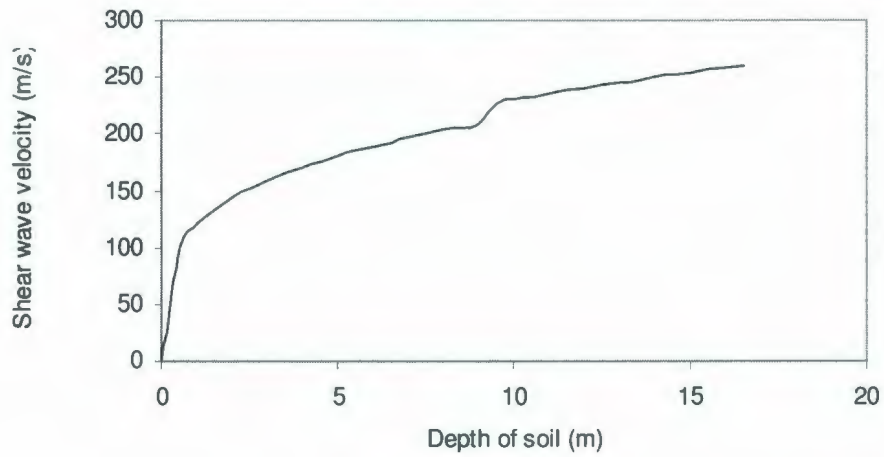


Figure B-5: Shear Wave Velocity Profile for the soil in Csp2 centrifuge model.

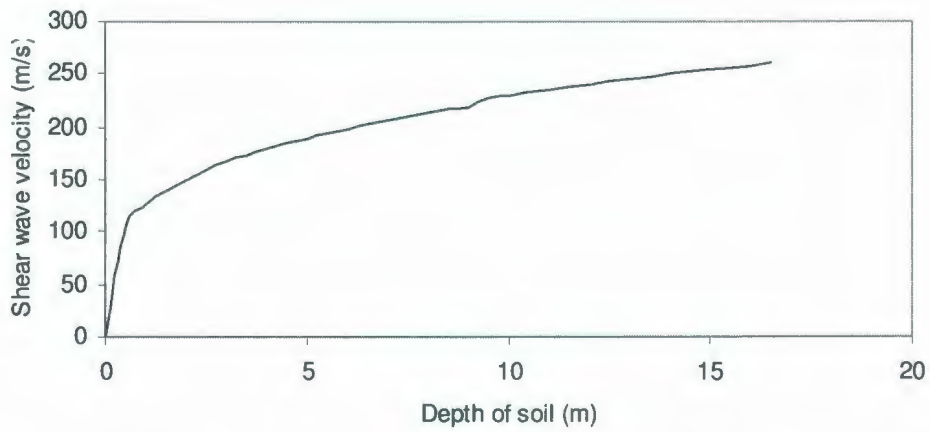


Figure B-6: Shear Wave Velocity Profile for the soil in Csp3 centrifuge model.

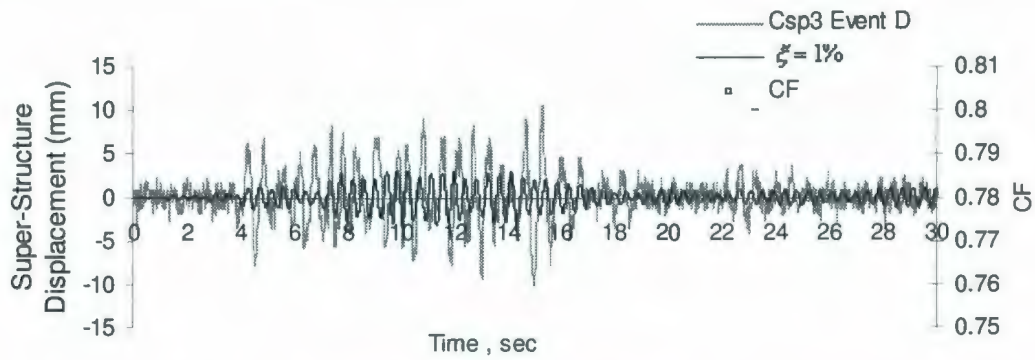


Figure B-7: Verification of the effect of time step 0.005 s on predicted response of the pile.

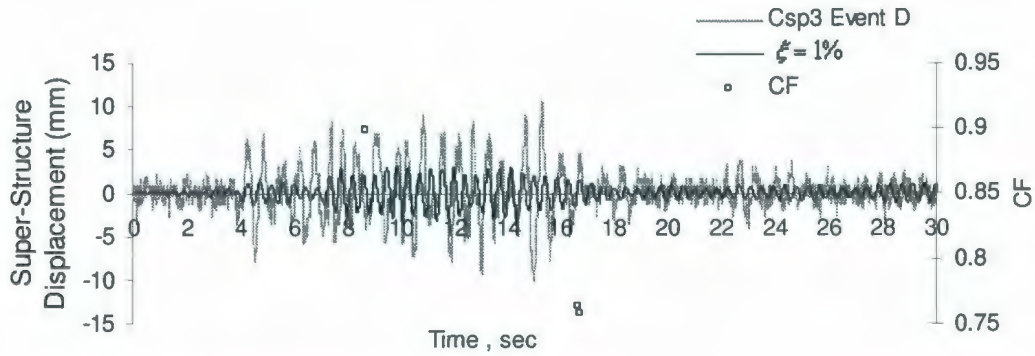


Figure B-8: Verification of the effect of time step 0.01 s on predicted response of the pile.

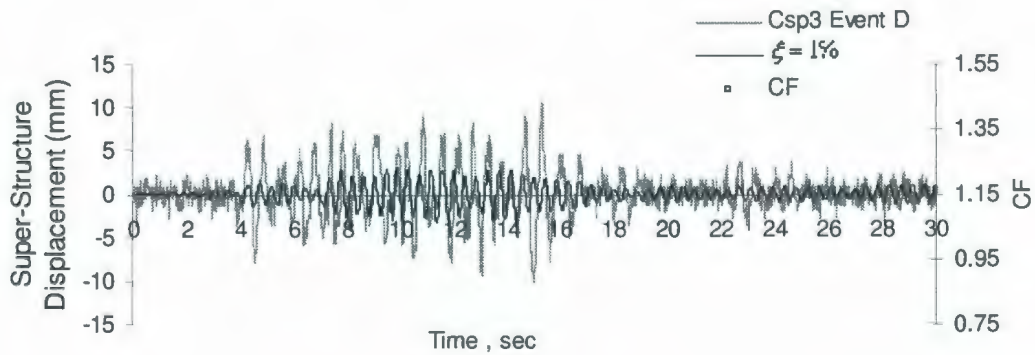


Figure B-9: Verification of the effect of time step 0.02 s on predicted response of pile.

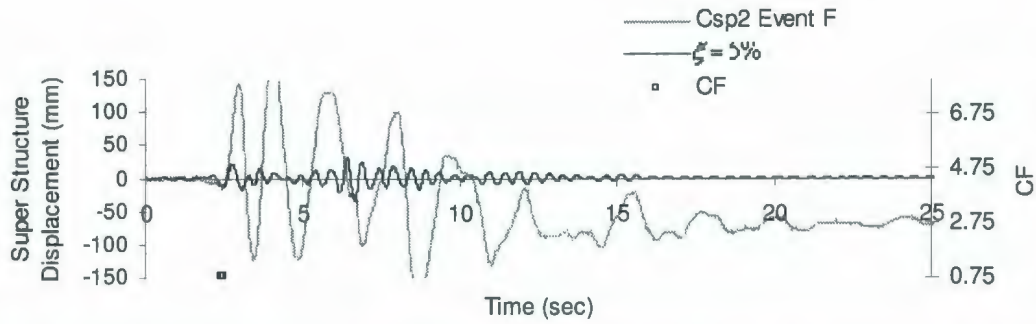


Figure B-10: Comparison of Superstructure Displacement Time History for Event F, Csp2.

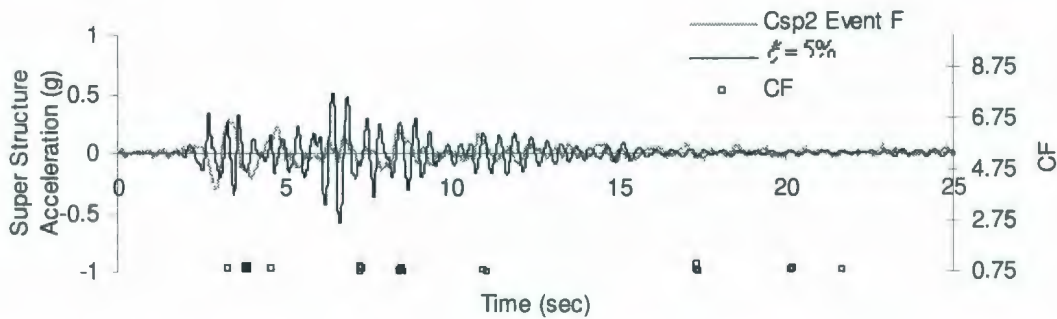


Figure B-11: Comparison of Superstructure Acceleration Time History for Event F, Csp2.

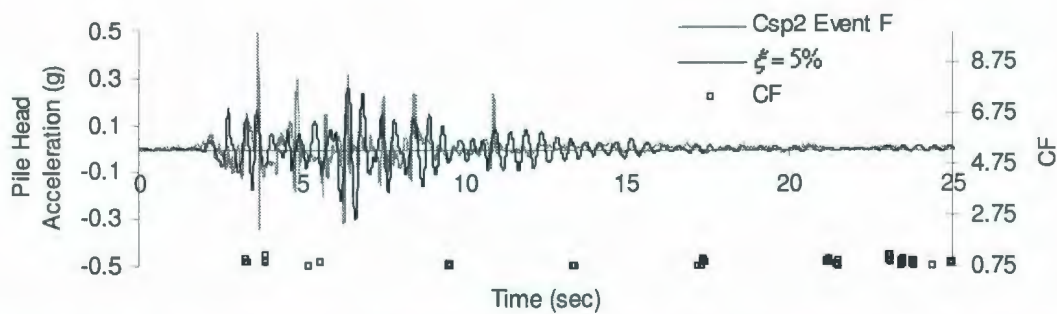


Figure B-12: Comparison of Pile Head Acceleration Time History for Event F, Csp2.

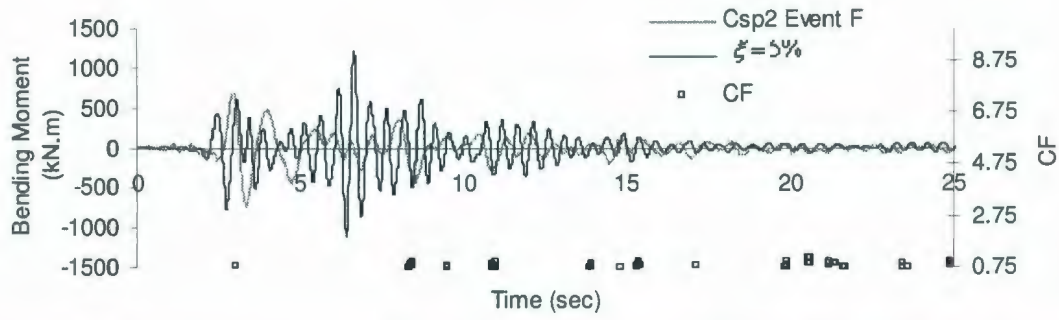


Figure B-13: Comparison of Bending Moment Time History for Event F, Csp2 at soil depth 0.5 m.

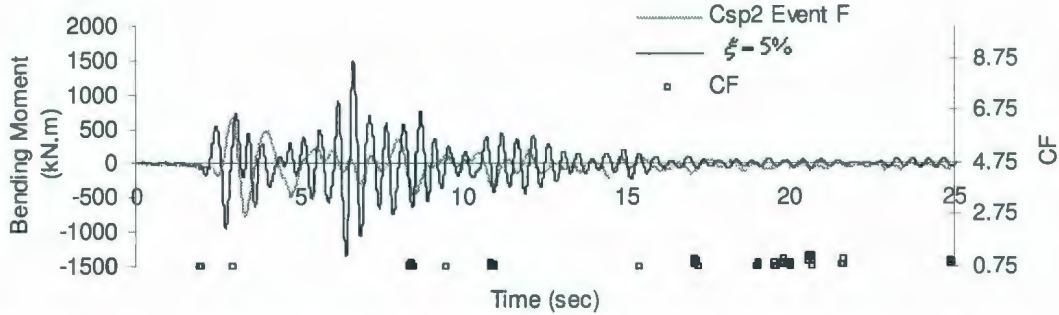


Figure B-14: Comparison of Bending Moment Time History for Event F, Csp2 at soil depth 1.5 m.

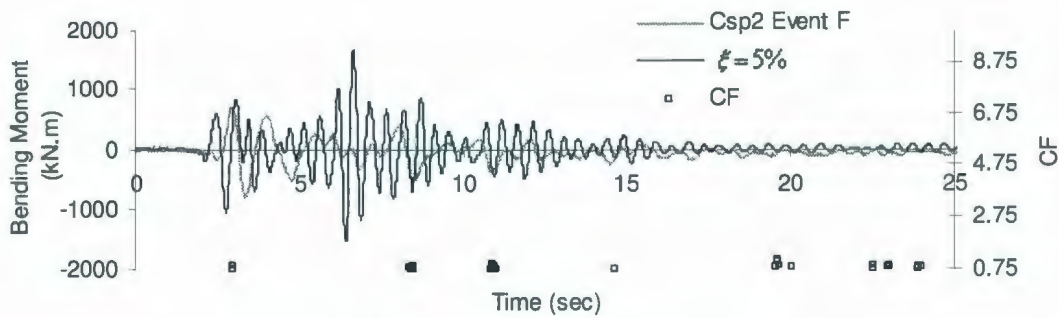


Figure B-15: Comparison of Bending Moment Time History for Event F, Csp2 at soil depth 2.5 m.

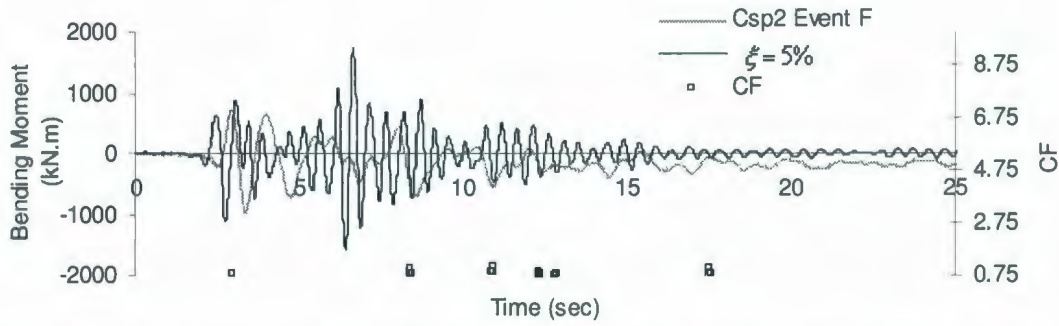


Figure B-16: Comparison of Bending Moment Time History for Event F, Csp2 at soil depth 4.0 m.

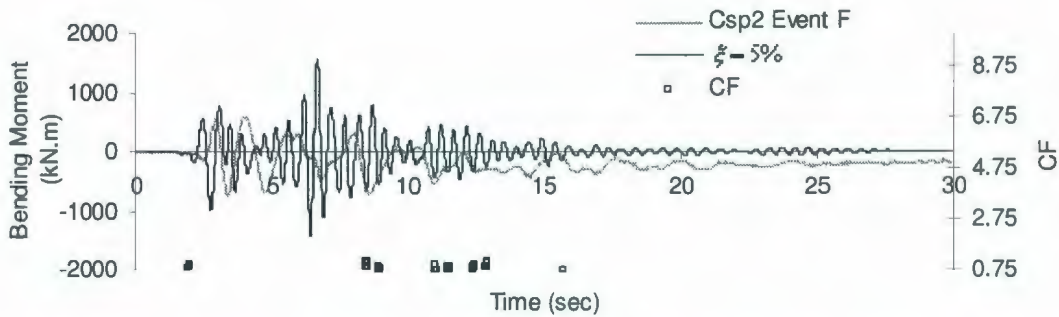


Figure B-17: Comparison of Bending Moment Time History for Event F, Csp2 at soil depth 5.5 m.

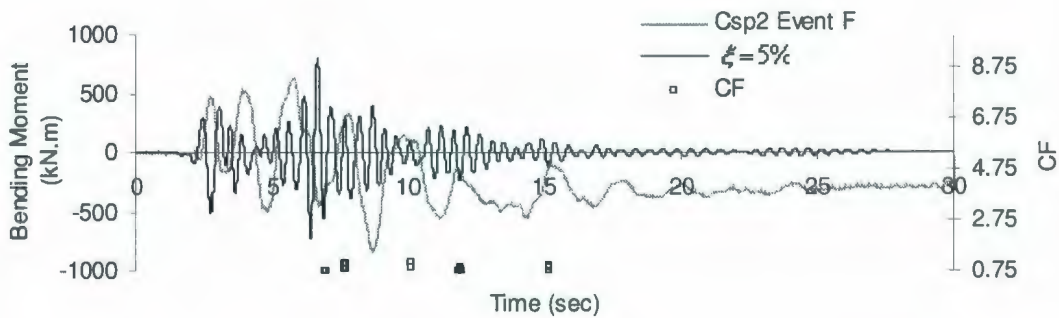


Figure B-18: Comparison of Bending Moment Time History for Event F, Csp2 at soil depth 8.5 m.

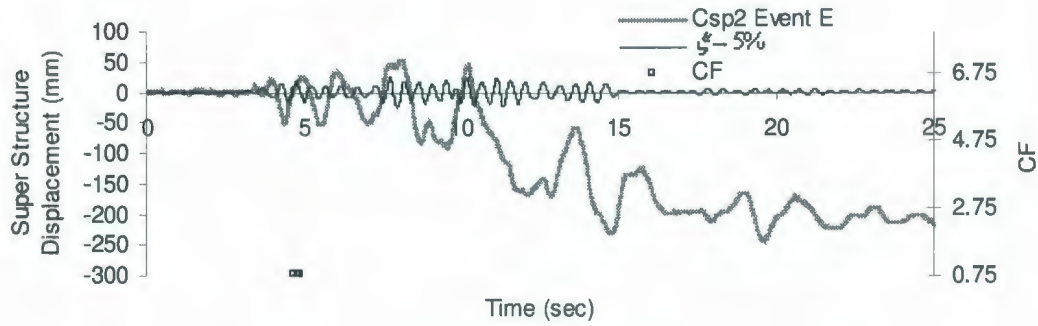


Figure B-19: Comparison of Superstructure Displacement Time History for Event E, Csp2.

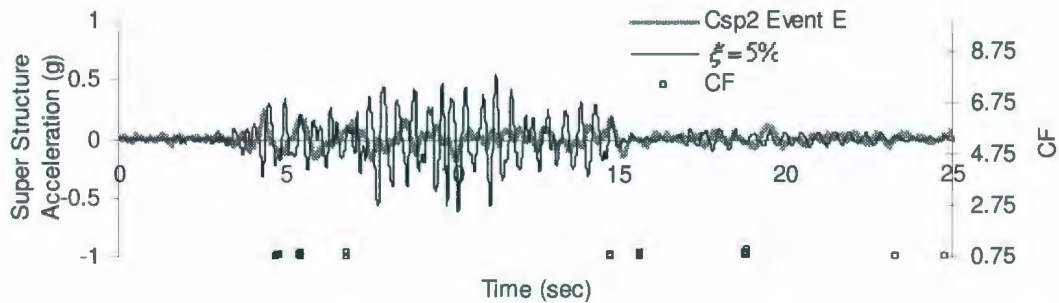


Figure B-20: Comparison of Superstructure Acceleration Time History for Event E, Csp2.

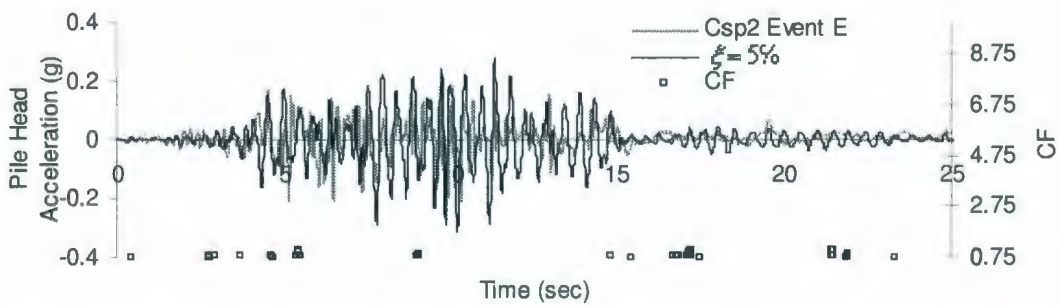


Figure B-21: Comparison of Pile Head Acceleration Time History for Event E, Csp2.

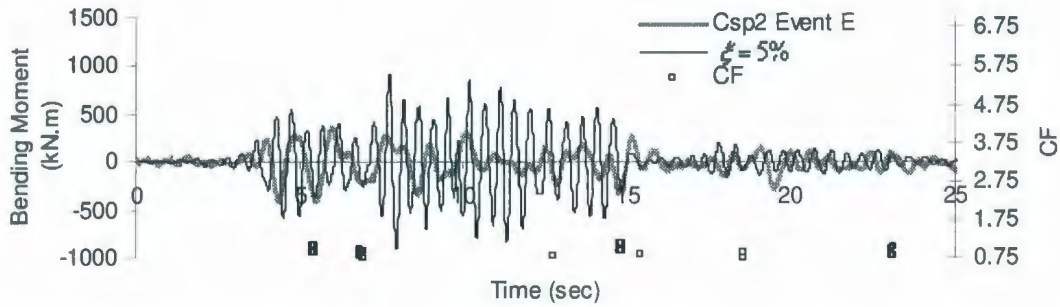


Figure B-22: Comparison of Bending Moment Time History for Event E, Csp2 at soil depth 0.5 m.

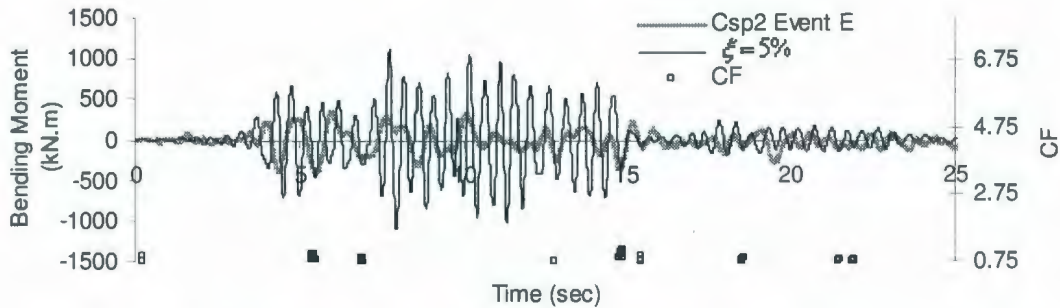


Figure B-23: Comparison of Bending Moment Time History for Event E, Csp2 at soil depth 1.5 m.

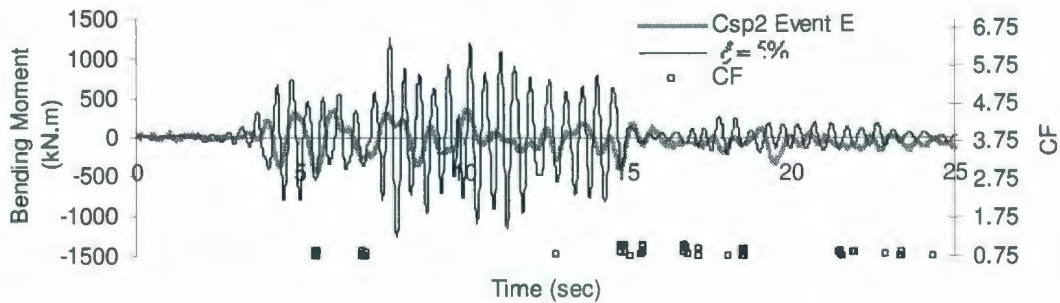


Figure B-24: Comparison of Bending Moment Time History for Event E, Csp2 at soil depth 2.5 m.

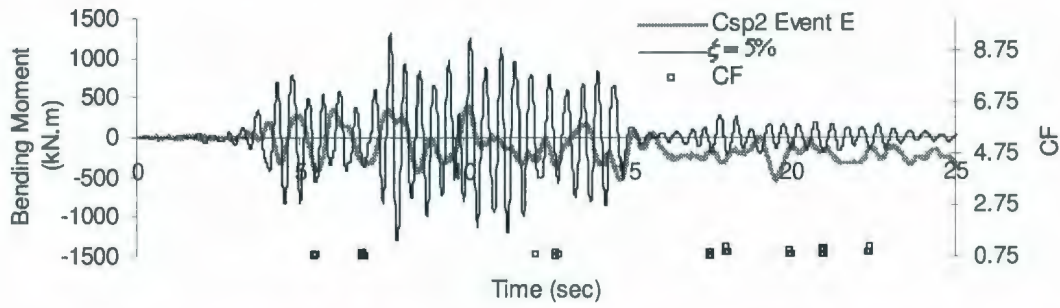


Figure B-25: Comparison of Bending Moment Time History for Event E, Csp2 at soil depth 4.0 m.

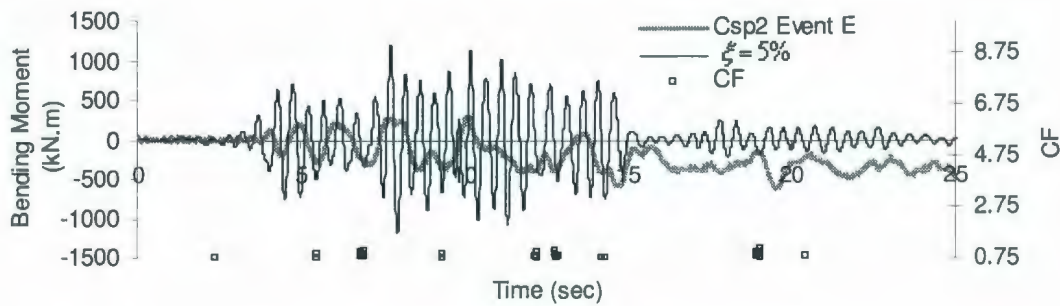


Figure B-26: Comparison of Bending Moment Time History for Event E, Csp2 at soil depth 5.5 m.

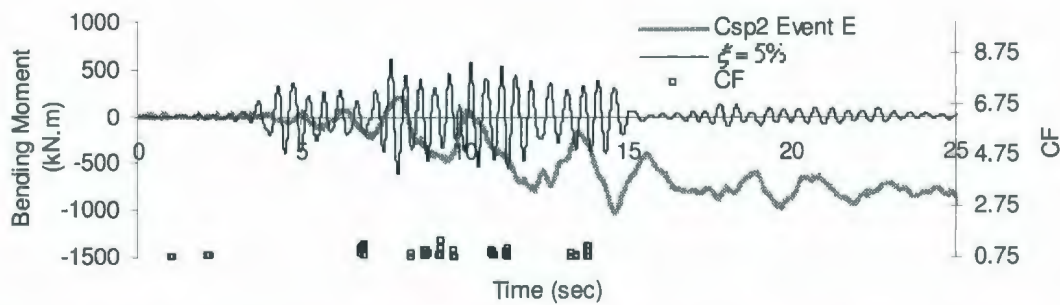


Figure B-27: Comparison of Bending Moment Time History for Event E, Csp2 at soil depth 8.5 m.

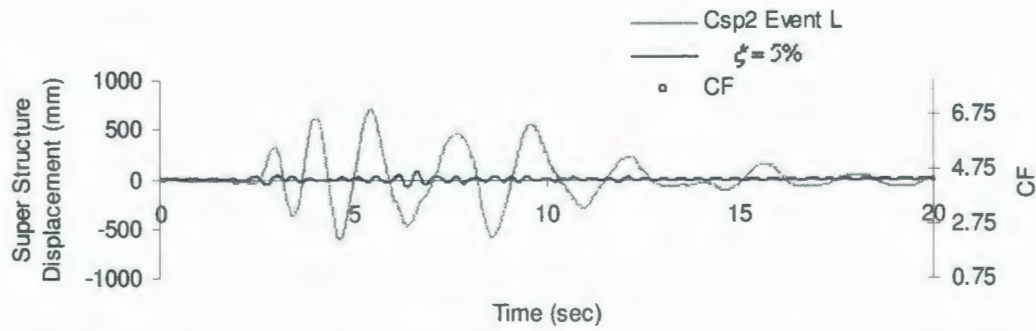


Figure B-28: Comparison of Superstructure Displacement Time History for Event L, Csp2.

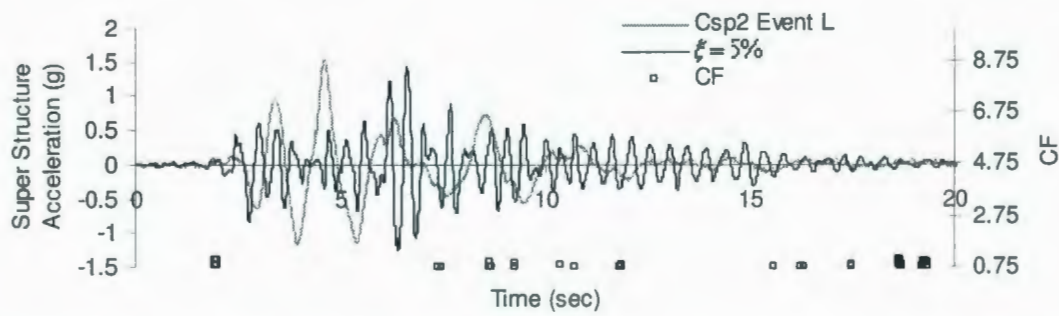


Figure B-29: Comparison of Superstructure Acceleration Time History for Event L, Csp2.

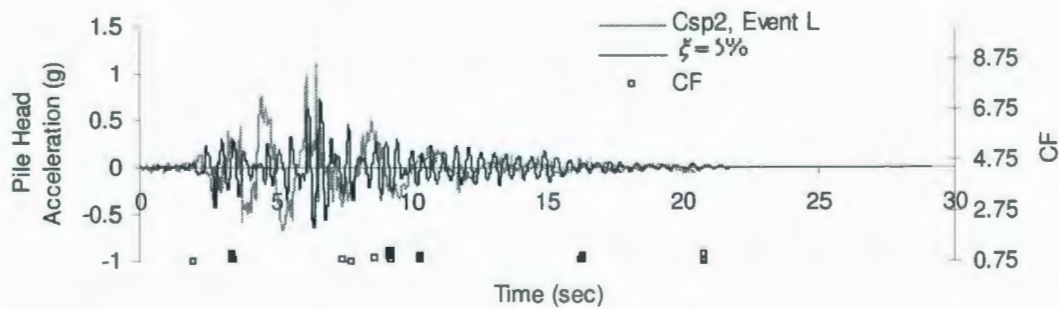


Figure B-30: Comparison of Pile Head Acceleration Time History for Event L, Csp2.

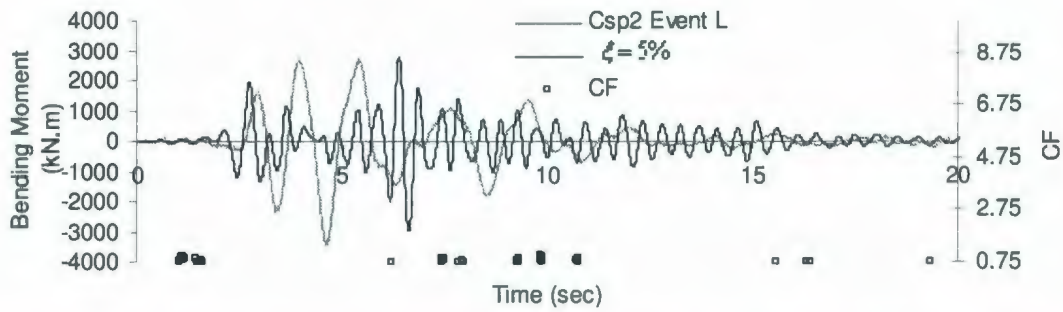


Figure B-31: Comparison of Bending Moment Time History for Event L, Csp2 at soil depth 0.5 m.

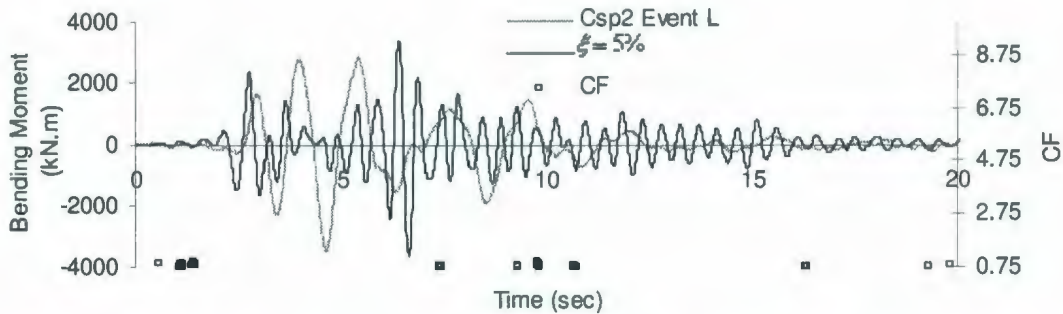


Figure B-32: Comparison of Bending Moment Time History for Event L, Csp2 at soil depth 1.5 m.

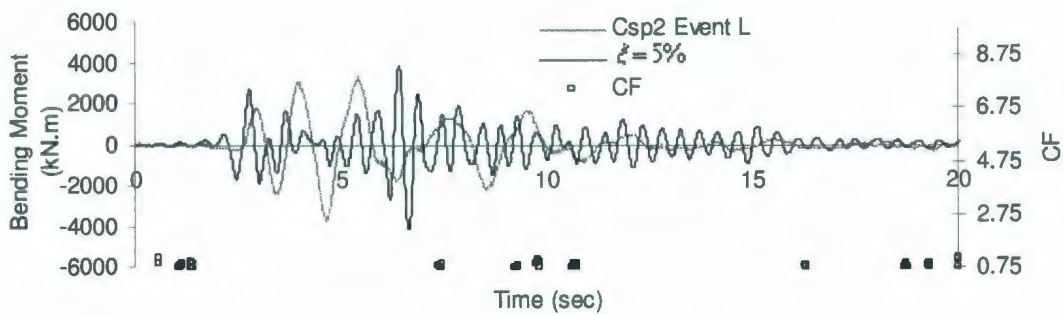


Figure B-33: Comparison of Bending Moment Time History for Event L, Csp2 at soil depth 2.5 m.

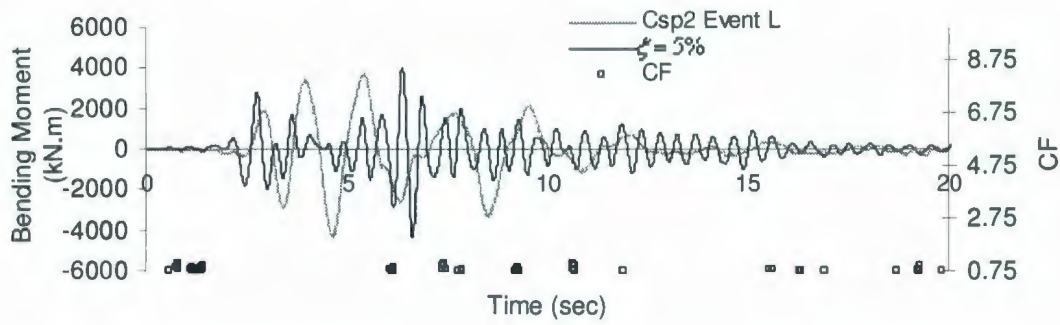


Figure B-34: Comparison of Bending Moment Time History for Event L, Csp2 at soil depth 4.0 m.

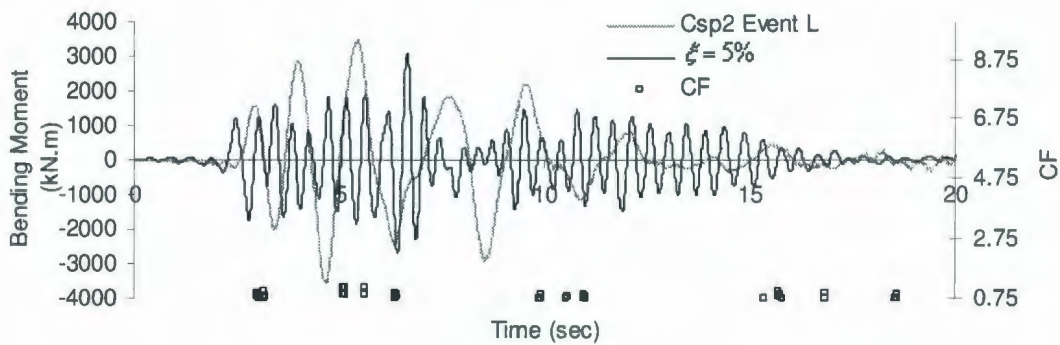


Figure B-35: Comparison of Bending Moment Time History for Event L, Csp2 at soil depth 5.5 m.

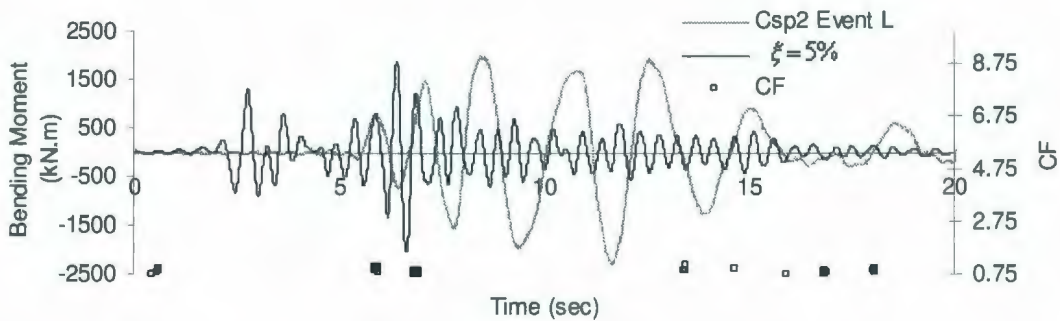


Figure B-36: Comparison of Bending Moment Time History for Event L, Csp2 at soil depth 8.5 m.

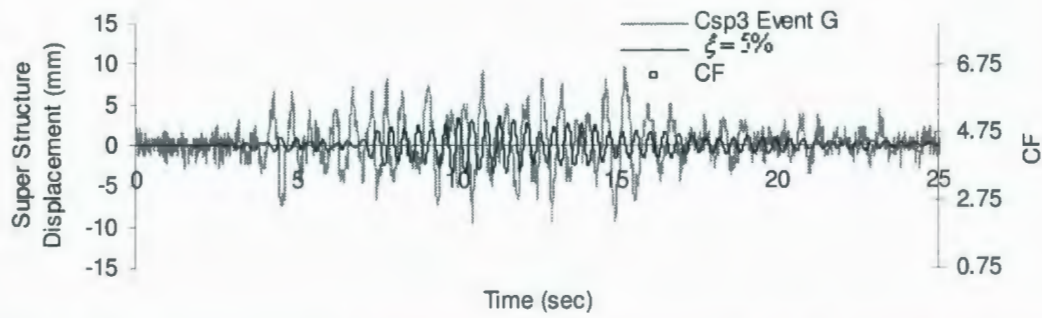


Figure B-37: Comparison of Superstructure Displacement Time History for Event G, Csp3.

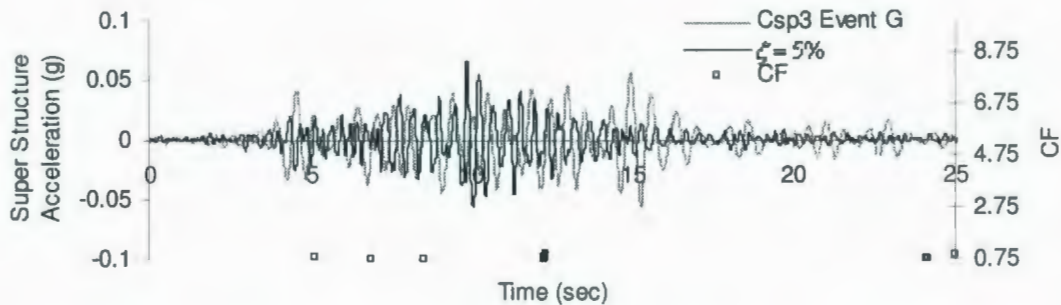


Figure B-38: Comparison of Superstructure Acceleration Time History for Event G, Csp3.

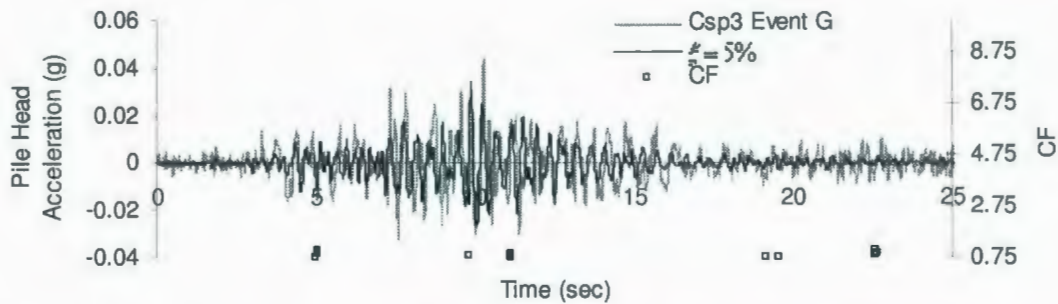


Figure B-39: Comparison of Pile Head Acceleration Time History for Event G, Csp3.

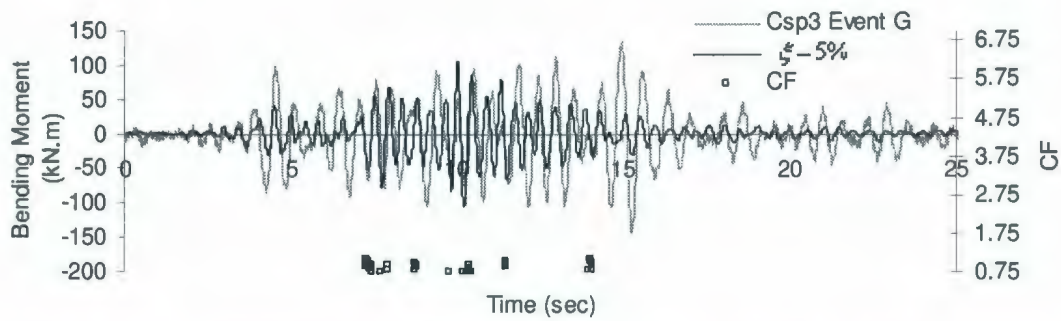


Figure B-40: Comparison of Bending Moment Time History for Event G, Csp3 at soil depth 0.5 m.

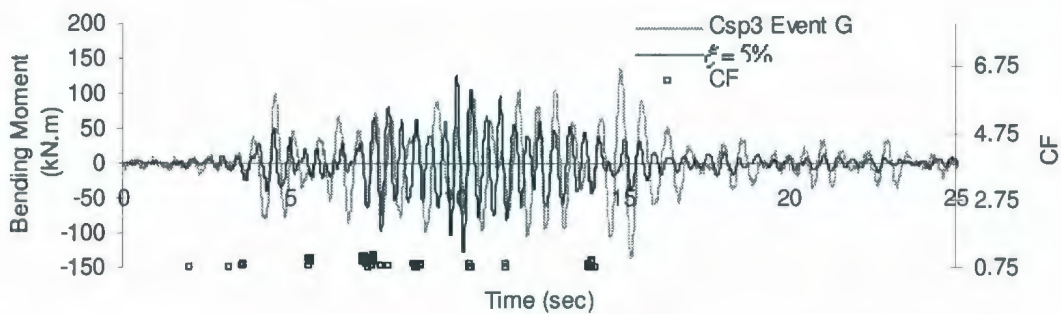


Figure B-41: Comparison of Bending Moment Time History for Event G, Csp3 at soil depth 1.5 m.

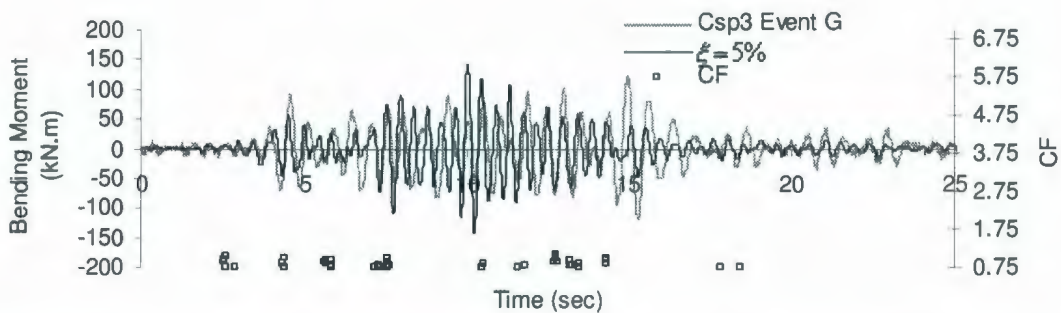


Figure B-42: Comparison of Bending Moment Time History for Event G, Csp3 at soil depth 2.5 m.

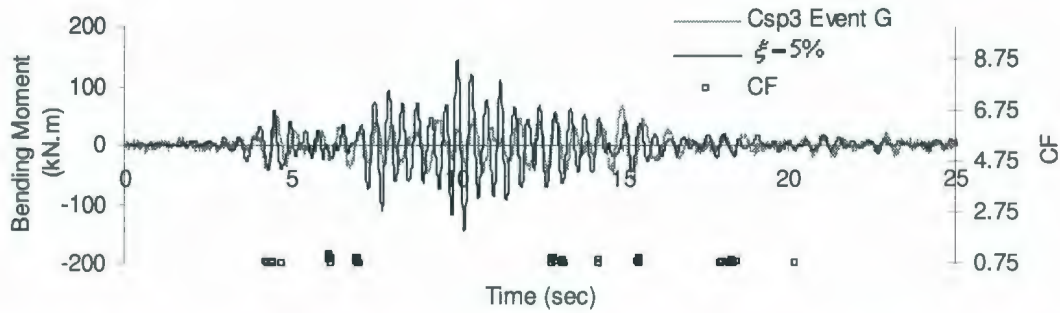


Figure B-43: Comparison of Bending Moment Time History for Event G, Csp3 at soil depth 4.0 m.

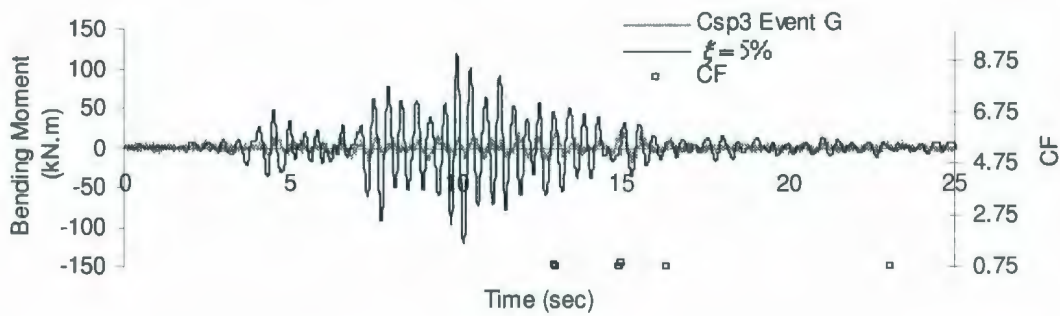


Figure B-44: Comparison of Bending Moment Time History for Event G, Csp3 at soil depth 5.5 m.

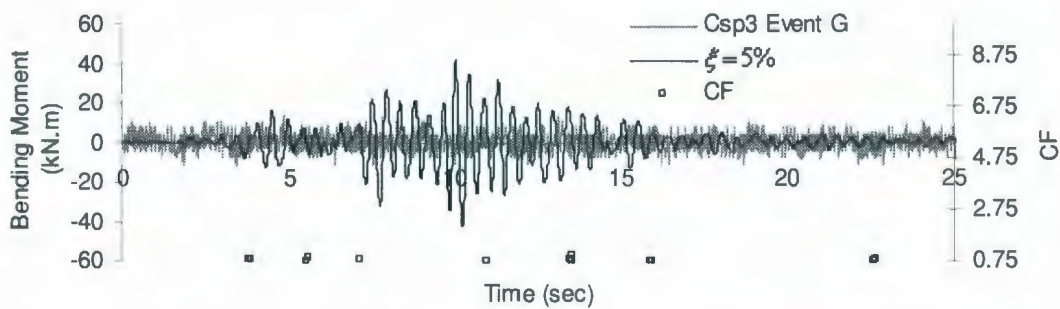


Figure B-45: Comparison of Bending Moment Time History for Event G, Csp3 at soil depth 8.5 m.

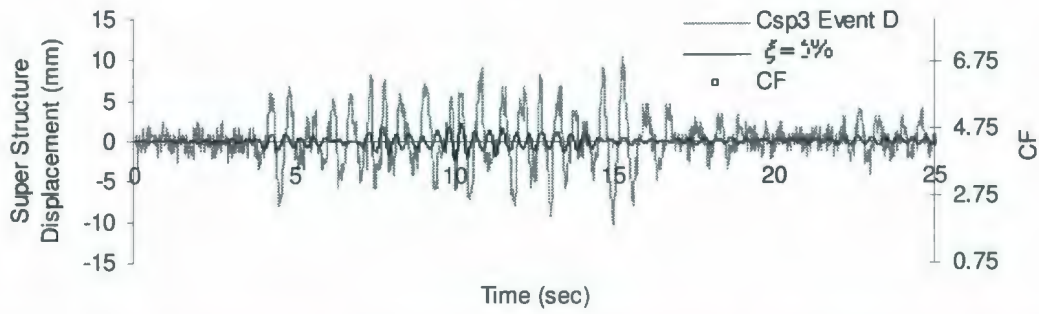


Figure B-46: Comparison of Superstructure Displacement Time History for Event D, Csp3.

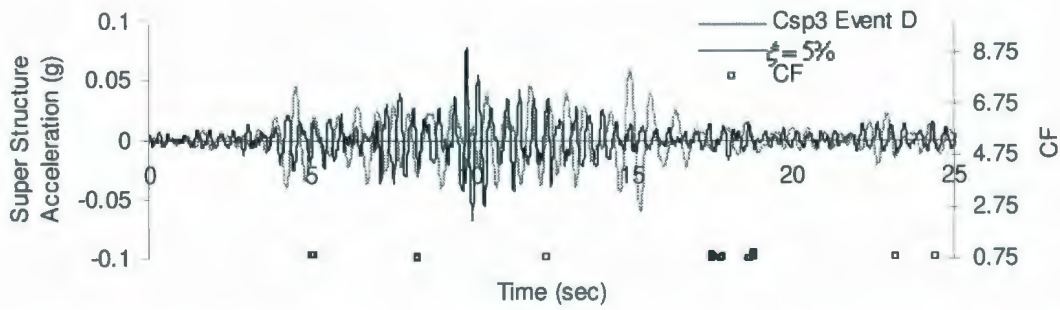


Figure B-47: Comparison of Superstructure Acceleration Time History for Event D, Csp3.

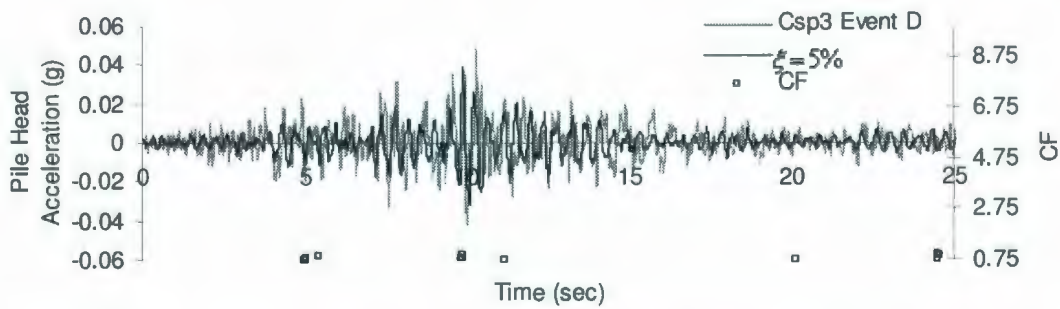


Figure B-48: Comparison of Pile Head Acceleration Time History for Event D, Csp3.

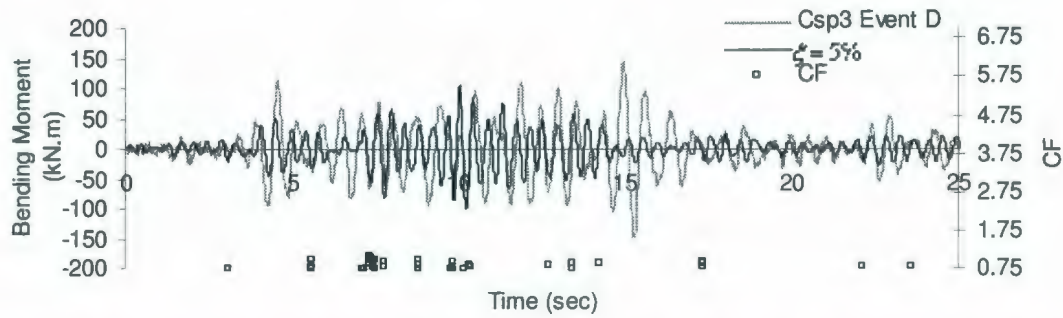


Figure B-49: Comparison of Bending Moment Time History for Event D, Csp3 at soil depth 0.5 m.

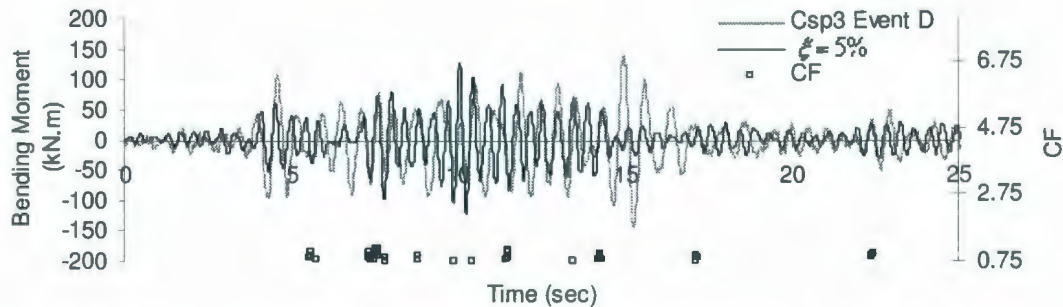


Figure B-50: Comparison of Bending Moment Time History for Event D, Csp3 at soil depth 1.5 m.

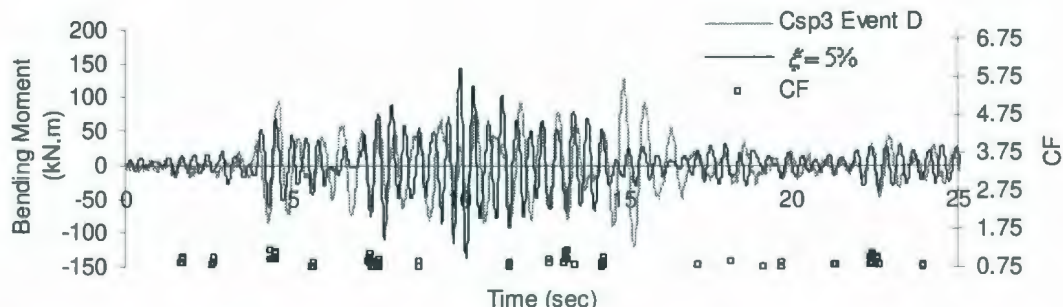


Figure B-51: Comparison of Bending Moment Time History for Event D, Csp3 at soil depth 2.5 m.

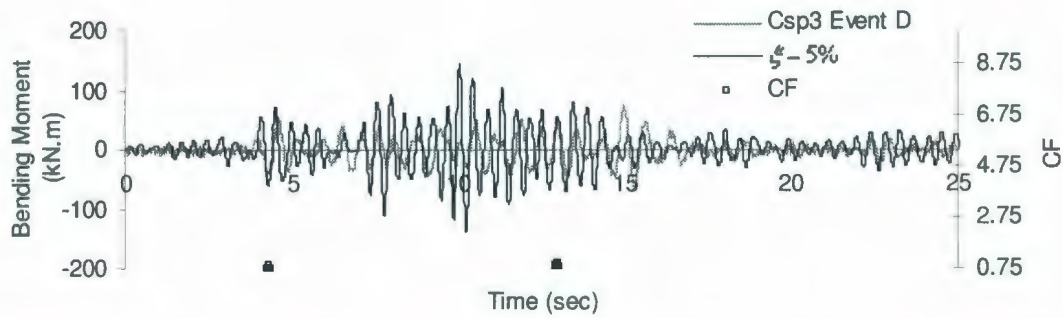


Figure B-52: Comparison of Bending Moment Time History for Event D, Csp3 at soil depth 4.0 m.

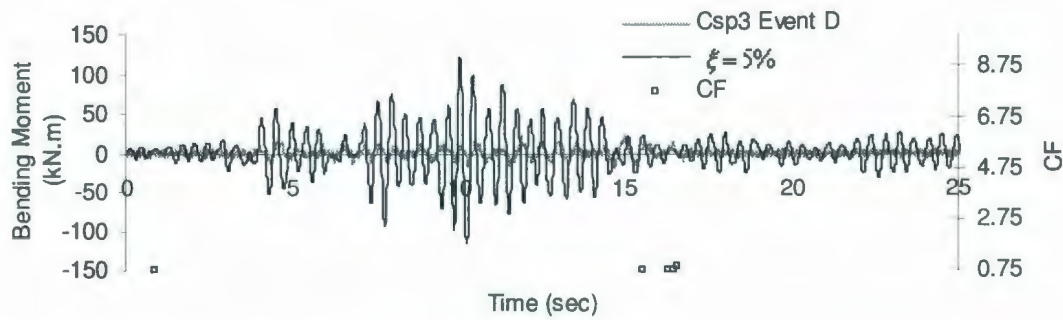


Figure B-53: Comparison of Bending Moment Time History for Event D, Csp3 at soil depth 5.5 m.

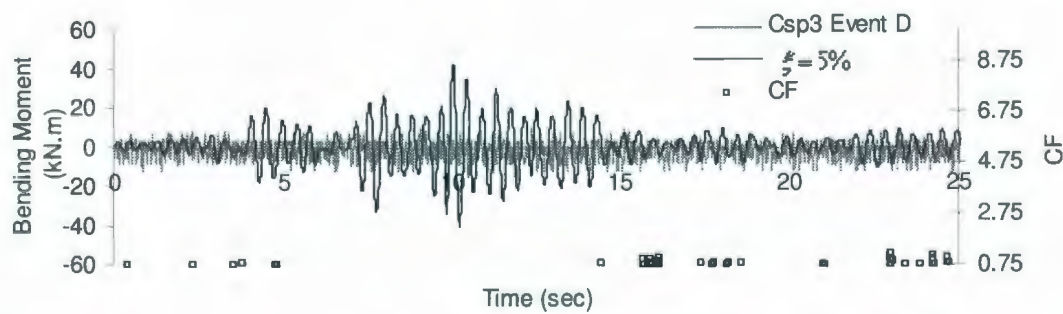


Figure B-54: Comparison of Bending Moment Time History for Event D, Csp3 at soil depth 8.5 m.

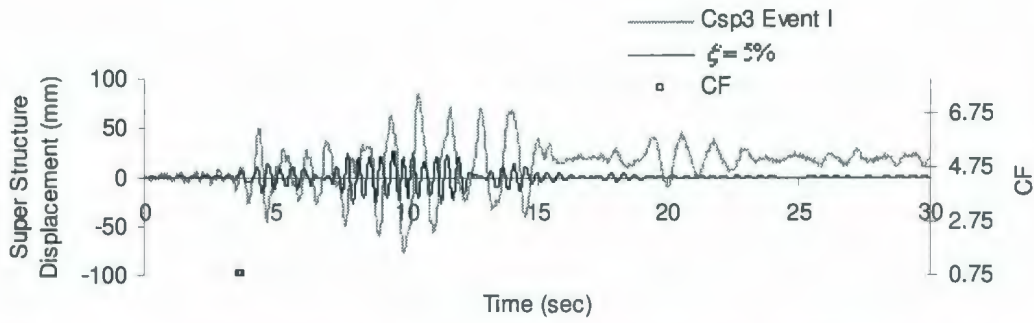


Figure B-55: Comparison of Superstructure Displacement Time History for Event I, Csp3.

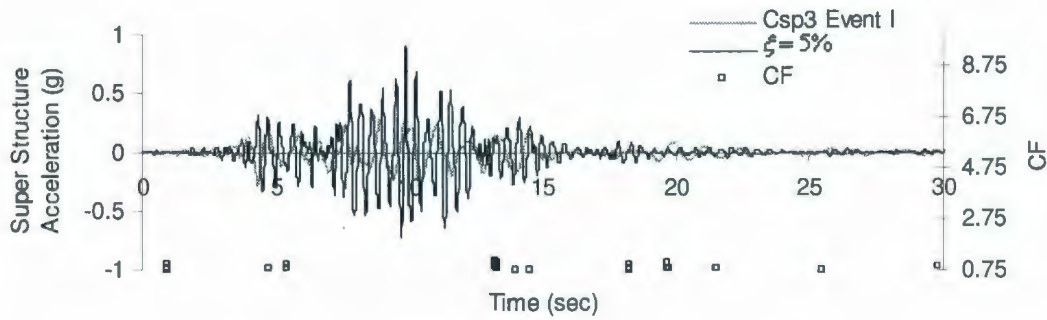


Figure B-56: Comparison of Superstructure Acceleration Time History for Event I, Csp3.

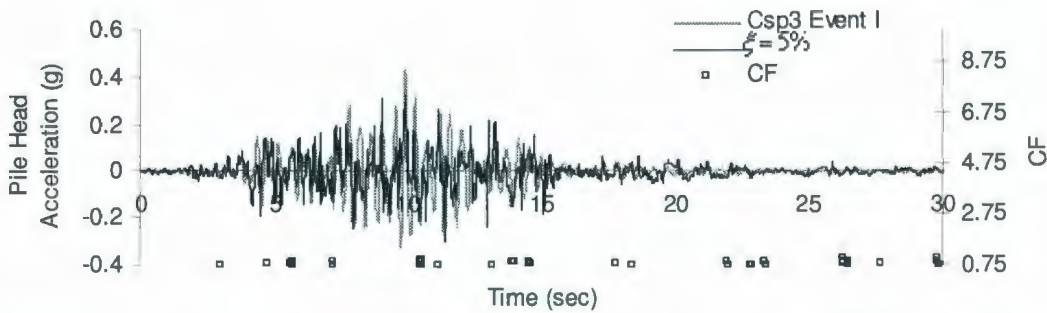


Figure B-57: Comparison of Pile Head Acceleration Time History for Event I, Csp3.

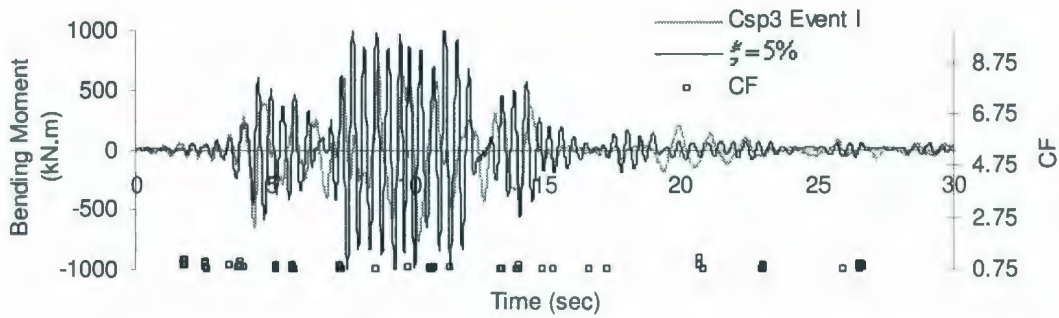


Figure B-58: Comparison of Bending Moment Time History for Event I, Csp3 at soil depth 0.5 m.

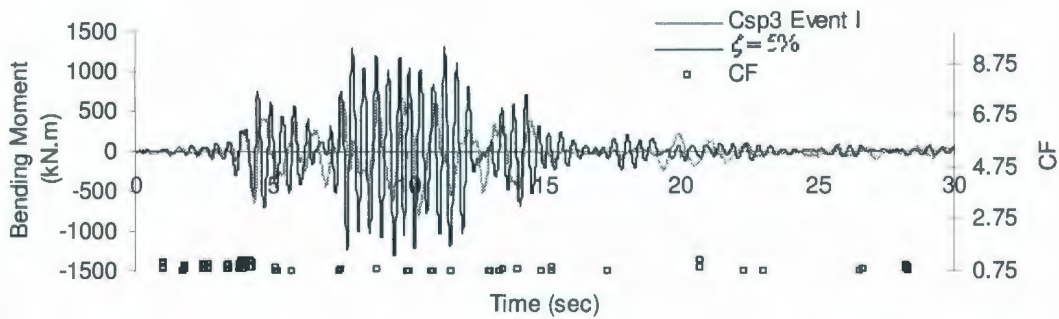


Figure B-59: Comparison of Bending Moment Time History for Event I, Csp3 at soil depth 1.5 m.

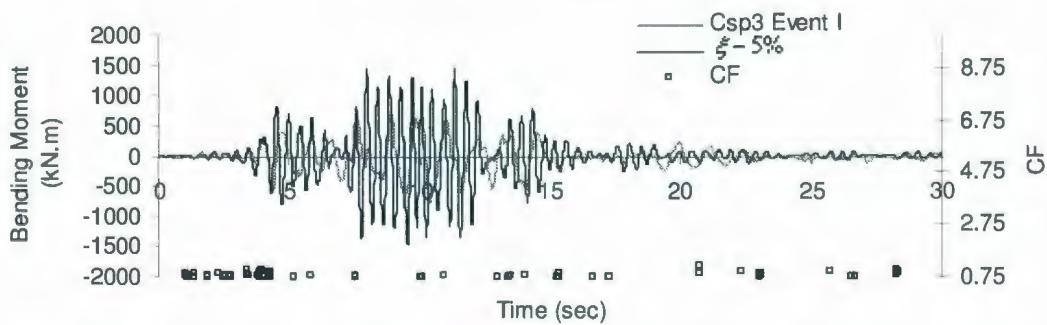


Figure B-60: Comparison of Bending Moment Time History for Event I, Csp3 at soil depth 2.5 m.

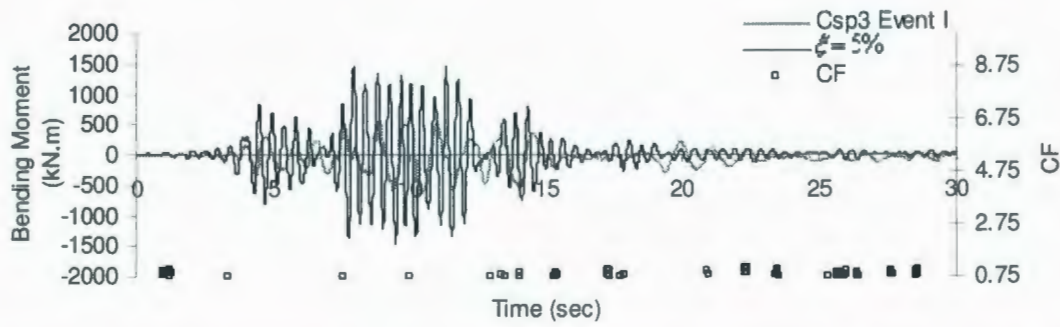


Figure B-61: Comparison of Bending Moment Time History for Event I, Csp3 at soil depth 4.0 m.

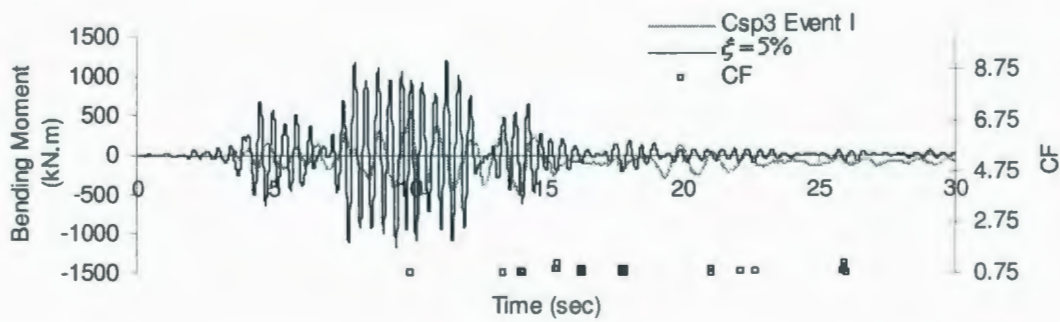


Figure B-62: Comparison of Bending Moment Time History for Event I, Csp3 at soil depth 5.5 m.

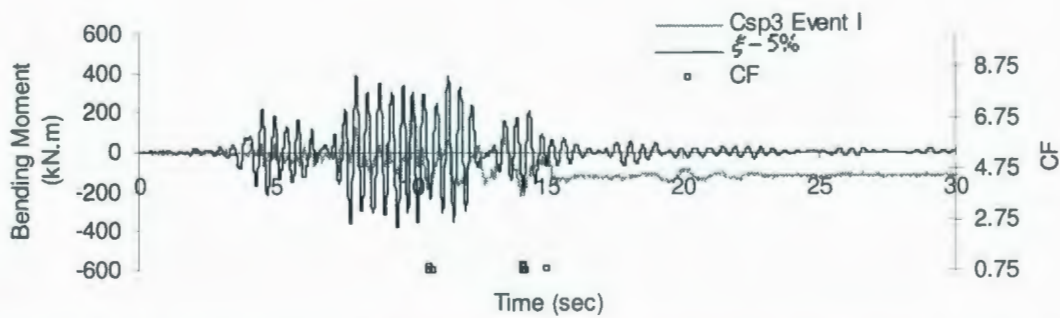


Figure B-63: Comparison of Bending Moment Time History for Event I, Csp3 at soil depth 8.5 m.

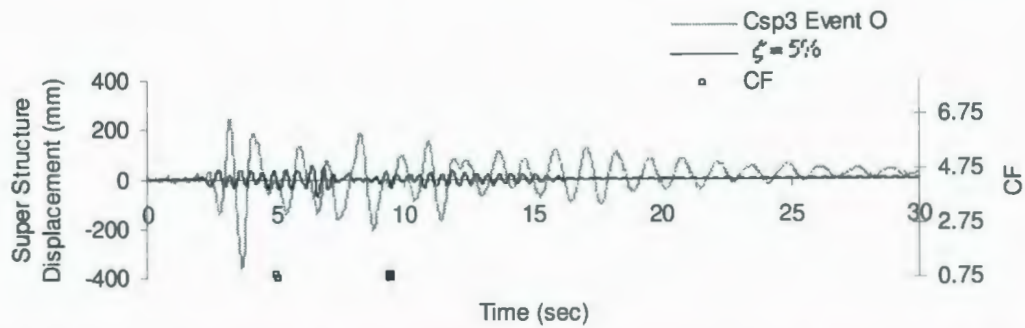


Figure B-64: Comparison of Superstructure Displacement Time History for Event O, Csp3.

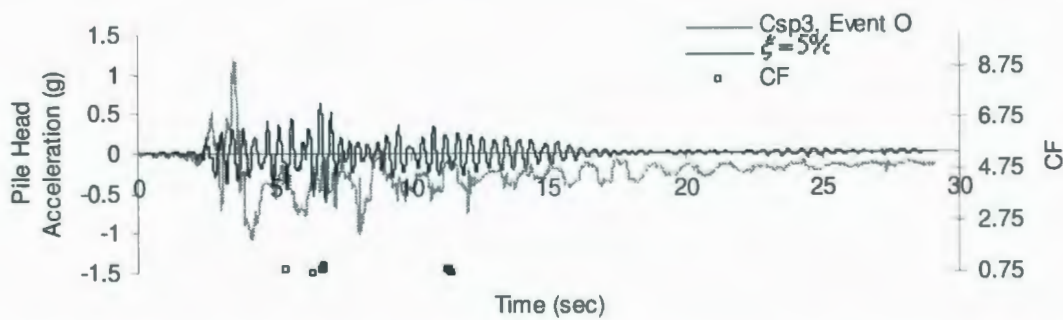


Figure B-65: Comparison of Superstructure Acceleration Time History for Event O, Csp3.

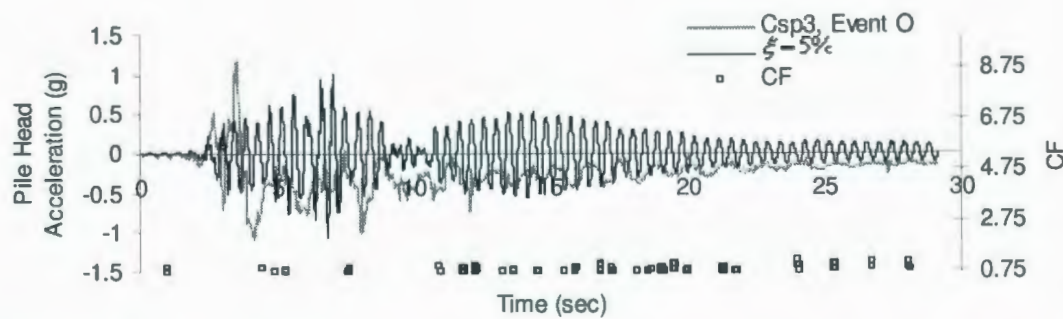


Figure B-66: Comparison of Pile Head Acceleration Time History for Event O, Csp3.

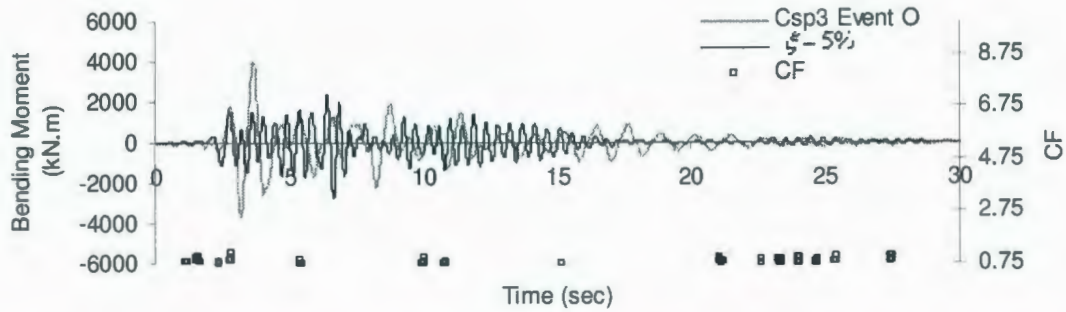


Figure B-67: Comparison of Bending Moment Time History for Event O, Csp3 at soil depth 0.5 m.

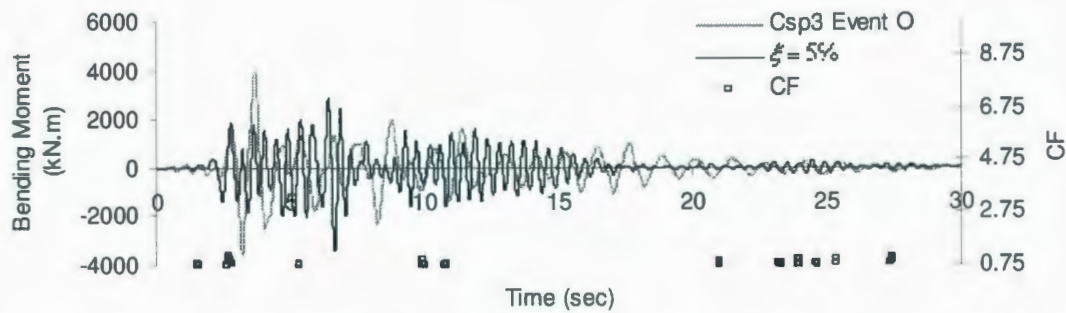


Figure B-68: Comparison of Bending Moment Time History for Event O, Csp3 at soil depth 1.5 m.

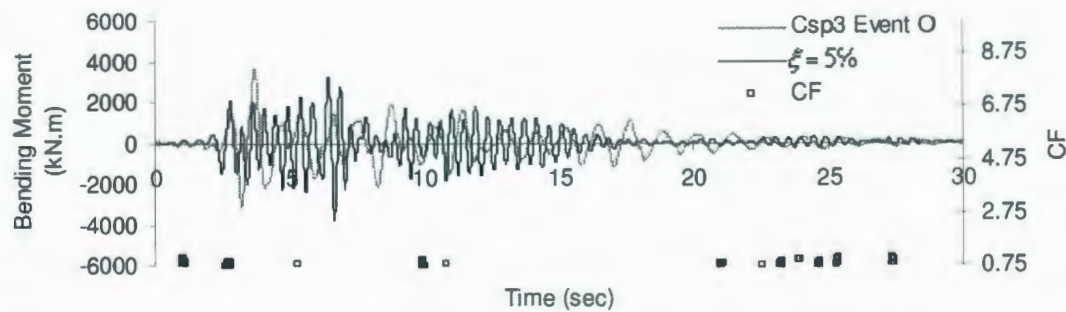


Figure B-69: Comparison of Bending Moment Time History for Event O, Csp3 at soil depth 2.5 m.

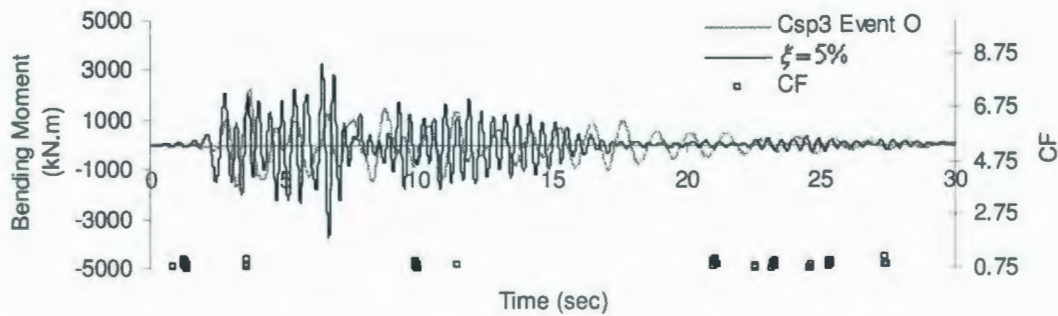


Figure B-70: Comparison of Bending Moment Time History for Event O, Csp3 at soil depth 4.0 m.

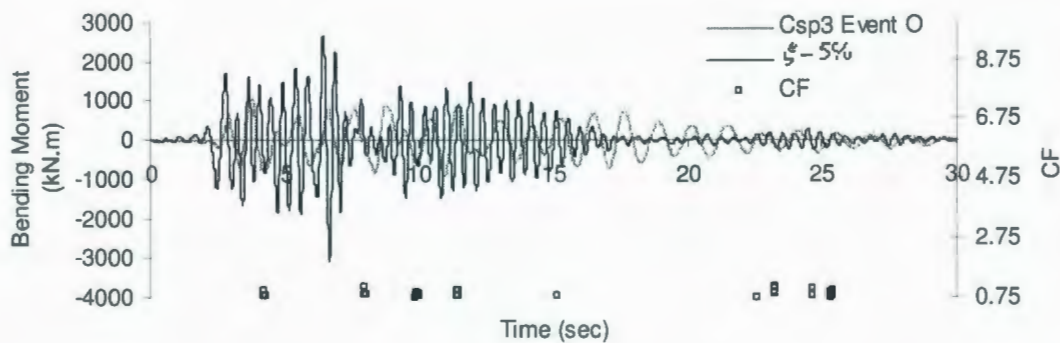


Figure B-71: Comparison of Bending Moment Time History for Event O, Csp3 at soil depth 5.5 m.

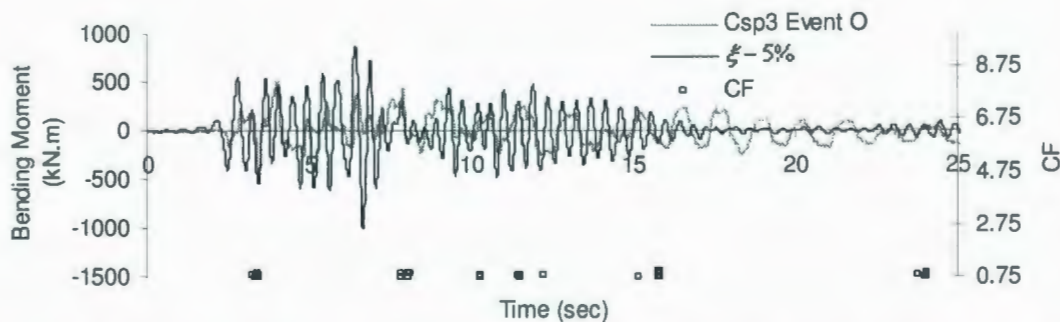


Figure B-72: Comparison of Bending Moment Time History for Event O, Csp3 at soil depth 8.5 m.

Appendix C: Pile Peak Bending Moment Profile

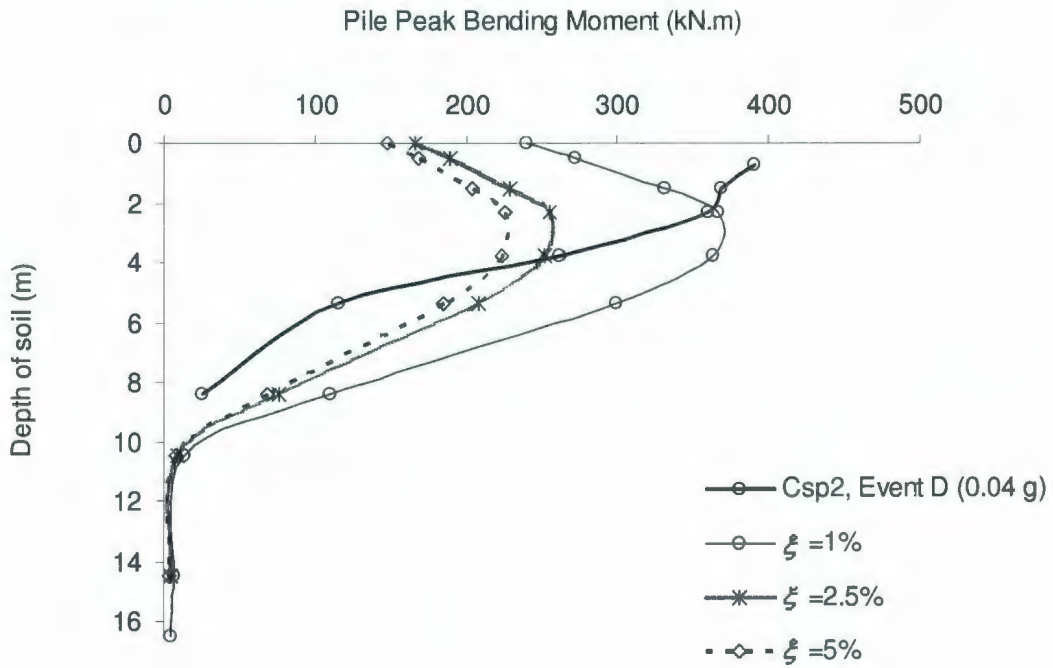


Figure C-1: Pile Peak Bending Moment (PPBM) in Event D of Csp2 test.

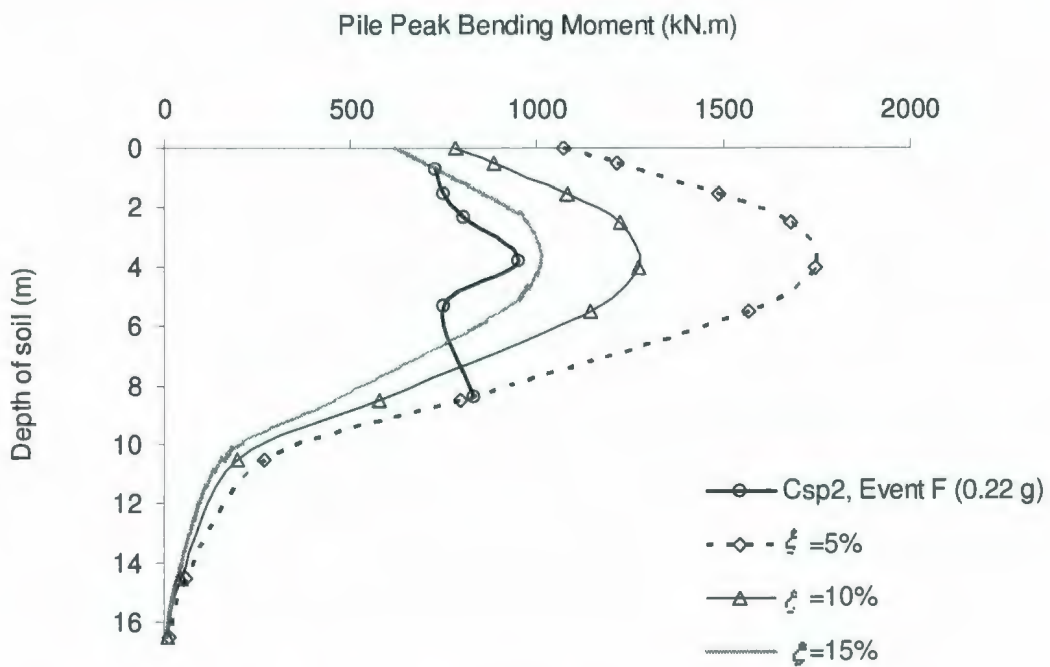


Figure C-2: Pile Peak Bending Moment (PPBM) in Event F of Csp2 test.

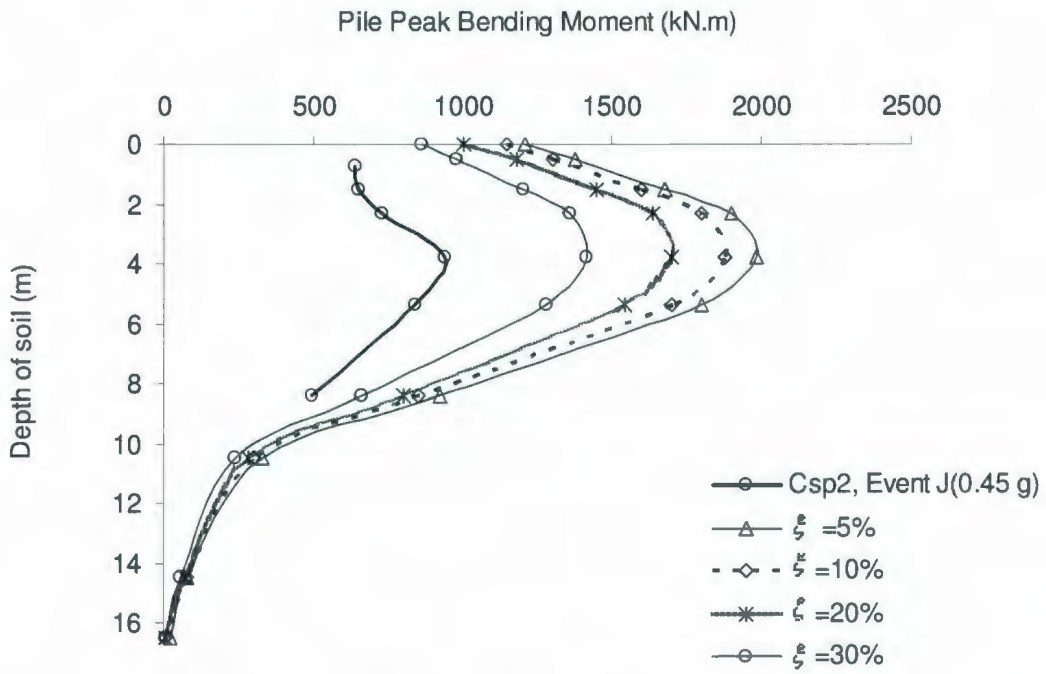


Figure C-3: Pile Peak Bending Moment (PPBM) in Event J of Csp2 test.

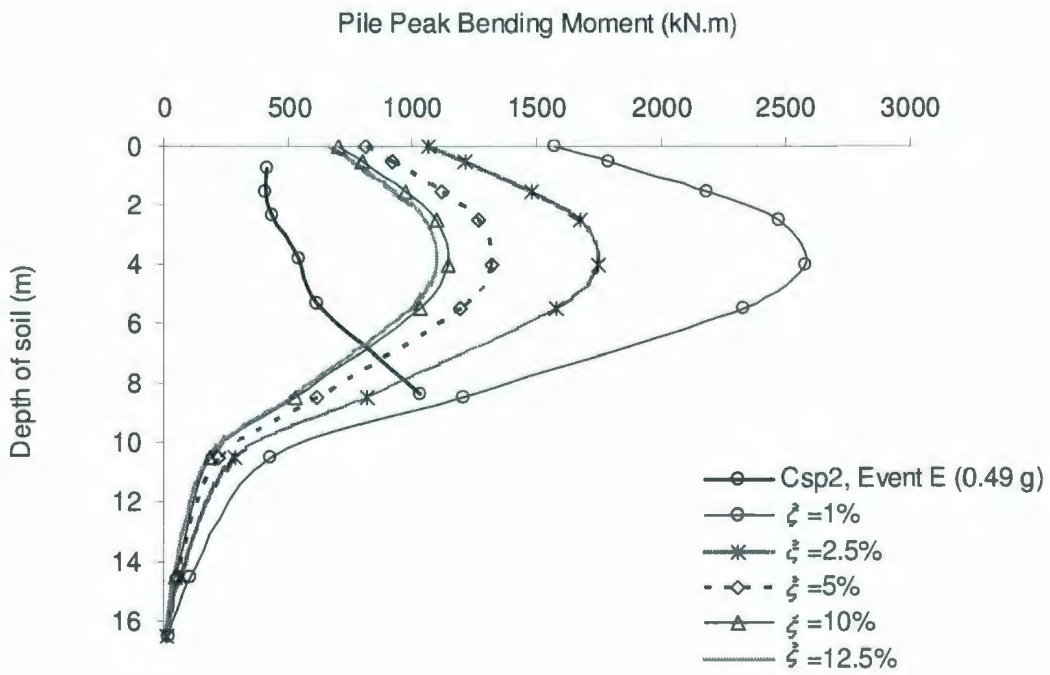


Figure C-4: Pile Peak Bending Moment (PPBM) in Event E of Csp2 test.

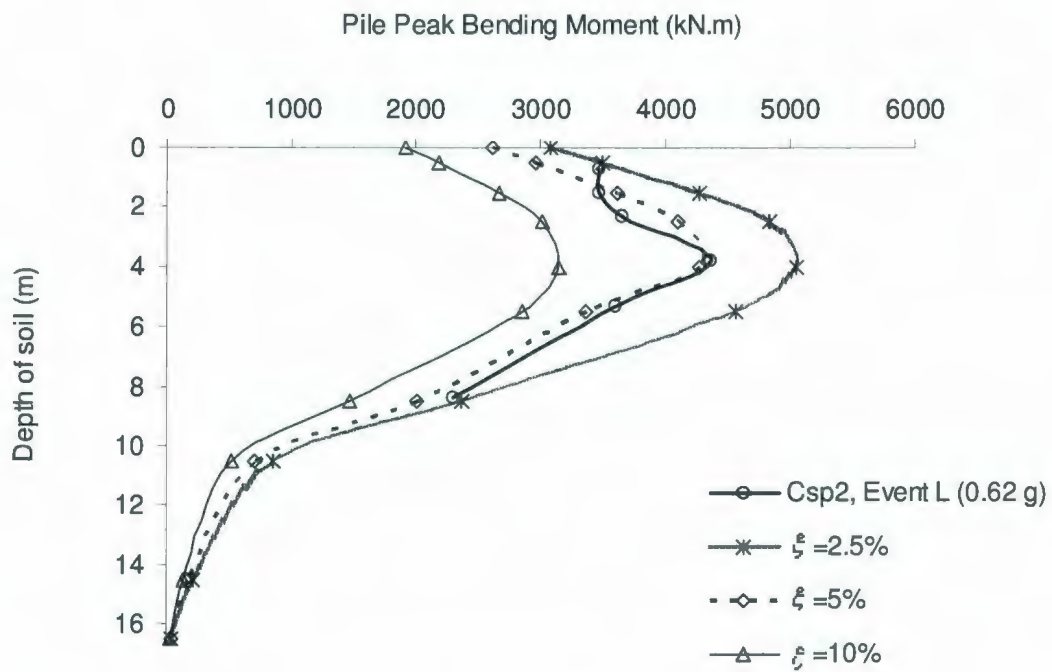


Figure C-5: Pile Peak Bending Moment (PPBM) in Event L of Csp2 test.

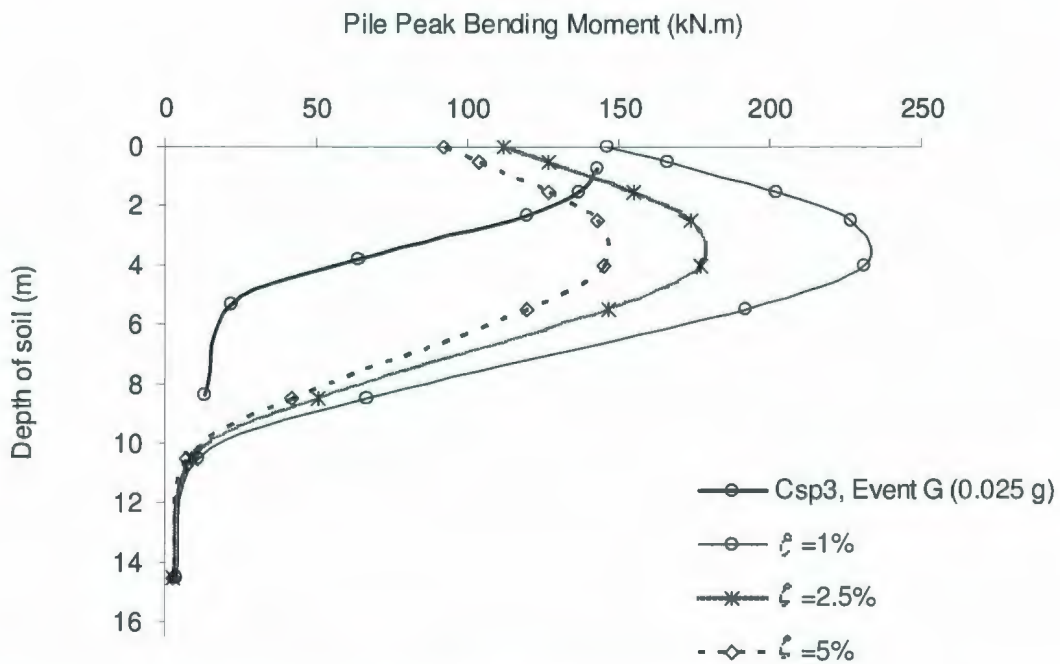


Figure C-6: Pile Peak Bending Moment (PPBM) in Event G of Csp3 test.

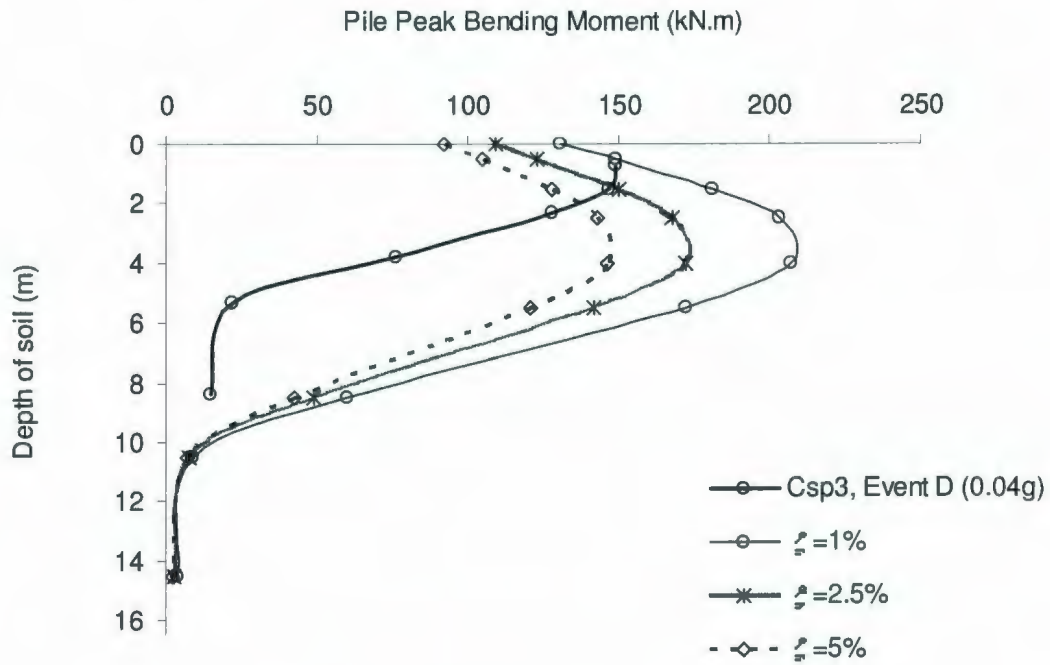


Figure C-7: Pile Peak Bending Moment (PPBM) in Event D of Csp3 test.

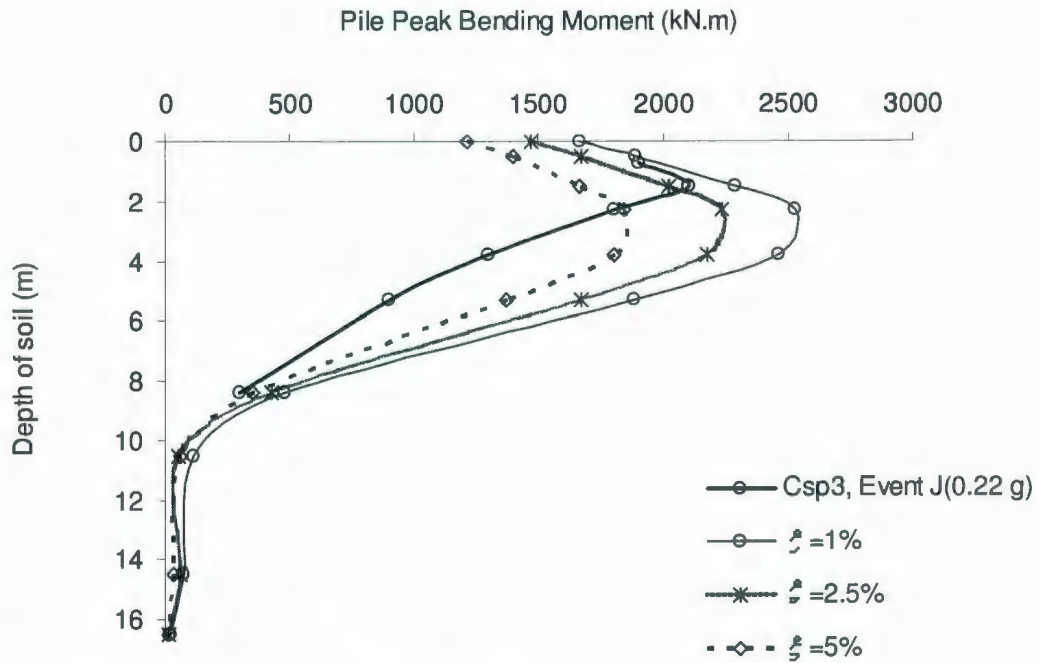


Figure C-8: Pile Peak Bending Moment (PPBM) in Event J of Csp3 test.

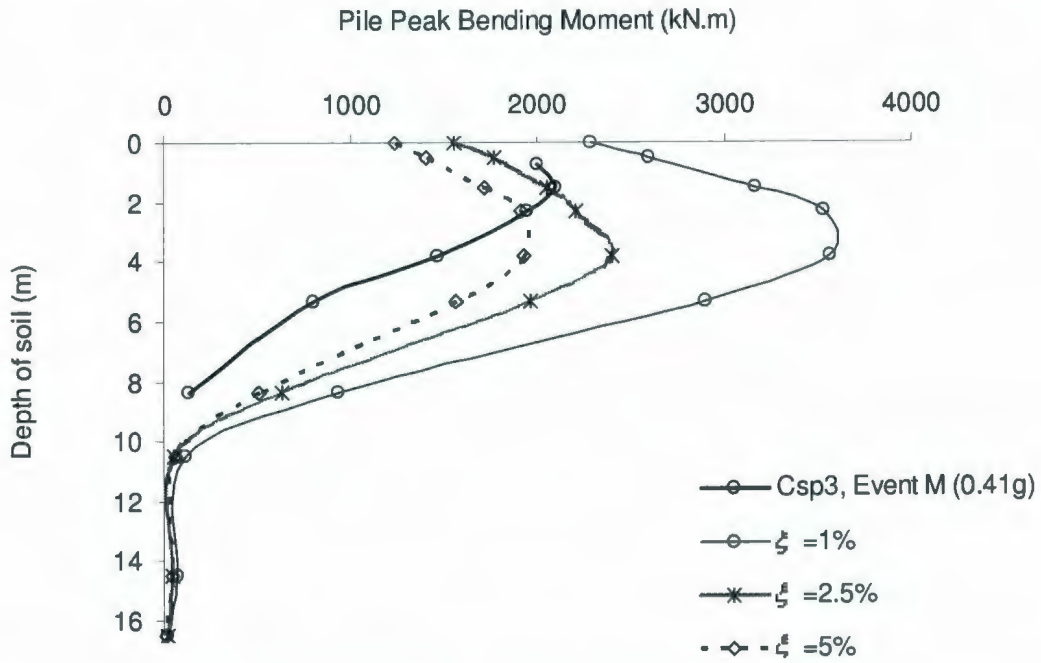


Figure C-9: Pile Peak Bending Moment (PPBM) in Event M of Csp3 test.

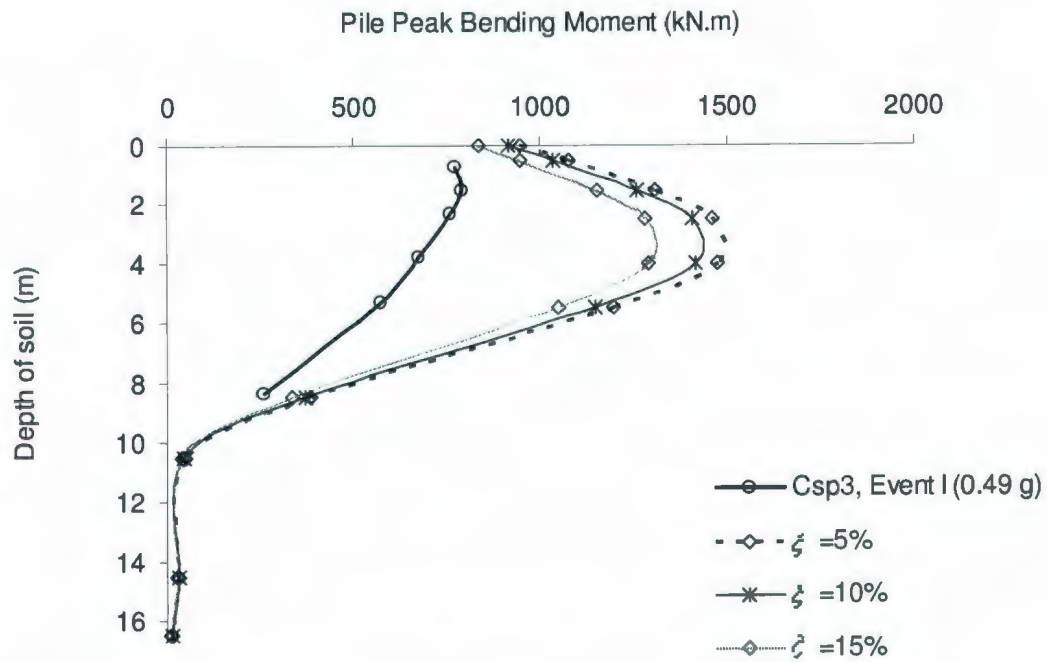


Figure C-10: Pile Peak Bending Moment (PPBM) in Event I of Csp3 test.

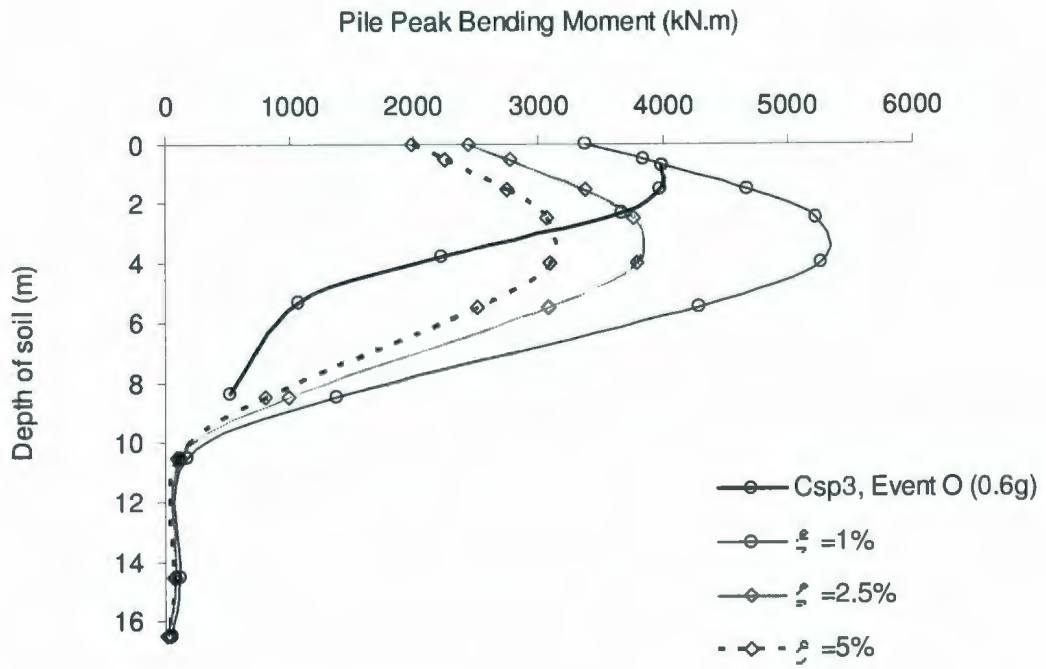


Figure C-11: Pile Peak Bending Moment (PPBM) in Event O of Csp3 test.



